Solid phase extraction and determination of indium using multi-walled carbon nanotubes modified with magnetic nanoparticles

Ehsan Zolfonoun [a,*]

[a] *Material and Nuclear Fuel Research school, Nuclear Science and Technology Research Institute, Tehran, Iran*

ABSTRACT

In this work MWCNTs-Fe_3O_4 nanocomposite was used as an adsorbent for extraction and preconcentration of indium from aqueous solutions. The magnetic MWCNTs with adsorbed analytes were easily separated from the aqueous solution by applying an external magnetic field. After elution of the adsorbed analytes, the concentration of indium was determined using inductively coupled plasma optical emission spectrometry determination. The effects of pH, sorbent amount, eluent type, chelating reagent concentration, sample volume, and time on the recovery of the In(III) were investigated. Moreover, under the optimum conditions, the detection limit for In(III) was 0.28 µg L^{-1}. The precision of the method, evaluated as the relative standard deviation obtained by analyzing a series of ten replicates, was 3.1 %. Ultimately, the method was successfully applied for the determination of In(III) in environmental water samples.

1. Introduction

Indium is an important element in the semiconductor industry, in the nuclear studies and in the production of high purity materials [1]. Indium and its compounds have numerous industrial applications including the manufacture of liquid crystal displays (LCD), semiconductors, low-temperature solders, and infrared *photodetectors* [2]. Also, indium compounds damage the heart, kidney, and liver. Thus, there is a need for specific and precise determination of indium traces in environmental and biological samples. The quantification of metal ions in various matrices has been performed by different techniques, including spectrophotometry, atomic absorption spectrometry (AAS), and inductively coupled plasma optical emission spectrometry (ICP-OES) [3]. In addition, using the mentioned methods directly for determining indium at very low concentrations is difficult because of insufficient sensitivity of this technique, as well as the matrix interferences which occur in real samples, and an initial sample pretreatment, such as preconcentration of the analyses (or analytes) and matrix separation, is often necessary [4]. Solid

phase extraction (SPE) is a routine extraction method for preconcentration of organic and inorganic analytes. This technique reduces solvent usage and exposure, disposal costs, and extraction time. In addition, based on the references, [5] and [6], various adsorbents have been used for adsorption of analytes in SPE methods.

Magnetic nanoparticles, mainly including Fe_3O_4 nanoparticles, received increasing attention in the recent years due to its unique properties and high potential applications in various fields such as cell separation, magnetically assisted drug delivery, enzyme immobilization, and protein separation [7, 8].. Recently, using magnetic nanoparticles for extraction of analytes in SPE methods is gaining research interest [9, 10]. In addition, multi-walled carbon nanotubes (MWCNTs) have received great attention due to their exceptional electronic, mechanical, thermal, chemical properties, and significant potential applications in many fields [11]. Owing to their large surface area and high reactivity, MWCNTs based adsorbents have been used for solid phase extraction and preconcentration of organic compounds and metal ions [12,13]. The decoration of MWCNTs with various compounds can modify their physicochemical properties. Also, this character makes them more suitable for chemical and biological applications. Functionalizing MWCNTs with magnetic nanoparticles can combine the features of magnetic nanoparticles and MWCNTs, which may result in materials with potential applications in biological labelling, drug delivery, and magnetic storage media [14, 15]. In this paper, a magnetic solid phase extraction method based on Multi-walled carbon nanotubes decorated with Fe_3O_4 nanoparticles is developed for the extraction and preconcentration of trace amounts of indium, prior to their determination by ICP-OES.

2. Experimental Procedure

2.1. Reagents

All reagents used were of analytical grade and were used as supplied. HNO_3, ammonia solution, $FeCl_3·6H_2O$, and $FeCl_2·4H_2O$, were purchased from Merck (Germany). MWCNTs (purity> 95%) were obtained from Sigma-Aldrich. Standard stock solution (1000 μg mL^{-1}) of In(III) was prepared by dissolving appropriate amounts of $In(NO_3)_3$ in water. A solution of $1.0×10^{-3}$ mol L^{-1} quinalizarine (Merck) was prepared by dissolving appropriate amounts of this reagent in 0.01 mol L^{-1} NaOH (Merck).

2.2. Instrumentation

All the measurements were carried out using a Perkin Elmer (Optima 7300 DV) simultaneous ICP-OES coupled to a concentric nebulizer and equipped with a charge coupled device (CCD) detector. Moreover, Metrohm model 744 digital pH meter, equipped with a combined glass-calomel electrode, was employed for the pH adjustments.

2.3. Preparation of MWCNTs-Fe$_3$O$_4$ nanocomposite

MWCNTs-Fe_3O_4 nanocomposite was synthesized according to the previously reported methods, which were mentioned in the references, [14] and [15]. First, MWCNTs were dispersed in concentrated nitric acid for 4 hours with ultrasonic treatment. Then purified MWCNTs were separated by filtering. Afterwards, they washed repeatedly with distilled water followed by ethanol and dried at 50 °C. The MWCNTs-Fe_3O_4 nanocomposite was prepared by chemical coprecipitation method. First, $FeCl_3·6H_2O$ (1.18 g) and $FeCl_2·4H_2O$ (0.43 g) were dissolved in 200 mL deionized water under nitrogen gas with vigorous stirring at 60 °C. Then 1.0 gram of MWCNTs was added in the solution with ultrasonic treatment for about 10 min. Finally, NH_4OH solution was added dropwise into the solution until its pH was adjusted to 11. After stirring for 30 min at 50 °C, the obtained MWCNTs-Fe_3O_4 nanocomposite was separated from the reaction medium by magnetic field, and

washed with 200 mL deionized water four times.

2.4. Magnetic solid-phase extraction procedure

A 100-mililiter sample or standard solution containing In(III) (pH 6), and QA (1.0×10^{-5} mol L^{-1}), was transferred in a glassware beaker. Then 5 mg MWCNTs-Fe_3O_4 nanocomposite was added into the sample solution. Afterwards, the mixture was stirred for 3 min. Subsequently, the sorbent particles were isolated by placing a strong magnet, and the supernatant was poured away. The preconcentrated target analyte was eluted using 1.0 mL of a 1 mol L^{-1} solution of HNO_3. Finally, the concentration of In(III) in acidic aqueous phase was determined by ICP-OES.

3. Results and discussion

3.1. Effect of pH

The effect of pH on the extraction of indium was studied in the range of 2.0–8.0 using nitric acid or sodium hydroxide. The resulting percent recovery-pH plots are shown in Fig. 1. These plots indicate that sorption is maximum and quantitative in the pH range of 6.0–7.0. Consequently, a solution pH of 6.0 was used in further experiments.

3.2. Effect of the sorbent amount

In order to study the effect of the sorbent, 2 to 10 mg of MWCNTs-Fe_3O_4 nanocomposite was added to 100 mL of the sample solution (Fig. 2).
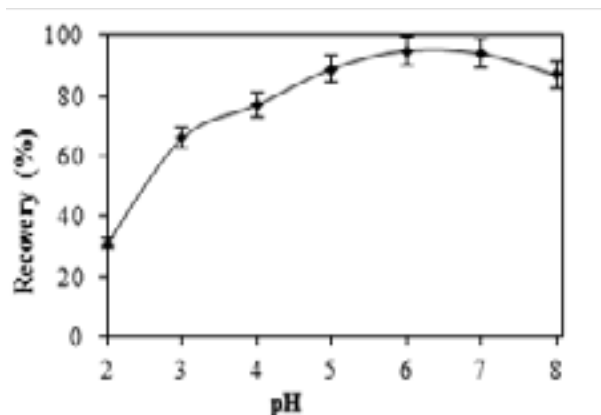
The obtained results showed that by increasing the sorbent amounts from 2 up to 5 mg due to increasing accessible sites, extraction recovery increased, and then it remained constant. A 5-miligram of the MWCNTs-Fe_3O_4 nanocomposite was selected for subsequent experiments.

3.3. Effect of eluent type

In order to find the best eluent, different eluting solutions such as HCl, H_2SO_4, HNO_3 and acetic acid, were tested. The results revealed that a 1.0-mililiter of 1.0 M concentration of all acids could afford the quantitative elution of In^{3+} from the sorbent. Finally, subsequent elutions of In^{3+} were carried out with 1 M HNO_3 solution

3.4. Effect of chelating reagent concentration

The effect of QA concentration on the extraction of indium was studied, and the results are shown in Fig. 3. Also, QA concentration in the range of 0 to 5.0×10^{-5} mol L^{-1} was investigated by us. Then, maximum recovery was obtained at a concentration of 1.0×10^{-5} mol L^{-1} of the ligand and at higher concentrations, the extraction recovery remained constant.

3.5. Effect of solution volume
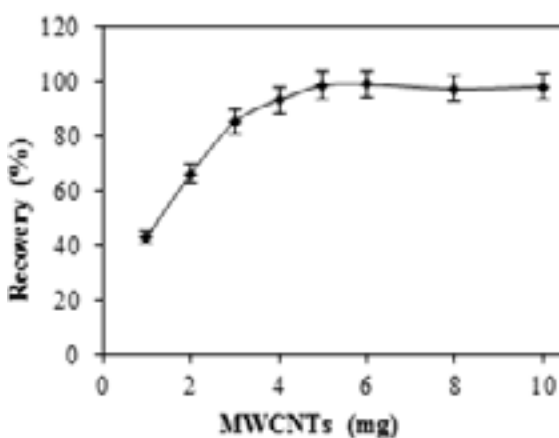
The effect of solution volume was examined by

Fig. 1. Effect of pH on the recovery of In(III) ion.

Fig. 2. Effect of the MWCNTs-Fe_3O_4 amount on the recovery of In(III) ion.
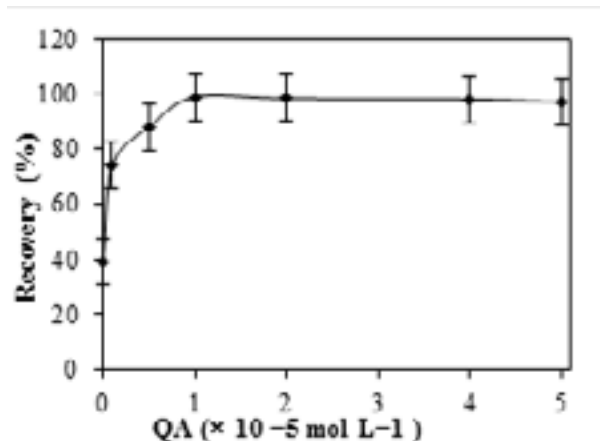
Fig. 3. Effect of chelating reagent concentration on the recovery of In(III) ion.

preconcentrating different volumes (20–250 mL) of aqueous solutions spiked with a constant mass of 10.0 μg of In(III), and the results are depicted in Fig. 4. The obtained results showed that when aqueous solution volume was up to 100 mL, recoveries above 95% were obtained. Thus, 100 mL was considered to be the maximal enrichment volume for water samples. Consequently, since the final solution volume to be measured by ICP-OES was 1.0 mL, the preconcentration factor for In(III) was evaluated as 100.

3.6. Effect of extraction time

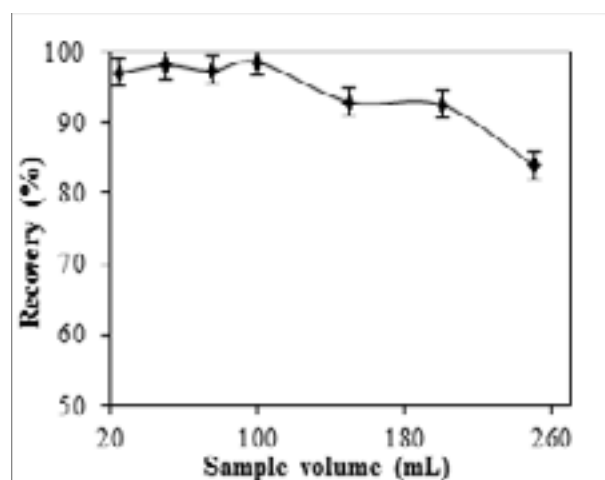The effect of extraction time on the extraction of

Fig. 4. Effect of sample volume on the recovery of In(III) ion.

In(III) was studied in the range of 1–15 min. The experimental results indicated that there was no significant effect on the extraction efficiency when the extraction time increased from 3 to 10 min. Based on the above considerations, the extraction time that is equal to 3 min was selected for further studies.

3.7. Effect of diverse ions on the recovery

In order to assess the possible analytical applications of the recommended procedure, the effect of common coexisting ions in natural water samples on the preconcentration and determination of indium ion was studied. In these experiments, 100 mL solutions containing 50 μg L^{-1} of indium and various amounts of interfering ions were treated according to the recommended procedure. In addition, tolerable limit was defined as the highest amount of foreign ions that produced an error not exceeding ±5% in the determination of investigated analyte ion. The results are summarized in Table 1. As seen, a large number of ions used have no considerable effect on the determination of indium.

3.8. Analytical figures of merit

In Table 2, the analytical characteristics of the proposed method, including linear range, limit of detection, reproducibility, and enrichment factor have been summarized. In the optimum conditions, a calibration graph was constructed by preconcentrating a series of the solutions according to the recommended procedure. There is an important tip, that the calibration curve for In(III) was linear form 1.0 to 500 μg L^{-1} with a regression

Table 1. Tolerance limits of some cations and anions on the sorption and determination of indium.

Ion	Tolerance limit (μg mL^{-1})
Li$^+$, Na$^+$, K$^+$, Cl$^-$, NO$_3^-$	>2000
Ca^{2+}, Mg^{2+}, Ba^{2+}, Sr^{2+}	1000
Ag$^+$, Hg^{2+}, SO$_4^-$	50
Cu^{2+}, Fe^{3+}, Pb^{2+}, Ni^{2+}, Co^{2+}, Cr^{3+}, Mn^{2+}, Cd^{2+}, Zn^{2+}	5

Table 2. Analytical parameters of the proposed method.

Parameter	Analytical feature
Linear range ($\mu g\,L^{-1}$)	1.0−500
r^2	0.995
LOD ($\mu g\,L^{-1}$)	0.28
R.S.D. % (n = 10)	3.1
Enrichment factor	100

coefficient of 0.995. The limit of detection (LOD) of the proposed method for the determination of indium was studied under the optimal experimental conditions. The LOD, defined three times by paying attention to the standard deviation of 10 measurements of the blank solution divided by the slope of the calibration curve, was 0.28 $\mu g\,L^{-1}$. The reproducibility of the proposed method for extraction and determination of 50 $\mu g\,L^{-1}$ indium (n= 10) was also studied. Finally, the relative standard deviations (R.S.D.) of these determinations were 3.1 %.

3.9. Application

The accuracy of the proposed method was tested by separation and determination of In(III) in tap water, mineral water, and well water samples. The obtained results are given in Table 3. The relative recoveries for the spiked samples were in the range of 94–109 %. The results demonstrated that the proposed method was suitable for the determination of In(III) in real samples.

4. Conclusions

In this study, a fast and simple method based was developed for the separation and preconcentration of indium, prior to ICP-OES determination. The use of NPs endued the SPE method with high extraction capacity and preconcentration factors. The magnetic separation greatly improved the separation rate while avoided the time-consuming column passing or filtration operation. The proposed preconcentration and determination method gives a low limit of detection and good R.S.D. values. Finally, the method can be successfully applied to the separation and determination of indium in real samples.

**Table 3.** Recovery of indium from water samples.

Sample	Indium		
	Added ($\mu g\,L^{-1}$)	Found ($\mu g\,L^{-1}$)	Recovery (%)
Tap water	0.0	<LOD	–
	10.0	9.7 (1.8)[a]	97
Mineral water	0.0	<LOD	–
	10.0	10.9 (1.4)	109
River water	0.0	<LOD	–
	10.0	9.4 (2.6)	94

[a] Values in parentheses are R.S.D.s based on three replicate analyses.

5. References

[1] M. Souad, C. Louage, J. Yves Doisy, L. Meunier, A. Benderrag, B. Ouddane, S. Bellayer, N. Nuns, M. Traisnel, U. Maschke, Extraction of indium-tin oxide from end-of-life LCD panels using ultrasound assisted acid leaching, Ultrason. Sonochem., 40 (2018) 929-936.

[2] J. Uhrovčík, J. Lesný, Determination of indium in liquid crystal displays by flame atomic absorption spectrometry, J. Ind. Eng. Chem., 21 (2015) 163-165.

[3] J.R. Dean, Practical inductively coupled plasma spectroscopy, Wiley., UK, 2005.

[4] B. Çelik, E. Akkaya, S. Bakirdere, F. Aydin, Determination of indium using vortex assisted solid phase microextraction based on oleic acid coated magnetic nanoparticles combined with slotted quartz tube-flame atomic absorption spectrometry, Microchem. J., 141 (2018) 7-11.

[5] M. Eftekhari, M. Gheibi, M. Akrami, F. Iranzad, Solid-phase extraction of ultra-trace levels of lead using tannic acid-coated graphene oxide as an efficient adsorbent followed by electrothermal atomic absorption spectrometry; response surface methodology – central composite design, New J. Chem., 42 (2018) 1159-1168.

[6] J.B. Ghasemi and E. Zolfonoun, Simultaneous spectrophotometric determination of trace amounts of uranium, thorium, and zirconium using the partial least squares method after their preconcentration by α-benzoin oxime modified Amberlite XAD-2000 resin, Talanta, 80 (2010) 1191-1197.

[7] Y. Li, Y.C. Liu, and J. Tang, Fe3O4-Al2O3 magnetic core-shell microspheres for rapid and highly specific capture of phosphopeptides with

mass spectrometry analysis, J. Chromatogr. A, 1172 (2007) 57-71.

[8] D. Horak, B. Rittich, J.A. Safar, A. Spanova, J. Lenfeld, and M.J. Benes, Properties of RNase A immobilized on magnetic poly(2-hydroxyethyl methacrylate) microspheres. Biotechnol. Prog., 17 (2001) 447-452.

[9] J.B. Ghasemi and E. Zolfonoun, Simultaneous spectrophotometric determination of trace amount of polycyclic aromatic hydrocarbons in water samples after magnetic solid-phase extraction by using projection pursuit regression, Environ. Monit. Assess., 185 (2013) 2297-2305.

[10] A. Mehdinia, M. Ramezani, A. Jabbari, Preconcentration and determination of lead ions in fish and mollusk tissues by nanocomposite of Fe3O4@graphene oxide@polyimide as a solid phase extraction sorbent, Food Chem., 237 (2017) 1112-1117.

[11] R.H. Baughman, A.A. Zakhidov, and W.A. deHeer, Carbon nanotubes-the route toward applications,Science, 297 (2002) 787-792.

[12] C. Herrero-Latorre, J. Barciela-García S. García-Martín R. M. Peña-Crecente, Graphene and carbon nanotubes as solid phase extraction sorbents for the speciation of chromium: A review, Anal. Chim. Acta, 1002 (2018) 1-17.

[13] Z. Dehghani, Firouzabadi, S. Dadfarnia, A.M. Haji Shabani, M.H. Ehrampoush, E.N. Tafti, Magnetic dispersive solid phase extraction using modified magnetic multi-walled carbon nanotubes combined with electrothermal atomic absorption spectrometry for the determination of selenium, Int. J. Environ. Anal. Chem., 98 (2018) 555-569.

[14] A. Pistone, D. Iannazzo, and M. Fazio, Synthesis and magnetic properties of multiwalled carbon nanotubes decorated with magnetite nanoparticles, Physica B, 435. (2014) 88-91.

[15] A. Masotti and A. Caporali, Preparation of Magnetic Carbon Nanotubes (Mag-CNTs) for Biomedical and Biotechnological Applications, Int. J Mol. Sci., 14 (2013) 24619-24642.

AMECJ
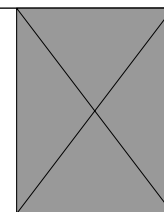
Room temperature imidazolium-based ionic liquids as scavengers for hydrogen sulfide removal of crude oil

Ali Akbar Miran Beigi[a,*], Maryam Yousefi[a,b], and Majid Abdouss[b]

[a] *Research Institute of Petroleum Industry, West Blvd. of Azadi Sport Complex, Tehran, Iran*
[b] *Department of Chemistry, Amirkabir University of Technology, P.O. Box 15875-4413, Tehran, Iran*

A B S T R A C T

Determination of H_2S amounts in crude oil was performed by a precise method instead of UOP163 that were developed in our pervious works. Evaluation of ILs and scavengers were done by two ways. The first one was based on variable concentration of ILs as the scavenger (dynamic method), and the second one was based on a constant concentration of the scavenger during H_2S removal process (static method). In the static method, design of experiments was performed for all three tested ILs and three parameters such as time, temperature, and dosage (injection volume) of ILs were investigated. A wide range of time and temperature was also studied according to operating conditions in petroleum terminals. The dose of ILs was obtained from the dynamic method. According to the obtained results, these ILs had a significant effect on H_2S reduction in crude oil, so that H_2S concentration in some conditions was less than 1 ppm. In comparison between ILs and commercial scavengers's performance can be properly understood that not only ILs reduced H_2S concentration, but also their dosage was very low, and mole ratio of [IL]/[H_2S] was 1:3 that it was negligible compared with commercial scavengers. Also the results showed that [EMIM][NTf$_2$] was more effective than the other ILs in H_2S removal.

1. Introduction

Hydrogen sulfide is one of the most abundant sulfur containing compounds in natural gas and light and middle distillate oil fractions as well as in atmospheric air effluents and pulp and paper industry. Hydrogen sulfide is undesirable, colorless, odorous, highly toxic, and poisonous for catalysts and corrosive to industrial gas and oil streams [1-3]. Also, it can be regarded as a major source of air pollution [4-6]. This acid gas is produced along with methane and light hydrocarbons in many oil and gas fields [7, 8]. According g to the international environmental regulations, H_2S contained in the acid gases should be effectively removed before emission to atmosphere [8, 9]. H_2S is commonly removed from natural and synthesis gases through chemical absorption using aqueous solutions of organic bases like single amines, amine mixtures, or mixtures of an amine and a salt of an amino acid [10-12]. Extensive research has been conducted by several groups on aqueous solutions of alkanolamines, especially

monoethanolamine (MEA), diethanolamine (DEA) and methyldiethanolamine (MDEA) for treating and sweetening [13-16]. All of them are volatile and they show a reversible reaction that it can reverse H_2S in refining processes and make the process economically expensive [17].

In contrast ionic liquids (ILs) provides a vaporless, thermally stable [18, 19], reusable "green" solvent and catalyst for chemical reactions, so ILs has very possibility for removal of H_2S. ILs are molten salts composed entirely of ions, and many of them are liquids at room temperature. Room temperature ionic liquids (RTILs), often referred to as 'designer solvents', have been the great focus of scientists in various fields since they can be tuned for specific applications [20-27]. Nowadays, the most commonly studied ILs normally contain, imidazolium, ammonium, phosphonium, pyridinium, and pyrrolidinium cations, and tetrafluoroborate, hexafluorophosphate, bistrifluorosulfonylimide and triflate anions [20, 25, 28-30]. In addition, the physicochemical properties of ILs can be finely tuned by slight structural changes of the corresponding cations and anions [23–26]. To better understand the nature of ionic liquids and rationally expand their applications especially as pollutant scavenger and electrolyte, knowledge of their thermophysical and electrochemical properties is required. In this work [Hmim][BF4], [Emim][Ntf$_2$] and [Bmim] [MeSO$_4$] were used as scavengers for H_2S removal from crude oil and then the results were compared with several commercial scavengers. Molecular structures of the three ILs are shown in Fig. 1.

In our previous work, physical and electrochemical properties of these ILs were investigated. Viscosity, solubility, thermal decomposition and electrochemical window of three ILs were studied more than the other properties. So these mentioned properties have been applied for H_2S removal. For example, the viscosity of selected ILs was fully compatible with the crude oil. Therefore, use of them in crude oil was not a problem. The thermal stability of ILs was very high and their ability at high temperatures was excellent. ILs may be have hydrophilic or lipophilic properties.

The hydrophilic and lipophilic ILs can remove H_2S of aqueous and organic parts of crude oil respectively. The decomposition temperature ranges of three ILs are shown in Table 1. Also, the experimental values of physicochemical properties of [HMIM][BF$_4$], [EMIM][NTf$_2$] and [BMIM][MeSO$_4$], such as density, refractive index, dynamic and kinematic viscosities, pH, and surface tension are listed in Table 2[20]. According to our previous studies these ILs are very suitable for H_2S
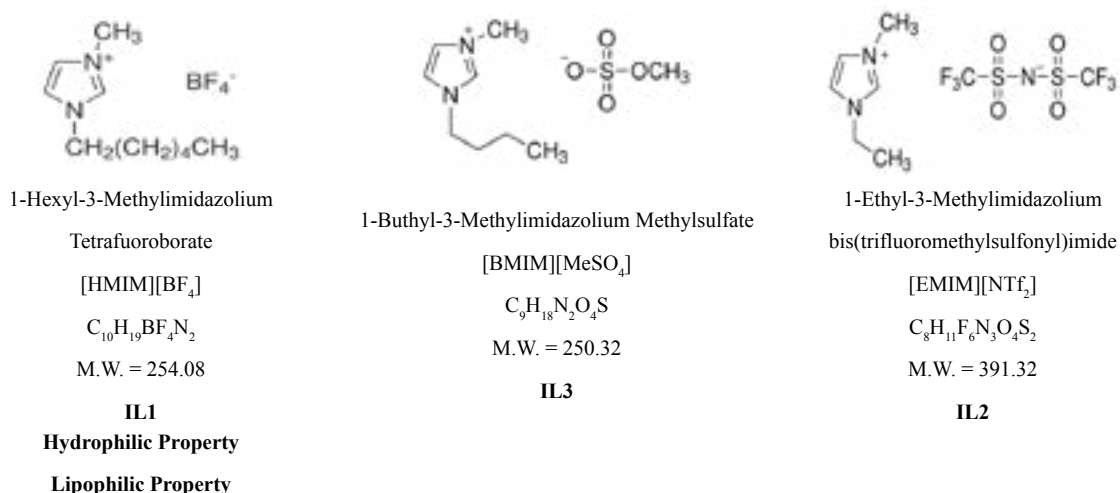

1-Hexyl-3-Methylimidazolium
Tetrafuoroborate
[HMIM][BF$_4$]
C$_{10}$H$_{19}$BF$_4$N$_2$
M.W. = 254.08
IL1
Hydrophilic Property

Lipophilic Property

1-Buthyl-3-Methylimidazolium Methylsulfate
[BMIM][MeSO$_4$]
C$_9$H$_{18}$N$_2$O$_4$S
M.W. = 250.32
IL3

1-Ethyl-3-Methylimidazolium
bis(trifluoromethylsulfonyl)imide
[EMIM][NTf$_2$]
C$_8$H$_{11}$F$_6$N$_3$O$_4$S$_2$
M.W. = 391.32
IL2

Fig. 1. Molecular structures of the three ILs

scavenging and to the best of our knowledge we didn't find any paper related to H_2S removal from crude oil by using ILs. In addition, these ILs unlike other scavengers don't have any disadvantages such as slow synthetics, high consumption, unstable in high temperatures, or increase salt and sediments content. Of course the elimination

Table 1. Thermal decomposition for investigated ionic liquids.

Ionic Liquid	Decomposition Temperature Range/°C
[HMIM][BF$_4$]	310-500
[EMIM][NTf$_2$]	390-510
[BMIM][MeSO$_4$]	317-438

Table 2. Density ρ, dynamic viscosity η, refractive index n_D, surface tension σ, thermal expansion a_p, and pH of the ionic liquids at different temperatures

t (°C)	ρ (g mL^{-1})	η (mPa s)	n_D	σ (mN m^{-1})	$10^4 a_p$ (K)	pH of 1% Solution
[HMIM][BF$_4$]						
10	1.1562	608.1	1.4265	41.4	5.343	
20	1.1492	311.7	1.4241	40.6	5.525	6.41
25	1.1461	220.0	1.4223	40.4	5.623	6.25
30	1.1425	167.3	1.4211	40.0	5.718	
40	1.1355	103.3	1.4183	39.8	5.909	5.77
50	1.1280	63.77	1.4158	39.0	6.104	
60	1.1214	52.22	1.4137	38.2	6.302	5.12
70	1.1122	28.48	1.4106	37.2	6.504	
80	1.1004	21.39	1.4080	36.6	6.709	4.49
90	1.0874	15.87	1.4051	36.3	6.918	4.17
95	1.0838	13.92	1.4038	35.9	7.025	
[EMIM][NTf$_2$]						
10	1.5311	55.92	1.4254	40.2	4.706	
20	1.5220	37.27	1.4232	39.8	5.518	6.48
25	1.5168	31.13	1.4220	39.4	5.929	6.5
30	1.5117	26.28	1.4206	39.0	6.344	
40	1.5020	19.67	1.4179	38.8	7.186	6.54
50	1.4907	14.96	1.4153	38.6	8.045	
60	1.4780	11.84	1.4127	38.0	8.925	6.60
70	1.4651	9.506	1.4101	37.2	9.828	
80	1.4494	7.820	1.4072	36.6	10.76	6.66
90	1.4292	6.539	1.4045	36.0	11.72	6.69
95	1.4230	6.054	1.4033	35.5	12.21	
[BMIM][MeSO$_4$]						
10	1.2117	220.6	1.4831	46.0	4.457	
20	1.2053	122.3	1.4777	44.4	4.810	7.60
25	1.2019	93.78	1.4771	43.7	4.988	7.55
30	1.1983	73.35	1.4765	43.4	5.167	
40	1.1923	46.85	1.4745	42.6	5.530	7.39
50	1.1853	32.21	1.4719	42.0	5.899	
60	1.1774	23.02	1.4694	41.2	6.274	7.18
70	1.1668	17.05	1.4673	39.8	6.656	
80	1.1538	13.14	1.4650	39.0	7.0453	6.96
90	1.1400	10.34	1.4626	38.1	7.443	6.85
95	1.1356	9.257	1.4615	37.6	7.645	

reaction mechanism is unknown and our further studies certainly will be in this field.

In present work determination of H_2S amounts in crude oil was performed by the method that was presented by researchers at Research Institute of Petroleum Industry method (RIPI). [31] Then ILs was used in two different ways as scavengers for H_2S removal. Finally, the results of both methods were compared with several commercial scavengers. Also, in our next work, metallic nanoparticles will be synthesized in ionic liquids media for H_2S removal from crude oil.

2. Experimental

2.1. Materials

All chemicals and three ionic liquids were purchased from Merck, Aldrich and Fluka companies. The chemicals were used without further purification. Crude oil samples included exported crude oil such as Balarood, Masjed Soleyman, Soomar, Bahregan, and Furoozan.

2.2. Experimental procedure

The RIPI method was applied for determination of H_2S amounts in crude oil. As we have previously reported this method was based on preliminary extraction with voltammetric detection. This method offers several inherent advantages for H_2S determination. Voltammetric detection methods are specific, since other species are electrochemically inactive at potentials where H_2S is detected. Also, this technique is very sensitive. Apparatus for determination of hydrogen sulfide in crude oil is shown in figure 2. After the measurement of H_2S content in crude oil, evaluation of several commercial scavengers and the ILs was done. Unfortunately there was not a systematic and standardized method to evaluate the efficiency of scavengers. In present work two methods was applied for evaluation. One is related to RIPI, was based on constant concentration of ILs or commercial scavengers and the other one was based on variable concentration of them that is related to
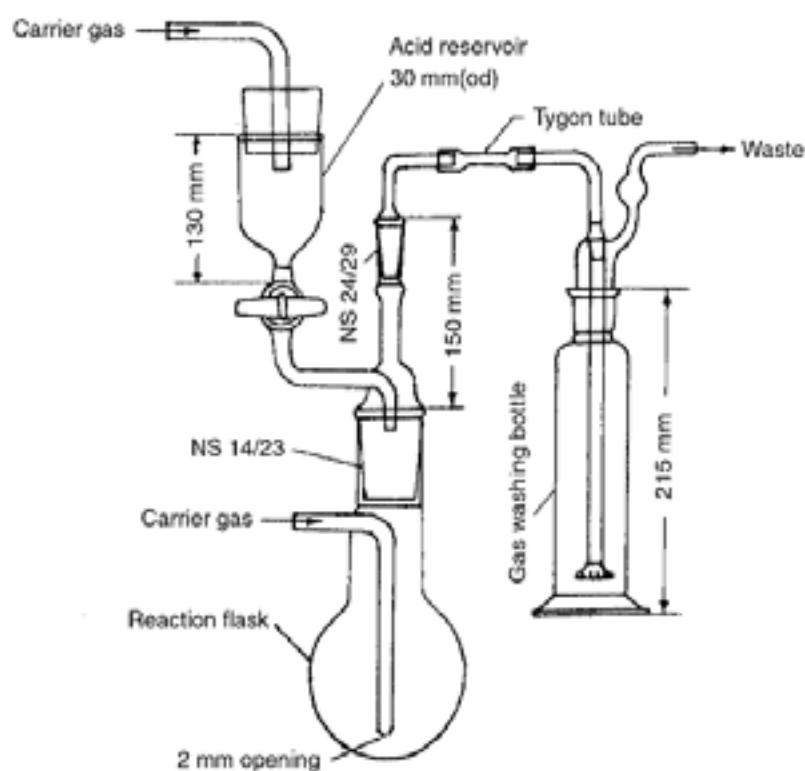

Fig. 2. The apparatus for determination of hydrogen sulfide in crude oil

oil export terminals. In the constant concentration method for ILs, design of experiment was applied by using Design Expert software.

3. Results and discussion

3.1. Evaluation of commercial scavengers

Evaluation of commercial scavengers was developed by two methods.

3.1.1 First method (Variable concentration)

This method has been developed by the RIPI, had high operating speed. The scavengers that were used had fast kinetic and high efficiency. Evaluation in this method was based on measuring and following potential variations of crude oil during addition of scavengers in a specified time. A potential variation of crude oil was shown in figure 3.

In the RIPI method, usually in the one minute intervals, approximately 50 µL of scavenger was added to the certain amount of crude oil (about 100 g) and potential changes versus time and volume

consumption of scavenger were recorded (Fig.3). Mutations that occurred in the potential curves were related to the equivalent point of H_2S titration by scavenger. In the equivalent point, almost all H_2S contents were neutralized by scavenger and crude oil are free of H_2S.

Primary investigations showed that electrode potential was depended on H_2S or S concentration in crude oil. As long as hydrogen sulfide was present in the crude oil, electrode potential, depending on the H_2S concentration in the specified range was nearly between -900 up to -1200 mV. It should be noted that beside H_2S concentration the electrode potential could be a function of temperature and electrolyte. Also, according to the Nernst equation, the electrode potential is depend on oxidative and reductive concentration, ions mobility and activity coefficient. Therefore, the potential ranges difference between -900 to -1200 mV may be due to one of the items listed above. In this method, evaluation of H_2S reduction was based on
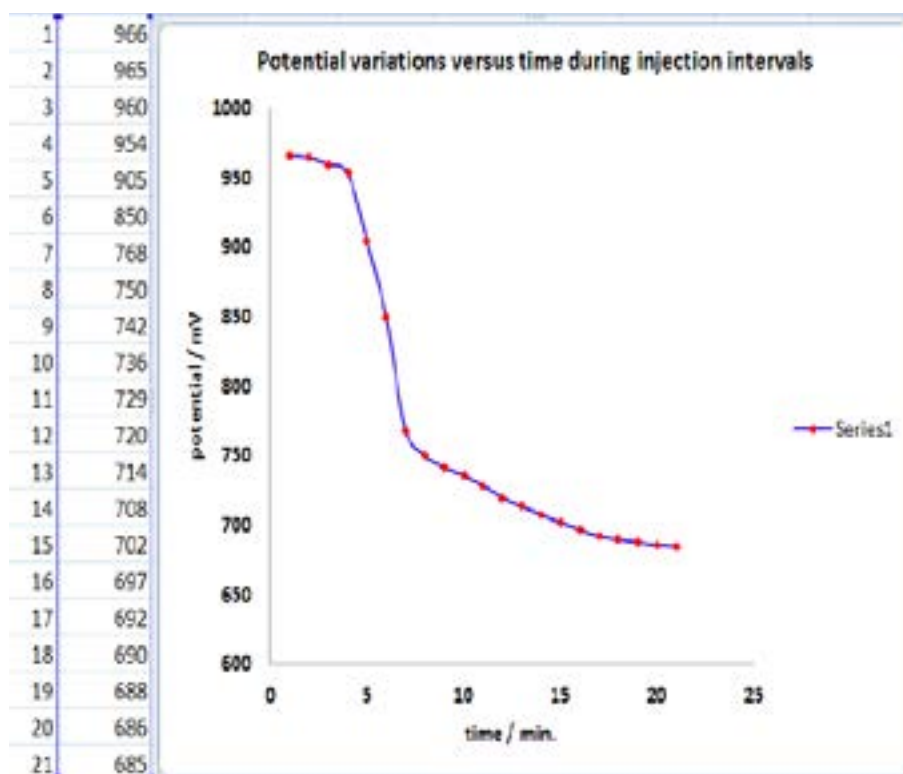

Fig. 3. Potential variations of crude oil by addition of a commercial scavenger versus time.

Table 3. Evaluation of commercial scavengers using RIPI method

Sample name	Injection volume/ml	E (initial)/mv	E (final)/mv	Treatment time/min
sulfavent 32	0.65	1100	805	15
sulfavent 42	0.55	1080	810	10
sulfavent 43	1	1000	860	7
sulfavent 44	1	1100	945	12

decreasing of the electrode potential. Experience indicated that when the crude oil was free of H_2S, electrode potential shifted to nearly less than -750 up to -800 mV. To more accurate investigations, 4 samples of commercial scavengers were tested using this method, and the results are given in Table 3.

As can be observed, sulfavent 32 and sulfavent 43 had better efficiency than the others. Lesser amounts of sulfavent 32 were used, on the other hand, Sulfavent 43 had higher speed. So that, for the neutralization of H_2S in crude oil, only 1 ml of scavenger was needed during 7 minutes. Although, both methods gave same results in the selection of scavengers, but the RIPI method provided more information, such as the effective time of scavenger and equivalent point.

3.1.2. Second method (Constant concentration)

This method was based on instructions of oil export terminals. First, the amount of H_2S was measured in crude oil and then specific dosage of scavengers was added to the crude oil. The consumed volume of scavenger (was related to H_2S concentration.

Here, H_2S concentration was based on the amount of hydrogen sulfide in crude oil, which is usually between 50 to 100 ppm of scavenger and depending on its efficiency, was about 2 to 5 times of the amount of H_2S in crude oil.

In a general evaluation, 100 g of a crude oil containing 75 ppm H_2S, was chosen. Then 225 ppm ([Scavenger]/[H_2S]:3) of the scavenger was added to it. After an hour stirring at room temperature, the H_2S concentration was measured with RIPI method. The same experimental conditions were done for an overnight and the results were reported and compared. Accordingly, all four samples were tested and the results are shown in Table 4.

Since the experiments were conducted on consecutive days, and there was no possibility of H_2S amount stabilization. So, the results were normalized in first and the last columns. As can be seen in the table, without any commercial scavenger, H_2S concentration has reached to 43 ppm after an overnight, but by mistake this reduction was generally considered to be scavenger. As a result, long reaction time was one of disadvantages in this method.

The result showed that all scavengers, with the exception of Sulfavent 44, had the ability to remove

Table 4. Evaluation of commercial scavengers using constant concentration of scavenger

sample name	H2S content in crude befor treatment / ppm	H2S content in crude after 1 hour treatment / ppm	H2S content in crude after overnight treatment / ppm	H2S content in crude before treatment after overnight / ppm
sulfavent 32	75	10.5	< 1.0	43
sulfavent 42	75	47.0	< 1.0	43
sulfavent 43	75	5.4	< 1.0	43
sulfavent 44	75	26.0	< 17	43

H_2S from crude oil. Whereas both Sulfavent 32 and 43 had satisfactory results after an hour. It seems that this method, where to store crude oil before loading, is appropriate. In the second method, which was developed by RIPI, those of scavengers that had rapid reaction kinetics (less than 15 min) will be successful in reduction or elimination of H_2S from crude oil.

3.2. Evaluation of Ionic Liquids

3.2.1 First method (Variable concentration)

The basis of this method, as was explained in the case of scavengers, was based on gradual addition of ionic liquids and measuring and following potential variations of crude oil. First, the amount of H_2S was measured in crude oil, then 20 ml of isopropyl alcohol and 30 ml of toluene was added to 50 g of crude oil that containing 100 ppm of H_2S. At the beginning, electrode potential was read, then certain amount of ionic liquid (approximately 10 µl) was added to crude oil in the same time intervals and potential variations was recorded. Fig. 4 shows the potential variations versus time for three ionic liquids. Also, in this method, the required volume

of ionic liquid to minimize concentration to less than 15 ppm of H_2S was determined.   When the electrode potential shifted to less than -800 mV, H_2S concentration was less than 15 ppm. As can be seen in this chart, the ILs have been able to reduce H_2S concentration to less than 1 ppm, in a short time (less than 30 minutes). Also, the mole ratio of [IL]/ [H_2S] was 2.3, 1.3, and 2.5 for [HMIM][BF_4], [EMIM][NTf_2], and [BMIM][$MeSO_4$] respectively that these were equal to 75 µl, 48 µl and 76 µl of ionic liquids. These values were negligible in comparison to commercial scavengers. Also among the three ionic liquids, [EMIM] [NTf_2] had a higher efficiency in H_2S removal from crude oil. Since [EMIM] [NTf_2] is lipophilic and its viscosity is closer to crude oil's viscosity, it can be better H_2S scavenger, moreover the consumed volume of IL_2 is less than the others.

3.2.2. Second method (Constant concentration)

In this method, the H_2S concentration was measured in 15 g of crude oil, then specific dosage or concentration of ionic liquid was added to the crude oil. In fact, according to the dynamic
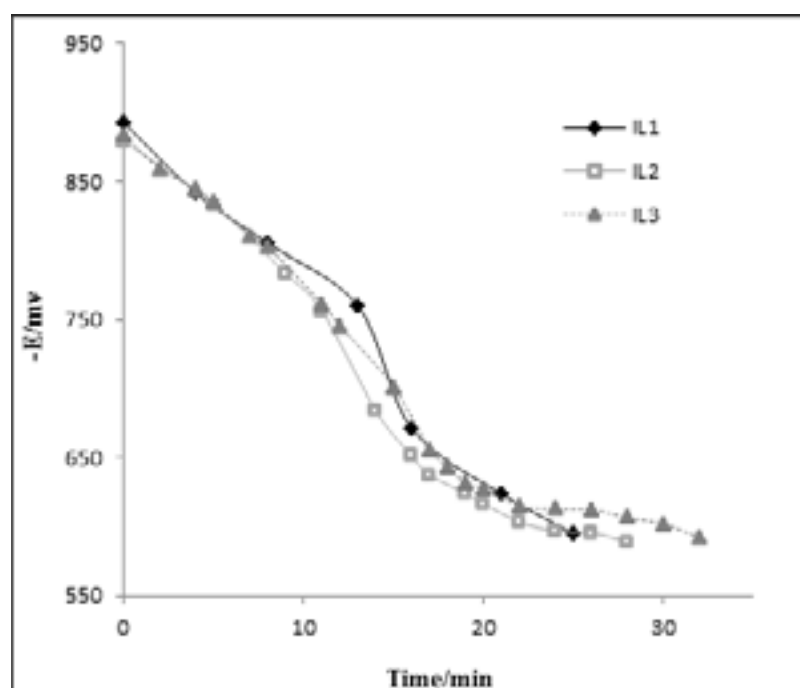

Fig. 4. The electrode response versus time during the gradual addition of the ionic liquid in crude oil.

method results and operating condition in crude oil terminals, the required time, temperature and dosage of ILs, were determined for H_2S removal. Finally, after considering the conditions in crude oil terminals (crude oil temperature, scavenger dosage and duration the crude oil passes through pipeline) and according to dynamic method results, it can be concluded that the required amount of ILs to remove H_2S should be selected from 1 to 3 [IL]/[H_2S] mole ratio, the reaction time from 25 min to 35 min and the temperature from 20° C to 50° C, should be selected. After identifying these factors design of experiment was performed for each IL, using Design Expert software.

3.2.3. Design of experiment
As mentioned, the effective parameters or factors on H_2S concentration was detected by using dynamic method. Then design of experiment was performed using Expert design software that

contained 20 runs or tests for each IL and various conditions such as dosage, temperature and reaction time, was applied separately for each run. The results are given in Table. 5. As can be seen in this table, first the concentration of H_2S was 100 ppm and after applying various conditions, such as dosage, time and temperature, H_2S concentration was reduced even less than 1 ppm. Columns 5 to 8 were normalized, because in some cases, H_2S concentration was more than 100 ppm, therefore all results were normalized to 100 ppm. It is obvious that if IL dosage, time and temperature was grater, H_2S concentration was lower.
Runs 4 and 14 for IL2 and crude oil sample without using ionic liquids are briefly reviewed in Table 6. H_2S concentration at the beginning was 113.27 ppm that was normalized to 100 ppm after 35 min stirring at 30 °C. The electrode potential shifted to -675 mV indicated that H_2S concentration was reached to less than 1 ppm. Also after run 14, H_2S

**Table 5.** Design of experiment for three ionic liquids

Run Order	Temp/ °C	Time /min	Dose [IL]/[H_2S]	ppm H_2S before treatment	ppm H_2S IL1	ppm H_2S IL2	ppm H_2S IL3
1	35	30	2	100	21.3	27.3	14.82
2	20	25	1	100	78.5	32.5	62.95
3	35	30	2	100	17.2	22.46	19.63
4	50	35	1	100	<1.0	<1	<1
5	20	35	3	100	<1.0	9.3	17.51
6	50	25	3	100	<1.0	4.02	<1
7	35	30	2	100	19.0	20.79	19.85
8	35	30	4	100	<1.0	7.3	3.1
9	35	30	0.4	100	38.5	48.9	27.46
10	11	30	2	100	32.3	41.83	26.27
11	35	30	2	100	18.4	18.55	19.04
12	60	30	2	100	<1.0	3.93	<1
13	35	22	2	100	21.4	30.47	35.79
14	35	38	2	100	<1.0	8.2	4.34
15	35	30	2	100	20.7	21.41	17.69
16	35	30	2	100	19.2	19.10	15.60
17	20	35	1	100	6.1	11.1	38.25
18	50	35	3	100	<1.0	<1	<1
19	50	25	1	100	8.4	11.3	<1
20	20	25	3	100	23.3	14.32	24.55

Table 5. Continue of Design of experiment for three ionic liquids.

	weight	Volume consumption of AgNO3	Initial potential (mV)	H$_2$S (ppm)	Condition		
					Time (min)	Temperature (°C)	Dose [IL]/[H$_2$S]
Crude oil	10.2	7.2	-1100	113.3	-	-	-
IL2 (Run 4)	15.0	-	-670	<1.0	35	50	1
IL2 (Run 5)	15.0	-	-575	<1.0	35	20	3
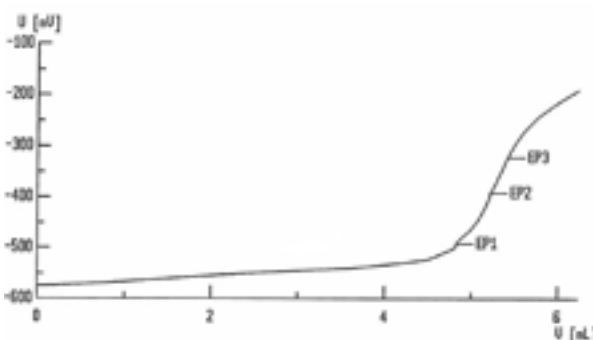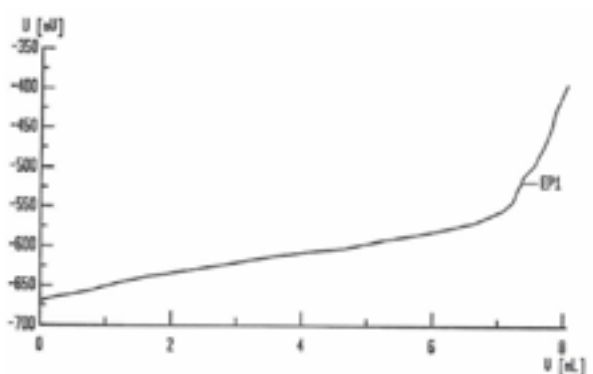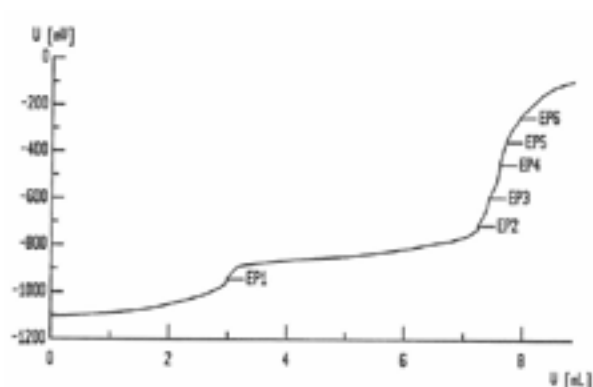
EP1	············	-926.9 mV	············	3.3854 mL
EP2	············	-850.7 mV	············	3.8148 mL
EP3	············	-735.7 mV	············	7.4372 mL
EP4	············	-585.0 mV	············	7.9573 mL
EP5	············	-461.4 mV	············	8.0852 mL
EP6	············	-378.5 mV	············	8.1808 mL
EP7	············	-279.3 mV	············	8.5390 mL
EP8	············	-184.0 mV	············	8.6572 mL
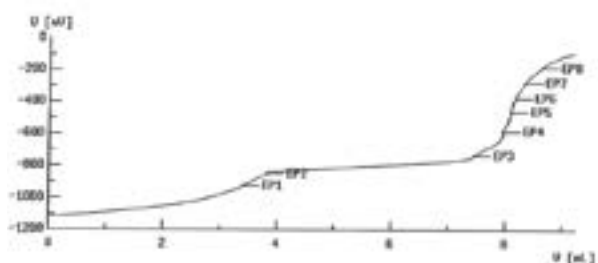
Fig. 6(a). The electrode potential versus volume of silver nitrate for H$_2$S measurement in crude oil that contains IL2.
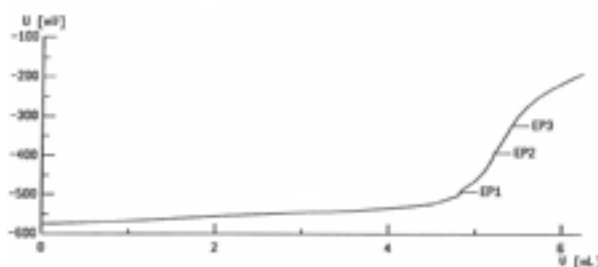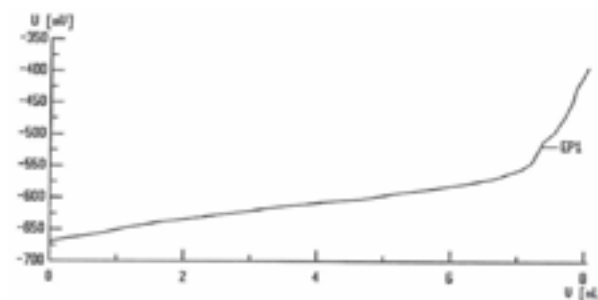
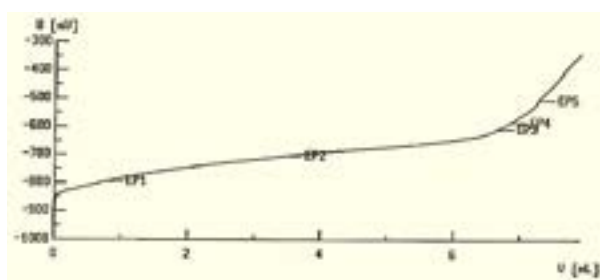|				
EP1	············	-518.4 mV	············	7.3420 mL

Fig. 6(b). The electrode potential versus volume of silver nitrate for H$_2$S measurement in crude oil that contains IL2

Fig. 5. The electrode potential versus volume of silver nitrate for H$_2$S measurement in crude oil.

concentration was decreased from 113.27 ppm to less than 1 ppm. The potentiometric curves for crude oil, runs 4 and 14 are presented respectively in figure 5.

The first chart showed H_2S concentration before addition of ionic liquids and the second one showed H_2S concentration after addition of ionic liquids in a special time and temperature. The electrode potential versus volume of silver nitrate was shown in Fig.5 and H_2S concentration can be calculated before and after of ILs addition, according to the following formula.

H_2S concentration before Run 4 and Run 14 for [EMIM][NTf$_2$] was 116.66 ppm as shown in figure 6a and 6b. H_2S concentration was diminished to less than 10 ppm after the Runs 4 and 14. figure 7 and 8 showed the electrode potential versus volume consumption of silver nitrate for runs 4 and 14 respectively. The EP3 (third equivalent point) for run 4 and EP1 for run 14 showed the required volume consumption of silver nitrate that neutralized H_2S amounts in crude oil.

Because the electrode potential was started with -675 mV, as a result H_2S concentrations is less than 1 ppm.

We found that all three parameters had significant effect in H_2S removal by obtained results of this software. Here a few charts are examined briefly in figure 8.

Fig. 7. The electrode potential versus volume of silver nitrate for H_2S measurement in crude oil that contains IL2.
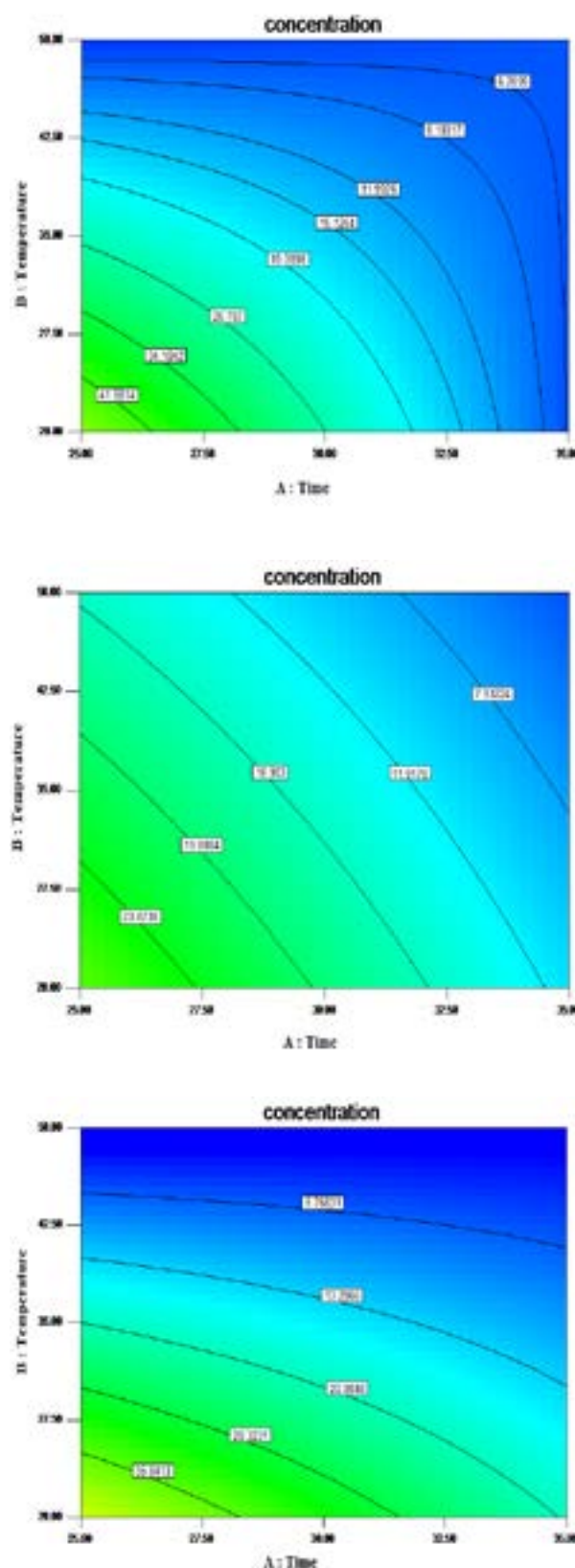

Fig. 8. Curves of temperature versus time at constant dosage.

These figures showed that at constant dosage, if temperature and time were grater, H_2S concentration was less. Also [EMIM][NTf$_2$] had better efficiency than the other ILs in H_2S removal, because it reduced H_2S concentration to less than 15 ppm in a short time.
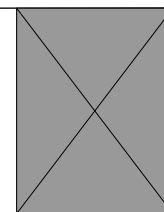
4. Conclusions

The results showed that all three ionic liquids were chosen correctly, because all of them are suitable for H_2S removal from crude oil. The investigation of chemical and physical properties of ionic liquids that all results were presented in our previous work, were indicated that some properties such as high thermal stability, pH, solubility, and wide electrochemical windows, defined them as a suitable scavenger to H_2S removal. Using ionic liquids in the limited situation, and at low concentrations of H_2S, is effective for crude oil sweetening. In comparison between commercial scavengers and ionic liquids and according to the obtained results from dynamic method and design of experiments, it is found by us that ILs is more effective than commercial scavengers because the volume consumption of ILs is less than the scavengers. Also, ILs could reduce H_2S concentration to less than 1 ppm. In design of experiments, three parameters (dosage, time and temperature) were investigated which all of them are effective in H_2S removal, and time is the most effective parameter. In addition, the results of dynamic method and design of experiment show that [EMIM][NTf$_2$] has better performance; in addition, the lower dosage of it has been spent.

5. References

[1] H. Sakhaeinia, V. Taghikhani, A. H. Jalili, A. Mehdizadeh, A. A. Safekordi, Solubility of H_2S in 1-(2-hydroxyethyl)-3-methylimidazolium ionic liquids with different anions, Fluid Phase Equilibria, 298 (2010) 303–309.

[2] R.C. Sahu, R. Patel, B.C. Ray, Removal of hydrogen sulfide using red mud at ambient conditions, Fuel Pro. Tech., 92 (2011) 1587–1592.

[3] N.N. Nassar, M.M. Husein, P. Pereira-Almao, Ultradispersed particles in heavy oil: part II, sorption of H_2S (g), Fuel Pro. Tech. 91 (2010) 169–174.

[4] N. Haimour, R. El-Bishtawi, A. Ali-Wahbi, Equilibrium adsorption of hydrogen sulfide onto CuO and ZnO, Desalination, 181 (2005) 145-152.

[5] T.H. Ko, H. Chu, H.P. Lin, C.Y. Peng, Red soil as a regenerable sorbent for high temperature removal of hydrogen sulfide from coal gas, J. Hazard. Mater., B136 (2006) 776–783.

[6] J.B. Chung, J.S. Chung, Desulfurization of H_2S using cobalt-containing sorbents at low temperatures, Chem. Eng. Sci., 60 (2005) 1515–1523.

[7] A.H. Jalili, A. Mehdizadeh, M. Shokouhi, A. N. Ahmadi, M. Hosseini-Jenab, F. Fateminassab, Solubility and diffusion of CO_2 and H_2S in the ionic liquid 1-ethyl-3-methylimidazolium ethyl sulfate, J. Chem. Thermodyn., 42 (2010) 1298–1303.

[8] Y. Duan, Y. Xiang, D. Xia, Removal of hydrogen sulfide from light oil with solid base, Fuel Pro. Technol., 86 (2004) 237–244.

[9] M.A. Sayyadnejad, H.R. Ghaffarian, M. Saeidi, Removal of hydrogen sulfide by zinc oxide nanoparticles in drilling fluid, Int. J. Environ. Sci. Tech., 5 (2008) 565-569.

[10] M.B. Shiflett, A. Yokozeki, Separation of CO_2 and H2S using room temperature ionic liquid [bmim][PF6], Fluid Phase Equilibria, 294 (2010) 105–113.

[11] W. Quan, X. Wang, C. Song, Selective removal of H_2S from biogas using solid amine-based "molecular basket" sorbent, Energy Fuels, 31 (2017) 9517–9528.

[12] R. T. Driessen, M. J. Bos, D. W. F. Brilman, A multistage fluidized bed for the deep removal of sour gases: proof of concept and tray efficiencies, Ind. Eng. Chem. Res., 57(2018) 3866–3875.

13] J. Li, Z. Dai, M. Usman, Z. Qi, L. Deng. CO_2/H_2 separation by amino-acid ionic liquids with polyethylene glycol as co-solvent. Int. J. Greenhouse Gas Control, 45(2016) 207–215.

[14] A.S. Rewar, S.V. Shaligram, U.K. Kharul, Polybenzimidazole based polymeric ionic liquids possessing partial ionic character: effects of anion exchange on their gas permeation properties, J. Membrane Sci., 497 (2016) 282-288.

[15] M.d. Sakinul Islam, K. N. Dhanavath, N. Kao, P. K. Bhattacharjee, B. Si-Ali, R.Yusoff, Carbon dioxide induced degradation of diethanolamine during absorption and desorption processes, Chinese J. Chem. Eng., 26 (2018) 293–302.

[16] S. Yar-Khan, M. Yusuf, A. Malani, Selection of amine in natural gas sweetening process for acid gases removal: A review of recent studies, petrol. petrochem. Eng. J., 1 (2017)1-7.

[17] F. L. Bernard, F. Dalla Vecchia, M. F. Rojas, R. Ligabue, M. O. Vieira, E. M. Costa, Vitaly V. Chaban, S. Einloft, Anticorrosion Protection by Amine–Ionic Liquid Mixtures: Experiments and Simulations, J. Chem. Eng. Data, 61 (2016) 1803–1810.

[18] H. Lü, C. Deng, W. Ren, X. Yang, Oxidative desulfurization of model diesel using $[(C_4H_9)_4N]_6Mo_7O_{24}$ as a catalyst in ionic liquids, Fuel Process. Technol., 119 (2014) 87–91.

[19] Y. Nie, C.X. Li, H. Meng, Z.H. Wang, N,N-dialkylimidazolium dialkylphosphate ionic liquids: their extractive performance for thiophene series compounds from fuel oils versus the length of alkyl group, Fuel Process. Technol., 89 (2008) 978–983.

[20] A.A. Miran Beigi, M. Abdouss, M. Yousefi, S.M. Pourmortazavi, A.Vahid, Investigation on physical and electrochemical properties of three imidazolium based ionic liquids (1-hexyl-3-methylimidazolium tetrafluoroborate, 1-ethyl-3-methylimidazolium bis(trifluoromethylsulfonyl) imide and 1-butyl-3-methylimidazolium methylsulfate), J. Mol. Liq., 177 (2013) 361–368.

[21] L. Wang, Y. Xu, Z. Li, Y. Wei, J. Wei, CO_2/CH_4 and H_2S/CO_2 selectivity by ionic liquids in natural gas sweetening, Energy Fuels, 32 (2018) 10−23.

[22] F. Billeci, F. D. Anna, H. Q. Nimal Gunaratne, N. V. Plechkova, K. R. Seddon, Ionic liquid gels: materials for sweetening of fuels, Green Chem., 20 (2018) 4260-4276.

[23] Y. Zhao, H. Gao, X. Zhang, Y. Huang, D. Bao, S. Zhang, Hydrogen Sulfide Solubility in Ionic Liquids (ILs): An Extensive Database and a new ELM model mainly established by imidazolium-based ILs, J. Chem. Eng., 61 (2016) 3970-3978.

[24] J.X. Zhou, J.B. Mao, S.G. Zhang, Calculations of the interaction between thiophene and ionic liquids, Fuel Process. Technol., 89 (2008) 1456–1460

[25] Cecilia Devi Wilfred, Chong Fai Kiat, Zakaria Man, M. Azmi Bustam, M. Ibrahim M. Mutalibb, Chan Zhe Phak, Extraction of dibenzothiophene from dodecane using ionic liquids, Fuel Process. Technol., 93 (2012) 85–89

[[27] W. Zhu, W. Huang, H. Li, M. Zhang, W. Jiang, G. Chen, C. Han, Polyoxometalate-based ionic liquids as catalysts for deep desulfurization of fuels, Fuel Process. Technol., 92 (2011) 1842–1848.

[28] D. Zhao, Y. Wang, E. Duan, J. Zhang, Oxidation desulfurization of fuel using pyridinium-based ionic liquids as phase-transfer catalysts, Fuel Process. Technol., 91 (2010) 1803–1806

[29] H. Shirkhanloo, Sara Davari Ahranjani, A lead analysis based on amine functionalized bimodal mesoporoussilica nanoparticles in human biological samples by ultrasoundassisted-ionic liquid trap-micro solid phase extraction, J. Pharm. Biomed. Anal., 157 (2018) 1–9

[30] A. Faghihi-Zarandi, H. Shirkhanloo, C. Jamshidzadeh, A new method for removal of hazardous toluene vapor from air based on ionic liquid-phase adsorbent, Int. J. Environ. Sci. Tech., Accepted: 16 August 2018, Doi.org/10.1007/s13762-018-1975-5.

[31] H. Sid Kalal, A.A. Miran Beigi, M. Farazmand, Sh.A. Tash, Determination of trace elemental sulfur and hydrogen sulfide in petroleum and its distillates by preliminary extraction with voltammetric detection, Analyst, 125 (2000) 903-908.

Research Article, Issue 1
Analytical Methods in Environmental Chemistry Journal
Journal home page: www.amecj.com/ir

AMECJ

The Investigation of precision of analytical methods for determination of salt content in Iranian crude oils

Ali Asghar Pasban[a*] **and Behrouz Nonahal**[a]

[a] *Research Institute of Petroleum Industry, Tehran, Iran*

A B S T R A C T
In crude oil analysis, the determination of salt content is one of the most important parameters especially for refining and exporting industries. In this study, extraction followed by volumetric titration and electrometric procedure are performed for determining salt content for several Iranian crude oils. Also, the effects of disturbing agents such as increasing associated water for determining salt in crude oil were investigated for both methods. The results show when water content in crude oil is less than 0.05 weight percent, both methods are equally accurate for determining salt content, but when there is an increase in associated water content in crude oil, the electrometric method followed by volumetric titration method shows more accurate results in comparison with the extraction procedure.

1. Introduction

Existing salt content in crude oils can lead to serious problems during petroleum production, refining process, transportation, and also some related chemical and petroleum engineering processes. [1]. Sodium, magnesium, and calcium chlorides are almost always present in crude oils. Moreover, calcium cement and calcium carbonate should also be mentioned. The amount of mineral salts in crude oil depends on the formation pattern of crude oil and can reach up to 200000 ppm [2-3]. In addition,

the pollution of the crude oil transportation route may also be somewhat effective. The presence of salts in crude oil in addition to corrosion causes the following problems.
During the production of crude oil, due to the minor evaporation of the associated water happens in the effect of pressure drop between the bottom and the top of the well, causing the chloride to settle sodium is at the entrance to the well wall and the diameter of the well decreases.
To cater for such issues, fresh water well is injected to the well. In refineries, the existence of salt along with other factors such as wax and asphaltene causes the formation of deposits inside the exchanger tubes.

Consequently, the formation of deposits inside the exchanger tubes reduces the heat transfer; moreover, the formation of deposits (or sedimentation) in furnace tubes will produce coke [4].

Also, the presence of water and salt in some crudes and heavy crudes will cause an increase in the acidity number. In order to control and reduce the effect of water and salt on the acidity number, water washing process (dehydration) is employed prior to the desalter unit [5-7].

In order to control the corrosion caused by salt, its content should be less than 4 ppm or 2 pounds in 1000 bpd of the crude oil [8]. In crude oil sales contracts, salt content is one of the important parameters whose permissible amount is mentioned in the contract, and the seller is obliged to control it when producing and exporting. Therefore, in the laboratory of exporting terminals, the salt content is determined, and if it exceeds the permissible limit, the cargo will not be shipped to the oil tanker. Also, if the buyer finds a discrepancy in the amount of salt received, inform the seller should be informed. Moreover, if the buyer's claim is confirmed, the seller will be obligated to pay compensation on the basis of the contract. It should be noted that a salt content increase in crude oil exports could be detrimental to the reputation of the exporting company in the oil market.

With reference to the above, standard salt content determination during production, transportation, storage, and exportation to a petroleum company are important. Crude oil producing company has to control this parameter in equipped laboratories. Oil companies can monitor the amount of salt along with other key parameters such as API grade, water and sediment, hydrogen sulfide, and sulfur on a daily basis [10-11]. In addition to controlling the quality of production of its subsidiaries, they can well defend the interests of participating in necessary situations and avoid unnecessary losses as much as possible. The National Iranian Oil Company (NIOC) has also created a hardware infrastructure and the necessary software in this field, and its experts try to carry out the necessary research and update the present standards. They use the best internationally accepted methods to control the quality of crude oil exports. For the time being, many of the production areas and exporting terminals use extraction and volumetric titration methods. Also, recently, it was stipulated or stated that volumetric titration method should be gradually replaced by the electrometric method.

The purpose of this research is to study the current methods of salt determination in petroleum laboratories and investigate comparative advantages and disadvantages of each method in conjunction with the project performed on "Salt content determination of Iran's crude oils at the Research Institute of Petroleum Industry in 2018".

2. Experimental Procedure
2.1. Material and Methods
In the laboratory investigation, crude oils with different characteristics for salt determination were selected to obtain a better comparison of the performance of standard methods at different conditions.

For this purpose, 6 samples of crude oils produced by National Iranian South Oil Company (NISOC) were selected. NISOC is regarded as one of the largest crude oil producers in the world and produces 85 percent of crude oil in Iran. The specifications of selected crudes are shown in Table 1.

In this study, for measurement of API grade of crude oils, a SVM equipment (model 2000) manufactured by Austrian company (Anton Paar) has been used to determine dynamic density and viscosity of the crude oils [12]. Also, for water and sediment tests, Hermle centrifuge (model ZK510) equipment manufactured by German company (Carlowitz) has been used along with ASTM D95 method [13].

For the determination of water content in crude oil, Carl Fisher (805 model titrando) test procedure has been adopted with the aid of ASTM D4377 [14]. For this purpose, a titration apparatus manufactured by Metrohm has been used. This apparatus uses a dual combination of platinum electrode to measure the amount of water in crude oil. The asphaltene is determined in weight percent using normal heptane and APD-500A automatic machinery manufactured by a Japanese Company called Cosmo which works

based on the ASTM D6560 which is equivalent to the standard IP 143 [15].

Also, a titration apparatus manufactured by Metrohm (805 Titrando model) is used to determine the estimate the effect of salt on the acidity number of the selected crudes. Moreover, the titration apparatus manufactured by Metrohm is equipped with a combination of a silver glass electrode and silver chloride (Ag/AgCl) as reference electrode surrounded by the same electrode [16].

The acidity number is the amount of consumed hydroxides for neutralization of one gram of sample mgKOH/gram oil. The results obtained in this study showed that the crude oils used in this study had low acidity numbers and did not cause much disorder in the performance of desalting units [17].

2.2. Salt content determination by standard method IP 77

In this method, salt content in the crude oil is separated by a glass system manufactured by Petrotest which is designed based on the standard IP 77 [14]. In this extraction method, the sample is heated by an electric heater in a glass flask with the volume of 55 cm^3. About 155 ml of crude oil with 155 ml of distilled water are poured inside the flask. After mixing, 100 milligrams of toluene and then 20 ml of acetone were added to the mixture. The flask is heated by the electric heater to the boiling point of the mixture, and the resulting vapors are cooled and returned to the flask by a vertical condenser mounted on top of the flask. This operation lasts for at least 45 minutes. To make sure that full salt extraction can be performed at a greater time. After completion of the extraction stage, the contents of the cooled water phases and organics are separated

and discharged through the valve embedded under the flask, and then the water phase is separated, and chlorine ion content in the water phase is neutralized by a mohair volumetric titration method. In this way, by using normal 0.01 silver nitrate, chloride ions are titrated in the presence of a few drops of potassium dichromate solution with a concentration of 50 gram. At the end of the neutralization of chlorine ions, the ambient color changes from yellow to light red. In this way, the concentration of chlorine ion is obtained in milligrams per cubic meter from Equation 1.

$$X = [VA/(V1-VB/V2)].N.58500.VE/VS \qquad (1)$$

where, VA is the volume of silver nitrate solution used for the titration extraction in ml, VB is the volume of silver nitrate used as the titration witness, V1 is the volume of consumed extraction used in titration, V2 is the volume used as witness in the titration process, VE is the total volume of the extract, VS is the sample volume of crude oil used, and N is the normality of the silver nitrate solution.

2.3. Salt content determination by ASTM method D3230

To determine salt content by the above method, a digital analyzer (694-SICT Model) is used which is manufactured by Kohler Corporation. This apparatus measures the electrical current passing through the crude oil solved in a beaker of solution mixture of alcohols with the aid of an electrode based on the electrometric measurement method [17]. With respect to standard calibration curve of the apparatus, the passing flow is reported in terms of Micro Siemens to milligrams which is directly converted to cubic meter and displayed on the monitor. The electrode used consists of two platinum

Table 1. The specification of crude oils.

Crude oil No.	API	Water Vol.%	Water and Sediments Vol.%	Acidity No. mgKOH/gr	Asphaltene wt.%
1	33.3	0.025	0.05	0.05	1.0
2	33.2	0.025	0.10	0.08	1.1
3	30.4	0.20	0.30	0.15	1.9
4	31.3	0.75	1.0	0.17	2.0
5	24.3	1.0	1.0	0.31	4.7
6	18.5	2.0	2.0	0.40	8.4

plates with the dimensions of 25 mm × 50 mm which are placed in parallel facing each other.

The spacing between the plates is 2 mm, and the maintaining material which holds the plates next to each other is insulated. For calibration of the system, according to ASTM D3230, standardization of apparatus solution has been carried out through a mixture of alcohols that were diluted in a mixture of sodium, magnesium, and calcium solution chlorides of 70%, 20% and 10% respectively. The purpose of dilution is to prepare salts mixtures with a concentration of 0.1 g/m³. The mixture of alcohols contains 37 % vol. of pure ethanol in isobutanol, for any liter of which, 3ml of distilled water is added. At this stage, a quantity of about 10 ml of an oil cut like paraffin was thoroughly dissolved in 40 ml of an organic solvent such as Xylene. Then 50 ml of alcohol mixture was added to this mixture and severely stirred. Then the final solution was poured inside a clean beaker and its conductivity was measured. This result is in fact, the amount of conductivity of the control solution. Then to completely cover measuring range of the apparatus (0-430 mg/cm³), standard solutions were used to match the table presented in ASTM standard D-3230 containing 50 ml of solution of mixture of alcohols with a suitable amount of salt mixtures. During each step, the conductivity was recorded on the apparatus. In this way, there are about 10 points to plot the calibration curve.

After calibration of the apparatus, salt content of crude samples were determined. To do this, 10 ml of each crude oil sample was dissolved in an organic solution containing xylene and 50^cc of alcohol mixtures. At this stage, the mixture was stirred for 90 seconds by hand. Then the sample remains constant for 5 minutes. Finally, the content was poured in the special beaker, and the salt content was measured.

3. results and discussion

Salt content of samples of crude oils were measured using extraction and volumetric method (IP 77). In addition, the electrical conductivity measurement method (ASTM D3230) reported in Table 1.

The results of salt determinations are reported in Table 2. As it can be seen from Table 2, at low salt concentrations in crude oils, the values obtained are close to each other by both methods, but at higher concentrations, the measured values in the electrical conductivity method are very different from extraction method and in the case of crude oil, the difference is approximately 1.5 times more than the amount of extraction method due to the restriction in neutralizing process IP 77 method because in volumetric titration, the 0.01 solution of normal silver nitrate is used. Silver nitrate reacts only with the chlorine ions of the water-soluble salts derived from the extraction, and since the amount of silver nitrate which has been consumed is the calculation criteria for the determination of salt, the presence of the other forms of salts in the aqueous phase cannot be reported in this method.

As stated in this standard, only the amount of chloride ion should be reported in the final report. Therefore, it is suggested that in laboratories, which crude oil quality control is performed, should not report the final result as salt content when working with this standard. In this study, for further analysis of the reasons for the difference in the results, associated water of 6 samples of crude oils related to desalting units were analyzed for the above-mentioned methods. Table 3 shows the analysis of the results of 6 samples of associated water with crude oils. For determination of ions in water of crude oils, despite high chlorine ions, the other ions are not negligible. By increasing associated water, the error of measurement of ions using the conductivity method was increased (Table 3). In addition, this difference is shown in figure 1. As shown in this figure, the results of the salt obtained through the electrometric method are higher than the extraction and volumetric method, which indicates that this method is more precise. As shown in Table 3 with increasing associated water in crude oil, the amount of salt will also increase proportionally. On the other hand, as shown in Table 3, sulphate, and bicarbonate foundations can also be problematic for refineries, and therefore, the salt determination for crude oil

Table 2. The results of salt determination in crude oils.

Crude Sample No.	Chlorine Ion (mg dm^{-3}) IP 77	Salt (mg dm^{-3}) ASTM D3230
1	33±2	34±1
2	65±1	72±3
3	146±5	160±2
4	194±7	295±5
5	203±6	344±4
6	207±12	395±9

should be calculated and total salt amounts should be reported for desalting units, so, the technical section will be able to control the output salt content by optimizing of parameters in desalting unit.

4. Conclusions

In this study, the determination of salt content in crude oils was evaluated by two methods which was exported and transported to domestic Iranian refiners. This procedure, was carried out on six petroleum products, produced by NISOC (National Iranian Southern Oil Company) using extraction and volumetric methods by (IP 77) and ASTM method D 3230. The results show that the electrometric method has some advantages in comparison to the extraction method, outlined as follows:

a) With respect to the need for refiners the salt content of the crude oil as feed should be reduced to less than 3 ppm. For such scenarios, only the ASTM method D 3230 should be used because the lowest limit of measurement for the IP 77 method is about 20 ppm.

b) Due to the nature of the IP 77 method, only chlorine ions in crude oil can be measured and, in the case of presence of salts in the form of sulfates or bicarbonates in the crude oil, these compounds cannot be calculated. Therefore, the total salt content of crude oil cannot be determined by this method.

c) In the electrometric method, a smaller sample volume is needed compared to the time-consuming extraction method.

d) Repeatability and reproducibility of the results in the electrometric method are better than the extraction method and volumetric analysis.

e) It is recommended that the electrometric method for determining salt content be used when the amount of water in the crude oil is high. Therefore, in this method, the passing flow through the medium is used. Moreover, in this method, the concentration of total ions can be calculated, and thus a more accurate calculation of the inorganic salts can be achieved. This method also helps the utilization of optimized operation of existing oil installations against damages inflicted from corrosion and sediments.

5. Acknowledgments

6. Refrences

[1] A. Kamari, A.Bahadori, and A.H.Mohammadi, On the Determination of Crude Oils Salt Content: Application of Robust Modeling Approaches, J. Taiwan Institute Chem. Eng., 44(2015)27-35.

[2] A.A. Pasban, S. Sadeghpour, M. Masoumi, and A.A.Miran Beigi, Acidity removal of Iranian heavy crude oils by nanofluid demulsifier: An experimental investigation, NanoAnalysis, 04 (2017) 112-118.

[3] E. Elhaddad and M.E. Abdel-Raouf, New Model to Eliminate Salts from Sarir Crude Oil: a Case Study, Int. J. Eng. Res. Sci. Technol., 2 (2013)182-189.

Table 3. Ion compounds in water with crude oil number of chlorine ion.

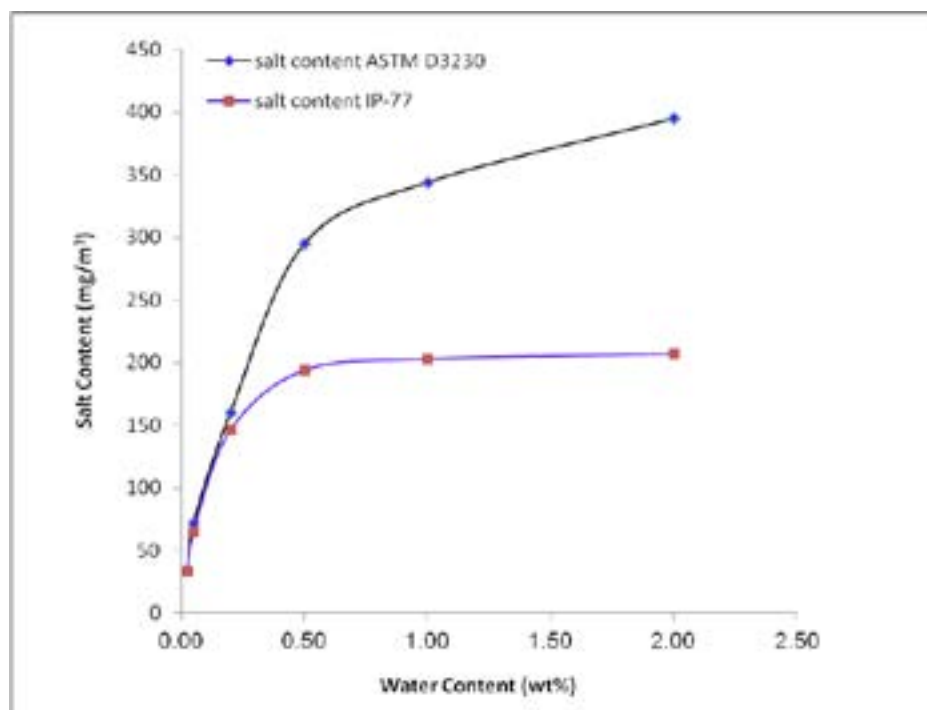| Sample No.	Chlorine Ion g L-1	Sulphate Ion g L-1	Bicarbonate Ion g L-1	Specific Gravity
1	81	0.41	0.27	0.9882
2	79	0.35	0.27	1.0006
3	85	0.34	0.27	1.0961
4	87	0.32	0.33	1.0983
5	91	0.47	0.28	1.1024
6	105	1.42	0.30	1.1196

Fig. 1. Effect of increasing associated water in salt content determination.

[4] U.B. Deshannavar, M.S,Rafeen, M.Ramasamy, and D,Subbarao, Crude oil Fouling:A Review, J. Appl. Sci., 10 (2010) 3167-3174.

[5] J.J. Sheng, Investigation of alkalineecrude oil reaction, Petroleum, 1 (2015) 31-39.

[6] C. Soltelo, A.Favela-Contreras,D. Sotelo,F. Beltran-Carajal, E.Cruz, Control Structure Design for Crude Oil Quality Improvement in a Dehydration and Desalting Process, Arab. J. Sci. Eng., 43 (2018) 6579-6594.

[7] H. Kiani, Study of a crude oil desalting plant of the national Iranian south oil company in Gachsaran by using artificial neural networks, Chem. Mol. Nucl. Mater. Metall. Eng., 7(12), (2013) 670–673.

[8] H.K Abdel-Aal., M.Aggour,M.A.Fahim,Petroleum and gas field processing, ASTM International, CRC Press, Florida, 2015.

[9] M.R Riazi-Aal., S.Eser, S.S. Agrawal, and J.L.Pena Diez, Petroleum refining and natural gas processing, 2nd ed., Taylor and francis, PA, USA, 2013.

[10] W. Y. Ayele, G. Juell-Skielse, A. Hjalmarsson, P. Johannesson, method for designing and refining digital Innovation contest measurement model, An Int. J. Inform. Technol., 11 (2018) 25-53.

[11] ASTM D4006, Standard test method for water content in crude oil by distillation, Annual Book of ASTM standards, 05.01, USA, 2017.

[12] ASTM D4007, Standard test method for water and sediment in crude oil by centrifuge method, Annual Book of ASTM standards, 05.01, USA, 2017.

[13] ASTM D4007, Standard test method for water content in crude oil by potentiometric Karl Fischer method, Annual Book of ASTM standards, 05.01, USA, 2017.

[14] IP 77, Determination of salt content- extraction and volumetric method, 2015.

[15] ASTM D3230, Standard test method for salts in crude oil (electrometric method) Annual Book of ASTM standards, USA, 05.01, 2017.

[16] ASTM D6560, Standard test method for determination of asphaltenes (heptanes insoluble) in crude petroleum and petroleum products, Annual Book of ASTM standards, USA, 05.02, 2017.

[17] ASTM D664, Standard test method for acid number of petroleum products by potentiometric titration, Annual Book of ASTM standards, USA, 05.01, 2017.
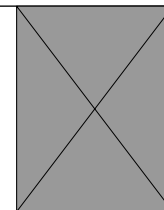
Investigation of Adsorption of Cobalt-phthalocyanine from Aqueous Waste Stream Using UVM-7/Ag

Amir Vahid[a]*, Majid Abdous[b], and Shahnaz Nayyeri[b]

[a] *Research institute of petroleum industry, Tehran, Iran.*
[b] *Faculty of chemistry, Amirkabir University of Technology, Tehran, Iran.*

A B S T R A C T

The effect adsorption of cobalt-phthalocyanine-3,4',4'',4'''-tetrasulfonicacid tetrasodium salt $[Co(tsPc)^{-4} \cdot 4Na^+]$ onto UVM-7/Ag mesoporous material was investigated. In addition, X-ray diffraction (XRD), scanning electron microscopy (SEM), and nitrogen adsorption-desorption measurement were used to examine the morphology and the microstructure of the obtained composite. Various parameters including solution adsorbent dosage, contact time, initial dye concentration and temperature were systematically studied. Equilibrium data fitted well the Langmuir models; moreover, the fitness suggests that the adsorption be monolayer and physical in nature. Kinetic studies showed that the adsorption process could be better described by the Lagergren pseudo-second-order models. Thermodynamic constant values ($\Delta G < 0$, $\Delta H < 0$ and $\Delta S < 0$) demonstrated that the adsorption reactions of $Co(tspc)^{-4}$ onto UVM-7/Ag were feasible, spontaneous, and exothermic under the examined conditions.

1. Introduction

Mercaptan and sulfur compounds present in the crude oil and petroleum cuts cause corrosion of pipes and different environmental pollutions[1]. There are various methods to remove mercaptan but the major one is the catalytic oxidation in the presence of caustic solution and air. phthalocyanine are effective catalysts for thiol and hydrosulfide oxidation by dioxygen[2-4]. Metal phthalocyanines (MPCS) are two dimensional (2D) organic macro cyclic molecular catalysts (MN4) with metal atoms at the center [5, 6].

One of the most important applications of MPCS has been in catalysis, including large-scale industrial processes. For instance, the Merox process, referred to as "sweetening" in the petroleum refining industry, involves catalytic oxidation of mercaptans in the presence of sulfonated cobalt phthalocyanines to remove a major part of sulfur from petrol [7]. The catalytic properties of MPCS depend on the metal and complex structure and can be tuned by appropriate structural modifications [8, 9]. This is the basis of the redox mechanism of catalytic oxidation of sulfur-containing compound.
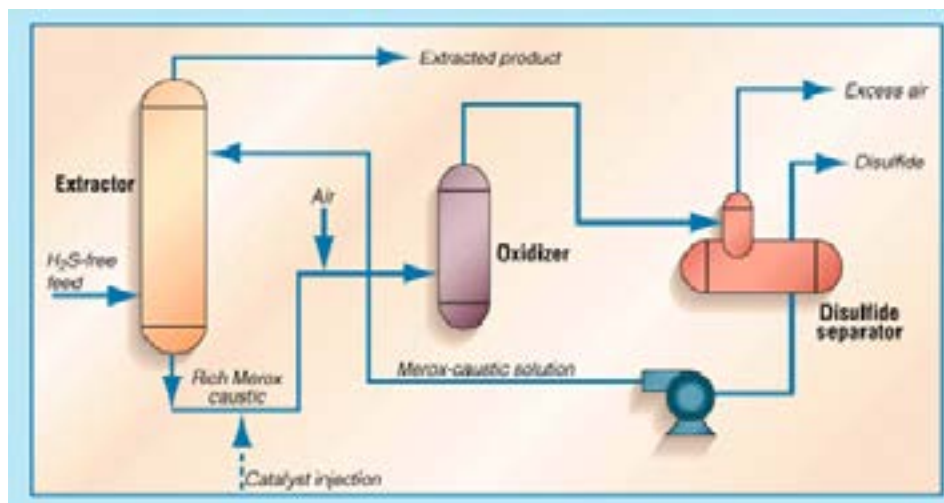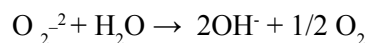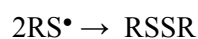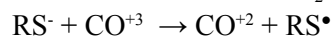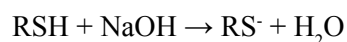
Fig. 1. Schematic representation of Merox unit.

These catalysts have found wide application in the catalytic oxidation of mercaptans in oil fraction as shown if Figure 1 [10].

In many systems using transition metal compounds as catalysts, the mechanism suggested by Wallace et al.[11] is:

$RSH + NaOH \rightarrow RS^- + H_2O$

$RS^- + CO^{+3} \rightarrow CO^{+2} + RS^\bullet$

$2RS^\bullet \rightarrow RSSR$

$O_2^{-2} + H_2O \rightarrow 2OH^- + 1/2\ O_2$

CoPC has a low solubility in water, the substitution of CoPc with hydrophilic sulfonic groups $[Co(tsPc)^{-4}]$
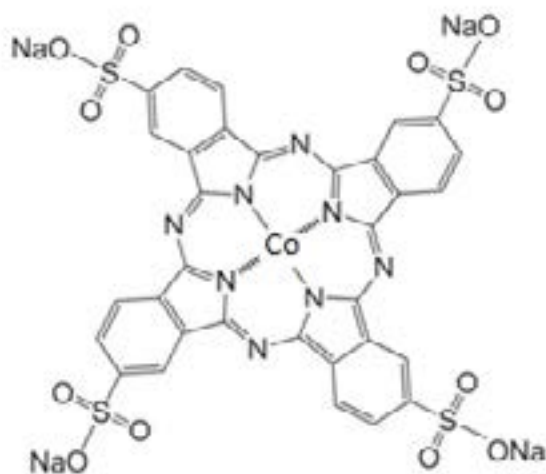
Fig. 2. Structure of the Co (II) tetra sulfophthalocyanine $[Co(tsPc)^{-4}.4Na^+]$ organometal.

as shown if Figure 2, makes this derivative easily soluble in aqueous solution. sulfonated metal phthalocyanine (MSPC) complexes, highly water-soluble molecule and very well recognized for its unique physicochemical properties and wide range of applications ranging from catalysis to sensing and photocatalysis .

The Merox catalyst is a heterogeneous blue powder dissolved in water.

Merox catalyst of caustic solution creates problems that in this work, co (II) tetra sulfophthalo cyanine $Co(TSPc)^{-4}$ catalyst removal from caustic solutions by using meso porous silica UVM-7 is studied. Functionalized with Ag and , γ-Alumina was prepared by sol-gel method and the synthesized nanoparticle was characterized by scanning electron microscopy (SEM) and X-ray diffraction (XRD).

Mesoporous materials can have large adsorption capacity, excellent selectivity and improved powder recoverability for removal of toxic compounds from aqueous solutions[12, 13]. The effects of adsorbent dosage, initial $Co(tspc)^{-4}$ concentration and contact time were studied. The adsorption was fit to different adsorption isotherms and also to kinetics of the adsorption was studied. Parameters affecting the removal of $Co(tspc)^{-4}$ from the aqueous solution was investigated and validated by

using three factorial Box– Behnken Design (BBD).

2. Experimental

2.1. Synthesis and characterization

The general procedure for the synthesis of UVM-7 is the atrane route, in which the presence of the polyalcohol is the key to balancing the hydrolysis and condensation reaction rates [18]. In a typical synthesis, TEOS was added to determined amounts of $TEAH_3$ (tri ethanolamine). The solution was heated up to 140ºC under vigorous stirring. After cooling down to 90ºC, CTAB (cetyl trimethylammonium bromide) was added to this solution. After that, water was added slowly to this solution under stirring until a white suspension resulted. This suspension was aged for 4 hours at room temperature. The solid was filtered, washed with sufficient amounts of water and acetone and dried in an oven at 80ºC overnight. Thermo calcination of the as synthesized UVM-7 was carried out under a flow of air up to 550ºC for 6 hours with a heating rate of 1 C/min to remove both the surfactant and $TEAH_3$ from the as-synthesized UVM-7. The final molar composition of the reactants was 1.0 TEOS : 3.5 $TEAH_3$: 0.25 CTAB: 90 H_2O.

2.2. Modification of UVM-7

For the modification of UVM-7 with Ag, 1 gram of calcined UVM-7 is mixed with 100 mL of distilled water contains 0.1 gram of $AgNO_3$ and stirred for 24 hours. The water was distilled using and automatic evaporator and calcined at 450 ºC for 5 hours.

3. Results and Discussion

3.1. Characterization UVM-7/Ag

TEM image of UVM-7/Ag is displayed in Figure 3. Mesochannels of the UVM-7 is obviously visible in this image. Furthermore, dark points in the image related to the higher contrast of heavy silver atoms with incident electron beam. BET surface area of the calcined UVM/7 was 838 m^2g^{-1}
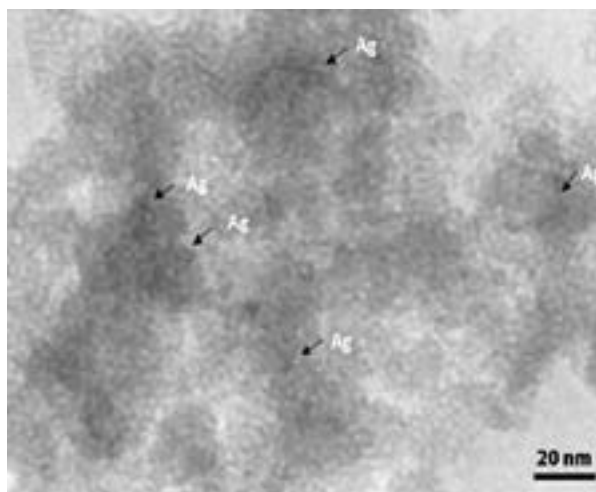

Fig. 3. TEM image of UVM-7/Ag.

which reached to 601 m^2g^{-1} after doping with silver. These are direct and indirect evidences of formation of ordered UVM-7 which contains silver nanoparticles.

XRD pattern of the as-synthesized and calcined UVM-7 are illustrated in Figure 4. As can be seen, a sharp peak at low angle about 1.5×2theta is characteristic of mesoporous materials. In case of calcined UVM-7 higher order diffraction, i.e. d_{110} and d_{200} are sign of better structural order which is usually seen in mesoporous materials after thermocalcination and condensation of silanol groups.

3.2. Adsorption studies

Adsorption behavior was studied by a batch method, which parameters that influence the adsorption process such as contact time, initial concentration, adsorbent dose, surfactant template, and reaction temperature was investigated. In addition, aqueous solutions of $Co(tsPc)^{-4}$ which its chemical structure is shown in Figure 1; moreover, with concentration ranging from 100 to 500 mg L^{1-}were prepared by dissolving $Co(tsPc)^{-4}$ in double distilled water. In each adsorption experiment, 10 mg adsorbent was added in 10 mL $Co(tsPc)^{-4}$ solutions. to study the effect of temperature the adsorption was carried out at four different temperatures (27, 35, 40 and 50 ⁰C) and for contact time studies the samples
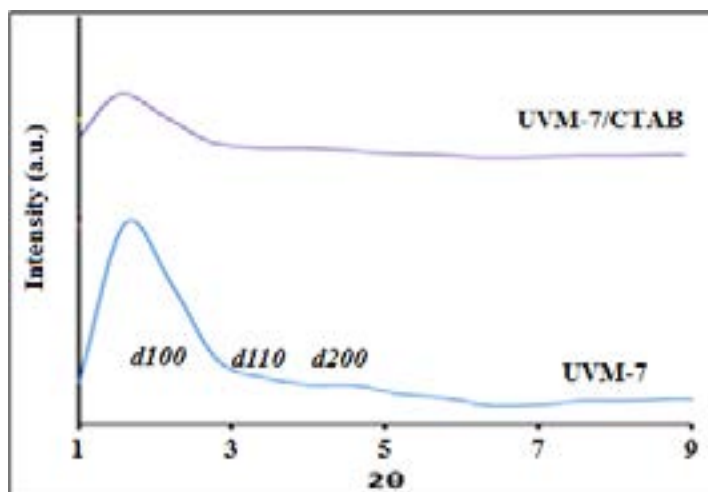
Fugire 4. XRD pattern of as-synthesized and calcined UVM-7.

were taken at predetermined time intervals (10, 20, 30, 40, 60, 80 and 100 min). After equilibrium, the concentration of the adsorbate in the residual solution was analyzed by a UV-spectrophotometer at λ max of 661 nm. The amount of $Co(tsPc)^{-4}$ adsorbed per unit mass of UVM-7/Ag the qe (mg g^{-1}) was calculated by the following equation:

$$q_e = \frac{(c_0 - c_t)V}{M}$$

where q_e is the adsorption capacity (mg g^{-1}) of the adsorbent at equilibrium; C_0 and C_e are the initial and equilibrium concentrations of solute (mg L^{-1}) respectively. Also, V is the volume of the aqueous solution (L). and W is the mass (g) of adsorbent used in the experiments.

The adsorptive removal efficiency (R) was determined according to the following equation:

$$R = \frac{(c_0 - c_t)}{c_o} \times 100$$

3.2.1. Effect of adsorbent dosage

The effect of adsorbent dosage (m) on the amount of $Co(tsPc)^{-4}$ adsorbed at equilibrium (qe, mg g^{-1}), was investigated by adding different weights of adsorbent UVM-7/Ag into 10 ml of solution 500 mg l^{-1} $Co(tsPc)^{-4}$ and shaking the mixture for 60 min at ambient temperature. It is evident from figure 5، qe increases by increasing m, can be attributed to the availability of greater surface area and more adsorption sites. that adsorption capacity of $Co(tspc)^{-4}$ increased when UVM-7/Ag dosage varied from 2 mg to 10 mg. However, the

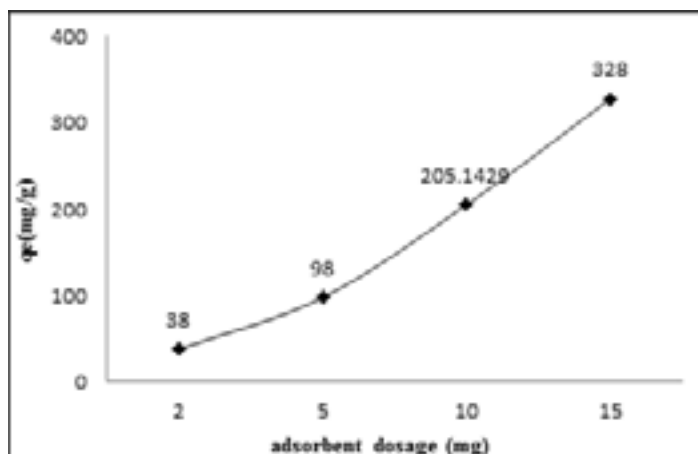**Figure 5.** .Effect of adsorbent dosage on the adsorption of $Co(tsPc)^{-4}$ by UVM-7/Ag.

adsorption capacity slowly as the adsorbent dosage increased from 10 mg to 15 mg. Thus 10 mg was chosen as the optimal UVM-7/Ag dosage in this study[14].

3.2.2. Effect of contact time

It is visible from Figure 6, that the amount of the adsorbed $Co(tsPc)^{-4}$ increases with time and then reaches a constant value. At this point, the amount of $Co(tsPc)^{-4}$ desorbing from the adsorbent is in a state of dynamic equilibrium with the amount of $Co(tsPc)^{-4}$ being adsorbed onto the mesoporous. The time required to attain this state of equilibrium is termed equilibrium time. estimate equilibration time for Calculation maximum adsorption Capacity and to know the kinetics of the adsorption It is seen that the rate of uptake is rapid.Required at the beginning, and time required for equilibrium

adsorption is 60 min. The adsorption rate was related to the content of the active adsorption sites on the matrix of the adsorbent[15].

3.2.3. Effect of temperature

The effect of temperature on the adsorption of $Co(tsPc)^{-4}$ onto UVM-7/Ag was investigated by adding 10 mg of the adsorbent into 10 mL of solution 500mg L^{-1} $Co(tsPc)^{-4}$ and shaking the mixture for 60 min at different temperatures of 27, 35, 40 and 50 °C in a water bath. The results indicated that the equilibrium adsorption amount (q_e) decreases with increasing temperature (Figure 7), indicating that the adsorption process is exothermic in nature[16]. In order to understand the effect of temperature on the adsorption process, thermodynamic parameters should be determined at various temperatures. For this reason, three basic thermodynamic parameters
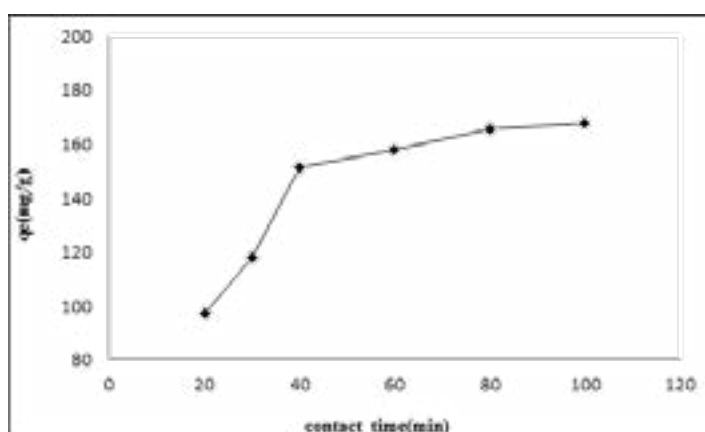

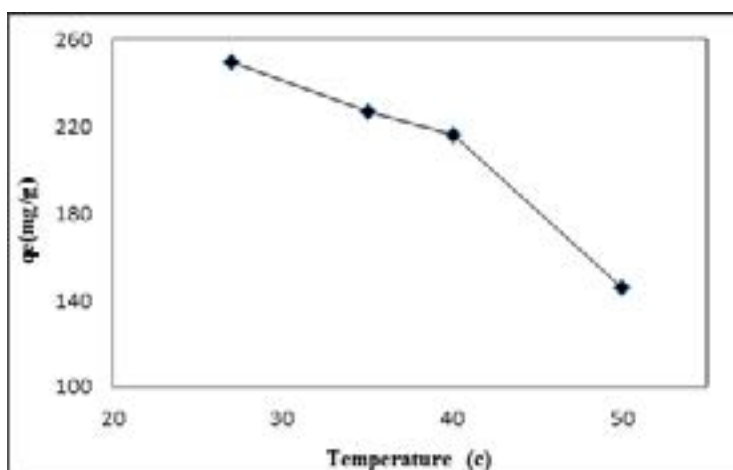**Fig. 6.** .Effect of contact time on the adsorption of $Co(tsPc)^{-4}$ by UVM-7/Ag

Fig. 7 .Effect temperature on the adsorption of $Co(tsPc)^{-4}$ by UVM-7/Ag

were studied: the Gibbs free energy of adsorption (ΔG), the enthalpy change (ΔH), and the entropy change (ΔS).The Gibbs free energy change of the adsorption process is related to the equilibrium constant (K_c). The thermodynamic parameters ΔG, ΔS and ΔH for this adsorption process were calculated from the following equations:

$$\Delta G = -RT \ln KC$$

where R is the gas constant (8.314 J mol^{-1} K^{-1}), T is the absolute temperature. K_c values were estimated as

$$Kc = Ca / Cb$$

where C_a is the equilibrium concentration of Co(tsPc)$^{-4}$ on adsorbent (mg L^{-1}), C_b is the equilibrium concentration of Co(tsPc)$^{-4}$ in the solution (mg L^{-1}). the ΔH and ΔS values were calculated from slope and intercept of the linear plot of lnK$_c$ versus 1/T[17, 18].

$$\ln Kc = \frac{-\Delta H}{RT} + \frac{\Delta S}{R}$$

The corresponding values of thermodynamic parameters are presented in Table 1. It shows that ΔH, ΔS and ΔG are negative for all experiments. The negative value of the standard enthalpy change for Co(tsPc)$^{-4}$ sorption indicates exothermic nature of adsorption[19] .The values of ΔG were calculated to be -6.3, -5.4, -4.4, -3.7 kJ mol^{-1} at the temperatures of 300, 308, 313 and 323 K, respectively. The negative ΔG indicates that the adsorption is a spontaneous process. The increase of ΔG values with rising temperature demonstrate a negative influence of temperature on the adsorption reaction. Moreover, negative ΔS values indicate a reduction of randomness at the solid–liquid interface during the adsorption process[20].

Therefore the optimal reaction temperature was 300 K.

3.2.4. Effect of initial dye concentration

The effect of initial Co(tsPc)$^{-4}$ concentration on adsorption behaviors was investigated in Figure 8. It can be seen that the majority of Co(tsPc)$^{-4}$ was removed by UVM-7/Ag in lower initial Co(tsPc)$^{-4}$ concentration, the Co(tsPc)$^{-4}$ removal efficiency decreased with increase initial Co(tsPc)$^{-4}$ concentration. also This effect can has been attributed to the ratio of surface active site to the total Co(tsPc)$^{-4}$ ions in the solution .while The result reveals that the amount of capacity adsorbed (qe) increases as the concentration increases. The initial concentration of Co(tsPc)$^{-4}$ can serve as an essential driving force for overcoming the mass transfer resistance of dye molecules between the aqueous solution and solid-phase adsorbent. As the initial concentrations of Co(tsPc)$^{-4}$ increased, the driving force became higher as well, which facilitated more dye molecules adsorbing onto the adsorbent, contributing to better adsorptive removal performance and higher adsorption capacity[21].

3.3. Effect of presence of surfactant template

When the surfactants in aqueous solution are beyond the critical micelle concentrations (CMC), micelles are formed and they act as templates for preparing UVM-7 materials. The existence of cationic template within the framework of UVM-7 materials causes the change in the surface chemistry and porosity of the sorbate, which in turn affects the sorption behavior of sorbate. CTAB/UVM-7 possesses high adsorption energy of

Table 1. Thermodynamics parameters for Co(tspc)$^{-4}$ adsorption onto UVM-7/Ag

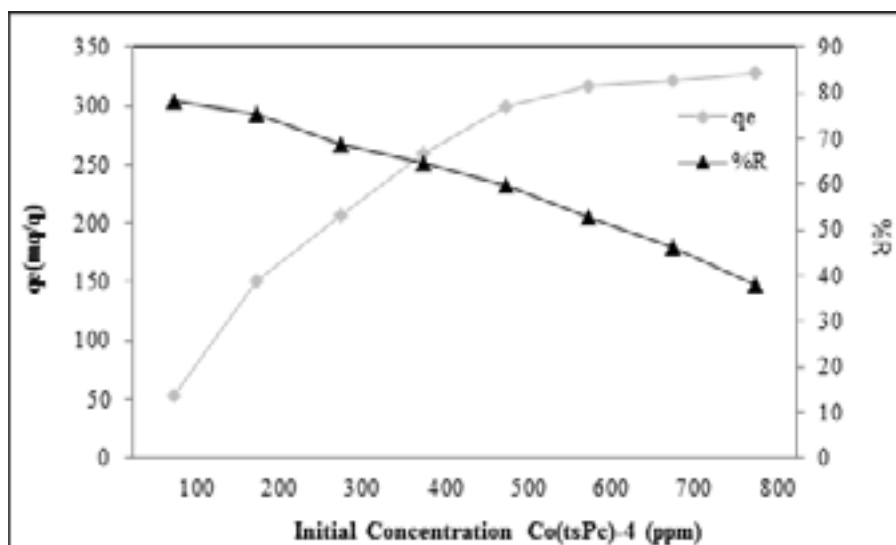| Temperature (k)	Thermodynamics quantities		
	ΔH(KJ mol^{-1})	ΔG(kj mol^{-1})	ΔS(kj mol^{-1}k^{-1})
300	-21.976	-6.3	-0.099
308	-21.976	-5.4	-0.099
313	-21.976	-4.4	-0.099
323	-21.976	-3.7	-0.099

Figure 8. Effect initial concentration on the adsorption of Co(tsPc)$^{-4}$ by UVM-7/Ag.

quaternary alkyl ammonium groups (Si–C–C–C–[N$^+$–(CH3)3]) contributed from cationic template. Apparently, the surfactant template can alter the surface chemistry and population of sorption sites of the materials. The cationic templates improve the sorption towards those species containing anionic groups. It is known that hydrophobicity, electrostatic interactions, p–p interactions, hydrogen bonding, dipole–dipole interactions, steric hindrance as well as a combination of them, are among the most important interactions which determine the retention behavior of substances in the absorbent. When the adsorbent is CTAB-containing mesoporous silica, the aromatic cycles could interact with the alkyl part of CTAB by hydrophobicity; the sulfonic acid groups interact with the positive polar heads of surfactants by electrostatic interactions. It is mentioned multiple interactions which give the surfactant-containing adsorbent excellent adsorption capability. As shown if Figure 9, The adsorption capacity of ''calcined'' adsorbent is weak and is generally due to the van der Waals interactions present between the molecules of dyes and adsorbent [22].

3.4. Adsorption isotherms

To optimize the design of an adsorption system for the adsorption of dyes, various isotherm equations like those of Freundlich, Langmuir and Temkin have been used to describe the equilibrium characteristics of the adsorption. For describing the relationship between the amount of adsorbate adsorbed on adsorbents at equilibrium (q_e) and the concentration cu(tspc)$^{-4}$ of the remaining in aqueous solution (c_e). The Langmuir relation assumes monolayer sorption on to the homogeneous surface with a specific number of equivalent sites. The Langmuir isotherm[23] is represented by the following linear equation:

$$\frac{c_e}{q_e} = \frac{1}{b\,q_m} + \frac{c_e}{q_m}$$

where C_e (mgL^{-1}) is the equilibrium concentration, qe (mgg^{-1}) the amount of adsorbate adsorbed per unit mass of adsorbent, qm (mg g^{-1}) is the Langmuir constant representing maximum monolayer capacity and b is the Langmuir constant related to the energy of adsorption. The Langmuir constants b and q_m were calculated from this isotherm and their values are listed in Table 2. The Freundlich isotherm is derived by assuming a heterogeneous surface with a non-uniform distribution of heat of adsorption over the surface. Finally, the Freundlich isotherm as follows:
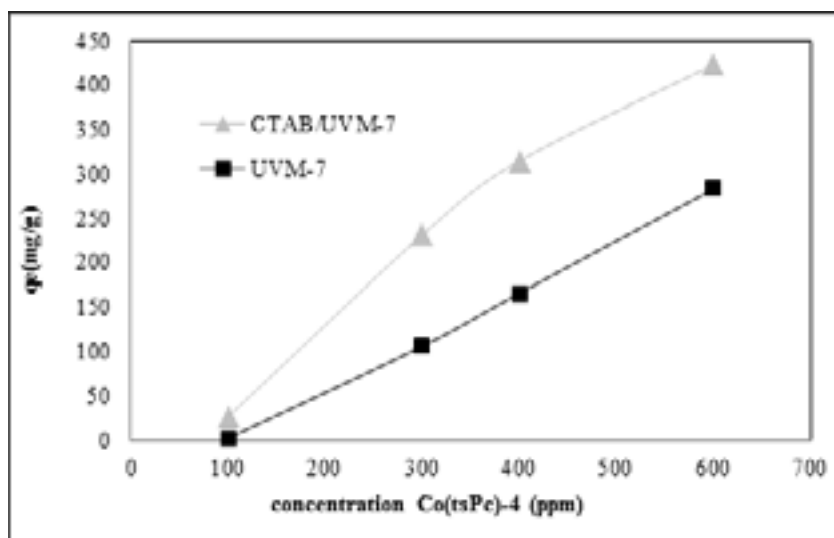
Fig. 9. Effect presence of surfactant template.

$$\log q_e = \log k_F + \frac{1}{n}\log c_e$$

where K_f is the Freundlich constant (mg g^{-1} (mg L^{-1})^n) and 1/n is the heterogeneity factor. The slope 1/n ranging between 0 and 1 is a measure of adsorption more intensity or surface heterogeneity, becoming heterogeneous as its value gets closer to zero. The plot of log qe versus log Ce, gives straight lines with slope 1/n [24].

The Temkin isotherm equation assumes that the heat of adsorption of all the molecules in the layer decreases linearly with coverage due to adsorbent–adsorbate interactions, and that the adsorption is characterized by a uniform distribution of the binding energies, up to some maximum binding energy [25, 26]. Temkin isotherm is given as:

$q_e = B \ln K_t + B \ln C_e$

K_t is the equilibrium binding constant (Lmg^{-1}) corresponding to the maximum binding energy, and constant B is related to the heat of adsorption. From Table 2, the Langmuir isotherm model yielded the best fit with the highest R^2 value (0.99) compared to the other two models.

3.5. Adsorption kinetics

The study of adsorption kinetics is desirable as it provides information about the mechanism of the adsorption process such as mass transfer and chemical reaction. In this context, the mechanism of the adsorption of Co(tspc)$^{-4}$ ion onto adsorbents, different kinetic models such as the pseudo-first-order and pseudo-second-order has been studied. The pseudo- first-order equation can be used to determine the rate constant for the adsorption process and describe the initial stage of the adsorption processas follows [27]:

$$\frac{1}{q_t} = \frac{k_1}{q_e}(\frac{1}{t}) + \frac{1}{q_e}$$

where q_e and q_t are the amounts of adsorbed Co(tspc)$^{-4}$ at equilibrium and any time t (mg g^{-1}), respectively, k_1 is the equilibrium rate constant of the first-order sorption (min^{-1}).

The pseudo-second-order rate equation of can be represented in the following form [28, 29] :

$$\frac{t}{q_t} = \frac{1}{k_2 q_e^2} + \frac{1}{q_e}t$$

where K_2 (g mg^{-1} min^{-1}) is the rate constant of the second-order equation, qt (mg g^{-1}) and qe (mg g^{-1}) Co(tspc)$^{-4}$ adsorbed at time t (min) and at equilibrium respectively [30]. Pseudo-second-order kinetics is based on the adsorption capacity,

Table 2. Isotherm parameters for Co(tspc)$^{-4}$ adsorption onto UVM-7/Ag.

Langmuir isotherm			Freundlich isotherm			Temkin isotherm		
qm (mg g^{-1})	b (L mg^{-1})	R^2	K_F (mg g^{-1})	N (L mg^{-1})	R^2	K_T (Lmg^{-1})	B	R^2
188.8	0.441	0.99	77624.72	15.38	0.982	1.52	11.53	0.709

which usually gives a good description of the whole adsorption process.

The rate constants and correlation coefficients of the two kinetic models can be obtained from the plot of experimental data (Table 3). The, pseudo-second-order kinetic with the higher correlation coefficient (R^2) suggests that cu(tspc)$^{-4}$ adsorption on to UVM-7/Ag predominantly follow the pseudo-second-order kinetic model.

4. Conclusion

Potential of UVM-7/Ag to adsorb Co(tspc)$^{-4}$ has been investigated in this study. Moreover, the adsorption of Co(tspc)$^{-4}$ was depend on adsorbent surface characteristics, temperature, contact time, adsorbent mass, and the initial Co(tspc)$^{-4}$ concentration in the solution. The adsorption kinetic studies showed that the adsorption process followed pseudo-second-order kinetic model. The Langmuir, Freundlich, and Temkin adsorption isotherm models were applied to the adsorption data of anionic dyes ont UVM-7/Ag . The Langmuir isotherm best fitted the adsorption equilibrium data for Co(tspc)$^{-4}$; moreover, the fitness suggests that the adsorption be monolayer and physical in nature. In addition, the thermodynamic calculations demonstrated the feasible, spontaneous, and exothermic nature of the adsorption reaction.

5. References

[1] M. Mirzaeian, A.M. Rashidi, M. Zare, R. Ghabezi, R. Lotfi, Mercaptan removal from natural gas using carbon nanotube supported cobalt phthalocyanine nanocatalyst, J. Natur. Gas Sci. Eng., 18 (2014) 439-445.

[2] M. Chanda, A. Grinshpun, K. O'driscoll, G. Rempel, Polymer-supported metal complexes as catalysts for the oxidation of thiosalts by molecular oxygen: V. The polythiosemicarbazide-Cu (II) complex, J. Mol. Catal., 26 (1984) 267-76.

[3] N. Reid , R. Barat, Impact of Fluorinated Cobalt(II) Phthalocyanine Catalysts on Aerobic Thiol Oxidation Kinetics, Chem. Eng. Commun., 203 (2016) 714-723.

[4] V. Iliev, Catalytic oxidation of mercaptans by charcoal-supported sterically hindered cobalt (II)-phthalocyanines, J. mol.catal., 85 (1993) L269-L273.

[5] D. Klyamer, A. Sukhikh, S. Gromilov , P. Krasnov , T. Basova , Fluorinated metal phthalocyanines: interplay between fluorination degree, films orientation, and ammonia sensing properties, Sensors, 18 (2018) 1-13.

[6] A.B. Sorokin, Phthalocyanine metal complexes in catalysis, Chem. Rev., 113 (2013) 8152-8191.

[7] B. Basu, S. Satapathy, A. Bhatnagar, Merox and related metal phthalocyanine catalyzed oxidation processes, Catal. Rev. Sci. Eng., 35 (1993) 571-609.

[8] Z. Tang, W. Wu, K. Wang, Review: oxygen reduction reaction catalyzed by noble metal clusters, Catalysts, 8 (2018) 1-18.

[9] Y. Cheng, J. Veder, L. Thomsen, S. Zhao, M. Saunders, R. Demichelis, C. Liu, R. De Marco, S. P. Jiang, Electrochemically substituted metal phthalocyanines, e-MPc (M = Co, Ni), as highly active and selective catalysts for CO2 reduction, J. Mater. Chem. A, 6 (2018) 1370-1375.

Table 3. Kinetic parameters for Co(tspc)$^{-4}$ adsorption onto UVM-7/Ag.

pseudo-first-order kinetics			pseudo-second-order kinetic		
qe (mg g^{-1})	K_1 (L min^{-1})	R^2	qe (mg g^{-1})	K2 (g mg^{-1}min^{-1})	R^2
250	29.5	0.957	250	0.000149	0.982

[10] A. Leitão, A. Rodrigues, Studies on the Merox process: Kinetics of n-butyl mercaptan oxidation, Chem. Eng. Sci., 44 (1989) 1245-1253.

[11] T. Wallace, A. Schriesheim, H. Hurwitz, M. Glaser, Base-Catalyzed Oxidation of Mercaptans in Presence of Inorganic Transition Metal Complexes, Ind. Eng. Chem. Process Des. Dev., 3 (1964) 237-241.

[12] M. Anbia, K. Mohammadi, An effective method for removal of dichromate ion and furfural from aqueous solutions using a nanoporous adsorbent, Asian J. Chem., 21(2009) 3347-3356.

[13] M. Anbia, M.K. Rofouei, S.W. Husain, Mesoporous lanthanum tungstate as a novel sorbent for removal of heavy metal ions from aqueous media. Asian J. Chem., 19 (2007) 3862-3873.

[14] D. Zhao, G. Sheng, J. Hu, C. Chen, X. Wang, The adsorption of Pb (II) on Mg 2 Al layered double hydroxide, Chem. Eng. J., 171(2011) 167-74.

[15] M.T. Yagub, T.K. Sen, S. Afroze, H.M. Ang, Dye and its removal from aqueous solution by adsorption: a review, Adv. Coll. Int. Sci., 209 (2014)172-184.

[16] A. Srivastav, V.C. Srivastava, Adsorptive desulfurization by activated alumina, J. Hazard. Mater., 170 (2009) 1133-1140.

[17] Y. Önal, Kinetics of adsorption of dyes from aqueous solution using activated carbon prepared from waste apricot, J. Hazard. Mater., 137 (2006) 1719-1728.

[18] M. Anbia, S.A. Hariri, Removal of methylene blue from aqueous solution using nanoporous SBA-3, Desalination, 261(2010) 61-66.

[19] A. Sari, D. Mendil, M. Tuzen, M. Soylak, Biosorption of palladium (II) from aqueous solution by moss (Racomitrium lanuginosum) biomass: equilibrium, kinetic and thermodynamic studies. J. Hazard. Mater., 162 (2009) 874-879.

[20] K. Foo, B. Hameed, Insights into the modeling of adsorption isotherm systems, Chem. Eng. J., 156 (2010) 2-10.

[21] V. M. Abbasov, H. C. Ibrahimov, Adsorptive Desulfurization of the Gasoline Obtained from Low-Pressure Hydro cracking of the Vacuum Residue Using a Nickel/Bentonite Catalyst, Energy Fuels, 31 (2017) 5840–5843.

[22] Y. Yongxing, J. Li, L. Guangqian, L. Zhang, Novel method to synthesize Ni2P/SBA-15 adsorbents for the adsorptive desulfurization of model diesel fuel, J. Alloys Compd., 745 (2018) 467-476.

[23] C. Almeida, N. Debacher, A. Downs, L. Cottet, C. Mello, Removal of methylene blue from colored effluents by adsorption on montmorillonite clay, J. coll. Int. Sci., 332 (2009) 46-53.

[24] N.R. Shinde, A.V. Bankar, A.R. Kumar, S.S. Zinjarde, Removal of Ni (II) ions from aqueous solutions by biosorption onto two strains of Yarrowia lipolytica, J. Environ. Manage., 102 (2012) 115-124.

[25] A. Bera, T. Kumar, K. Ojha, A. Mandal, Adsorption of surfactants on sand surface in enhanced oil recovery: isotherms, kinetics and thermodynamic studies, Appl. Surf. Sci., 284 (2013) 87-99.

[26[R. Labied, O. Benturki, A. E.Hamitouche, Adsorption of hexavalent chromium by activated carbon obtained from a waste lignocellulosic material: Kinetic, equilibrium, and thermodynamic study, Adsorp. Sci. Technol., 36 (2018) 1066–1099.

[27] A. Dada, A. Olalekan, A. Olatunya, O. Dada, Langmuir, Freundlich, Temkin and Dubinin–Radushkevich isotherms studies of equilibrium sorption of Zn2+ unto phosphoric acid modified rice husk, J. Appl. Chem., 3 (2012) 38-45.

[28] A. Rong, L. Meng, P. Liping, Y. Dongsheng, J. Wang , Y. Zhou, Kinetics Study of Gas Pollutant Adsorption and Thermal Desorption on Silica Gel, Appl. Sci., 7, 609 (2017) 1-11.

[29] M. Anbia, A.H. Davijani, Synthesis of L-Cysteine grafted nanoporous carbon (CMK-3) and its use as a new cadmium sorbent, Chem. Eng. J., 223(2013) 899-907.

[30] M. Gouamid, M. Ouahrani, M. Bensaci, Adsorption equilibrium, kinetics and thermodynamics of methylene blue from aqueous solutions using date palm leaves, Energy Procedia, 36(2013) 898-907.

A green approach to electrosynthesis of chromeno[3',4':5,6] pyrano [2,3-d] pyrimidines by electrochemistry

Reyhaneh Kazemi Rad[a*]

[a] *Department of Chemistry, Rasht Branch, Islamic Azad University, Rasht, Iran*

ABSTRACT

Eletrochemistry is a broad, useful, and selective technique method in many research fields. Among them, the investigation of performance of electrochemical methods in determination, synthesis and selective reduction/oxidation of different elements and molecules have attracted growing attention due their intrinsic advantages such as selectivity, low cost, and high yield of synthesis. Moreover, electrocatalytic synthesis of organic molecules is known as a green and environmentally benign method. In the present form, electrocatalytic multicomponent transformation of barbituric acid, aromatic aldehydes, and 4-hydroxycumarin was carried out. The electrocatalytic transformation was done in alcohols in the presence of tetrabutylammounium flouride as an electrolyte in an undivided cell containing an iron electrode as the cathode and a Pt electrode as the anode at a constant current leads to substituted chromeno[3',4':5,6] pyrano[2,3-d] pyrimidines in good to high yields (54-92%) at room temperature. The yield of reaction was obtained by gravimetric analysis and calculated upon theoretical conversion. The application of the effective electrocatalytic cascade method to the formation of chromeno-pyrano-pyrimidines is also beneficial from the viewpoint of diversity-oriented large-scale processes and represents an example of facile environmentally benign synthetic concept for electrocatalytic multicomponent reactions. The products were characterized with proper analytical methods such as elemental analysis (CHN), FT-IR, ^{1}H-NMR, and ^{13}C-NMR spectrometry. Finally, the obtained results showed that the desired products were synthesized.

1. Introduction

Chromene derivatives have attracted great interest due to biological and pharmacological activities such as anti-coagulant, anti-cancer, spasmolytic, diuretic, anti-anaphylatic, etc. Furthermore, the chromene derivatives are widely found in natural alkaloids, flavonoids, tocopherols, and anthocyanins [1-6].

Pyrano[2,3-*d*]pyrimidines have also received considerable attention over the past years due to their wide range of the diverse pharmacological action such as antitumor, cardiotonic, hepatoprotective, antihypertensive, anticoagulant and antibronchitic activity [7-12]. Moreover, pyranopyrimidine derivatives occur widely in the structures of various natural products [13].

Thus, chromeno pyrano[2,3-*d*]pyrimidine system appears to be of the interest because it incorporates a chromene and a pyrano[2,3-*d*]pyrimidine heterocyclic ring, which are both promising with respect to biological responses.

To the best of our knowledge, there are only a few reports on the three-component coupling of 4-hydroxycoumarin, aldehydes, and cyclic 1,3-dicarbonyl compounds [14,15].

Due to the extensive research on the electrochemistry of organic compounds, electrosynthesis has become a useful method in modern organic chemistry [16,19]. Electrochemical organosynthetic methods have received significant attention because of their benefit to the environment. In these procedures, electricity acts as a 'green' oxidative and reductive agent.

2. Experimental Procedure
2.1. Material and Methods
All reagents were purchased from Merck and Fluka and used without further purification. The melting points were obtained in open capillary tubes and were measured on an Electrothermal IA 9100 apparatus. IR spectra were recorded on KBr pellets with a Shimadzu FT-IR 8600 spectrophotometer. ^{1}H and ^{13}C NMR spectra were determined with a Bruker DRX-400 Avance instrument at 400 and 100 MHz. Elemental analysis were carried out on a Thermo Finnigan Flash EA 1112 series instrument.

2.2. General procedure for the synthesis of 4a-g
A mixture of barbituric acid **1** (2 mmol), aromatic aldehyde **2a-g** (2 mmol), 4-hydroxycoumarin **3** (2 mmol), and TBAF (0.04 g, 0.2 mmol) in n-PrOH/H$_2$O (15/5 mL) were electrolyzed in an undivided cell equipped with a magnetic stirrer, a platinum anode and an iron cathode at room temperature under a constant current density of 4 mA/cm^2 (I = 20 mA, electrodes square 5 cm^2). Progress of the reaction was monitored by thin layer chromatography. After electrolysis was finished, the precipitation of the products were obtained at pH = 7. In addition, filter cakes were washed twice with hot ethanol to give pure target products **4a-g.**

2.3. Experimental characterisation data for compounds 4a-g
7-phenyl-chromeno[3',4':5,6]pyrano[2,3-d]pyrimidine-6,8,10(7H,9H,11H)-trione (4a):
Yellow solid; mp (dec.) > 300°C. IR (KBr): ν_{max} = 3400, 3209, 3029, 2943, 1684, 1612, 1568, 1390, 1190 cm^{-1}; ^{1}H-NMR (400 MHz, DMSO-d$_6$): δ = 6.11 (s, 1H), 7.04-7.08 (m, 2H), 7.13-7.16 (m, 3H), 7.25-7.29 (m, 2H), 7.51-7.55 (m, 1H), 7.78-7.81 (m, 1H), 9.93 (s, 1H, NH), 10.12 (s, 1H, NH); ^{13}C-NMR (100 MHz, DMSO-d$_6$): δ = 166.2, 165.9, 165.4, 165.0, 152.6, 151.5, 143.8, 131.6, 128.0, 127.1, 125.1, 124.3, 123.6, 119.4, 116.0, 105.9, 89.8, 34.0; Anal. Calcd for C$_{20}$H$_{12}$N$_2$O$_5$: C, 66.67; H, 3.36; N, 7.77. Found: C, 66.54; H, 3.24; N, 7.98.

7-(3-nitrophenyl)-chromeno[3',4':5,6]pyrano[2,3-d]pyrimidine-6,8,10(7H,9H,11H)-trione (4b):
Yellow solid; mp (dec.) > 300°C. IR (KBr): ν_{max} = 3400, 3211, 3072, 2980, 1684, 1612, 1570, 1525, 1351, 1282, 1183 cm^{-1}; ^{1}H-NMR (400 MHz, DMSO-d$_6$): δ = 6.22 (s, 1H), 7.25 (t, J = 7.6 Hz, 1H), 7.31 (d, J = 8.4 Hz, 1H), 7.46-7.58 (m, 3H), 7.80 (d, J = 7.6 Hz, 1H), 7.86 (s, 1H), 7.97 (d, J = 7.6 Hz, 1H), 10.03 (s, 1H, NH), 10.17 (s, 1H, NH); ^{13}C-NMR (100 MHz, DMSO-d$_6$): δ = 166.2, 164.9, 164.7, 152.7, 151.4, 148.1, 146.9, 134.2, 131.8, 129.7, 124.6, 124.4, 123.7, 123.6, 121.5, 120.6, 116.1, 104.9, 89.3, 34.2; Anal. Calcd for C$_{20}$H$_{11}$N$_3$O$_7$: C, 59.27; H, 2.74; N, 10.37. Found: C, 59.22; H, 2.74; N, 10.39.

7-(4-nitrophenyl)-chromeno[3',4':5,6]pyrano[2,3-d]pyrimidine-6,8,10(7H,9H,11H)-trione (4c):
Orange solid; mp (dec.) > 300°C. IR (KBr): ν_{max} = 3415, 3213, 3055, 2962, 1686, 1610, 1569, 1512, 1379, 1346, 1183 cm^{-1}; ^{1}H-NMR (400 MHz, DMSO-d$_6$): δ = 6.21 (s, 1H), 7.25-7.32 (m, 4H), 7.54 (t, J = 8.4 Hz,1H), 7.79-7.80 (m, 1H), 8.06

(d, J = 8.8 Hz, 2H), 9.97 (s, 1H, NH), 10.09 (s, 1H, NH); ^{13}C-NMR (100 MHz, DMSO-d$_6$): δ = 168.9, 166.0, 153.4, 152.8, 151.4, 145.5, 143.6, 131.8, 128.3, 124.6, 123.7, 123.5, 123.4, 119.3, 116.0, 105.0, 89.8, 34.7; Anal. Calcd for C$_{20}$H$_{11}$N$_3$O$_7$: C, 59.27; H, 2.74; N, 10.37. Found: C, 59.12; H, 2.78; N, 10.50.

7-(2-chlorophenyl)-chromeno[3',4':5,6] pyrano[2,3-*d*]pyrimidine-6,8,10(7*H*,9*H*,11*H*)-trione (4d):

White solid; mp (dec.) > 300°C. IR (KBr): ν$_{max}$ = 3433, 3197, 3057, 2964, 1686, 1612, 1568, 1402, 1188 cm^{-1}; ^{1}H-NMR (400 MHz, DMSO-d$_6$): δ = 5.99 (s, 1H), 7.08-7.17 (m, 2H), 7.21-7.27 (m, 3H), 7.33 (d, J = 7.2 Hz, 1H) , 7.50 (t, J = 7.2 Hz, 1H), 7.76 (d, J = 7.2 Hz, 1H), 9.86 (s, 1H, NH), 10.00 (s, 1H, NH); ^{13}C-NMR (100 MHz, DMSO-d$_6$): δ = 168.4, 165.6, 165.4, 164.0, 152.5, 151.5, 141.8, 133.2, 131.4, 130.7, 129.7, 127.2, 126.2, 124.2, 123.6, 119.5, 115.9, 106.0, 88.3, 34.1; Anal. Calcd for C$_{20}$H$_{11}$ClN$_2$O$_5$: C, 60.85; H, 2.81; N, 7.10. Found: C, 60.74; H, 2.93; N, 7.13.

**7-(4-chlorophenyl)-chromeno[3',4':5,6] pyrano[2,3-*d*]pyrimidine-6,8,10(7*H*,9*H*,11*H*)-trione (4e):**

White solid; mp (dec.) > 350°C. IR (KBr): ν$_{max}$ = 3429, 3217, 3068, 2920, 1686, 1612, 1572, 1373, 1188 cm^{-1}; ^{1}H-NMR (400 MHz, DMSO-d$_6$): δ = 6.08 (s, 1H), 7.05 (d, J = 8.0 Hz, 1H), 7.07 (t, J = 8.0 Hz, 1H), 7.22 (d, J = 8.4 Hz, 2H), 7.27 (d, J = 8.4 Hz, 2H), 7.51 (d, J = 7.2 Hz, 1H) , 7.78 (t, J = 7.2 Hz, 1H), 9.90 (s, 1H, NH), 10.07 (s, 1H, NH); ^{13}C-NMR (100 MHz, DMSO-d$_6$): δ = 166.0, 164.8, 152.7, 151.4, 143.1, 131.6, 129.6, 129.0, 127.9, 124.4, 123.6, 119.4, 116.0, 105.5, 89.6, 33.7; Anal. Calcd for C$_{20}$H$_{11}$ClN$_2$O$_5$: C, 60.85; H, 2.81; N, 7.10. Found: C, 60.74; H, 2.93; N, 7.13.

7-(3-bromophenyl)-chromeno[3',4':5,6] pyrano[2,3-*d*]pyrimidine-6,8,10(7*H*,9*H*,11*H*)-trione (4f):

White solid; mp (dec.) > 350°C. IR (KBr): ν$_{max}$ = 3333, 3167, 3060, 2933, 1684, 1612, 1576, 1468, 1398, 1188 cm^{-1}; ^{1}H-NMR (400 MHz, DMSO-d$_6$): δ = 6.11 (s, 1H), 7.06-7.14 (m, 3H), 7.24-7.29 (m, 3H), 7.52-7.55 (m, 1H), 7.79 (s, 1H), 9.97-10.08 (brs, 2H, NH); ^{13}C-NMR (100 MHz, DMSO-d$_6$): δ = 166.1, 164.7, 152.7, 151.4, 147.4, 131.7, 130.3, 129.7, 128.0, 127.1, 126.4, 126.0, 124.4, 123.7, 121.7, 119.4, 116.0, 105.2, 89.4, 34.0; Anal. Calcd for C$_{20}$H$_{11}$BrN$_2$O$_5$: C, 54.69; H, 2.52; N, 6.38. Found: C, 54.35; H, 2.64; N, 6.63.

7-(4-bromophenyl)-chromeno[3',4':5,6] pyrano[2,3-*d*]pyrimidine-6,8,10(7*H*,9*H*,11*H*)-trione (4g):

White solid; mp (dec.) > 300°C. IR (KBr): ν$_{max}$ = 3400, 3210, 3084, 2930, 1684, 1612, 1568, 1377, 1184 cm^{-1}; ^{1}H-NMR (400 MHz, DMSO-d$_6$): δ = 6.06 (s, 1H), 6.99 (d, J = 8.0 Hz, 2H), 7.23-7.29 (m, 2H), 7.32 (d, J = 8.0 Hz, 2H), 7.51 (d, J = 7.6 Hz, 1H), 7.78 (t, J = 7.6 Hz, 1H), 9.88 (s, 1H, NH), 10.06 (s, 1H, NH); ^{13}C-NMR (100 MHz, DMSO-d$_6$): δ = 168.0, 166.0, 152.5, 151.4, 148.4, 143.7, 131.6, 130.8, 129.5, 124.4, 123.6, 120.3, 119.4, 118.0, 116.0, 105.4, 89.8, 33.7; Anal. Calcd for C$_{20}$H$_{11}$BrN$_2$O$_5$: C, 54.69; H, 2.52; N, 6.38. Found: C, 54.62; H, 2.45; N, 6.50.

3. Results and discussion

Simple alcohols (methanol, ethanol, propanol) or alkanes (heptane, hexane) are environmentally preferable solvents, whereas the use of dioxane, acetonitrile, acids, formaldehyde, and tetrahydrofuran is not recommendable from an environmental perspective [20, 21]. In continuation of our work [15, 22-24] on the development of efficient and convenient procedures using electrogenerated base, we were prompted to design
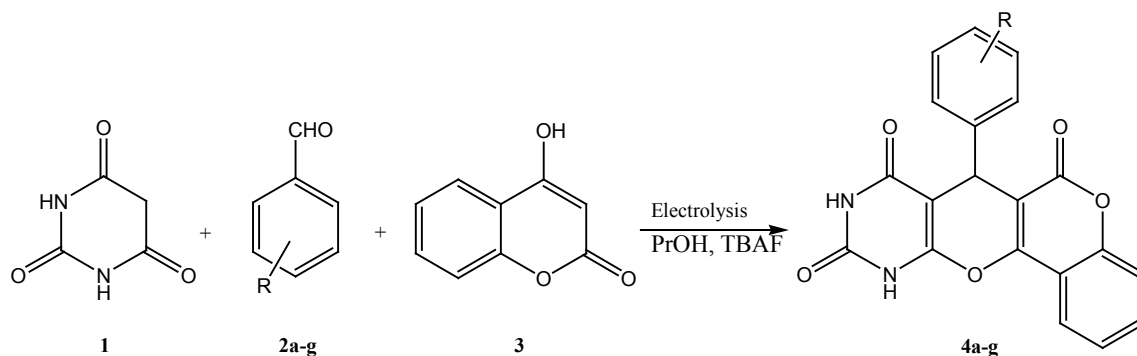
Scheme 1. Synthesis of chromeno pyrano[2,3-d] pyrimidine.

Table 1. Electrocatalytic transformation of barbituric acid (**1**), 3-nitrobenzaldehyde (**2b**), and 4-hydroxycoumarin (**3**) into **4b**[a].

Entry	Alcohol	I (mA)	Current density (mAcm^{-2})	Time (min)	Electricity passed (F mol^{-1})	Yield (%)
1	MeOH	20	4	20	0.25	88
2	EtOH	20	4	20	0.25	90
3	PrOH	20	4	20	0.25	94
4	PrOH	10	2	40	0.25	80
5	PrOH	30	6	13.5	0.25	90
6	PrOH	50	10	8	0.25	87

[a] 3-nitrobenzaldeyde (2 mmol), barbituric acid (2 mmol), 4-hydroxycumarin (2 mmol), TBAF (0.2 mmol), alcohol/water (15/5 ml), iron cathode (5 cm^2), platinum anode (5 cm^2), r.t.

a green and environmentally benign methodology for the synthesis of chromeno pyrano[2,3-*d*] pyrimidine compounds based on electrochemically induced multicomponent reaction of barbituric acid, aromatic aldehydes and 4-hydroxycumarin in an undivided cell containing an iron electrode as cathode and a Pt electrode as anode in the presence of tetrabutylammounium flouride as electrolyte in alcohols at room temprature.

First, to evaluate the synthetic potential of the procedure proposed and to optimize the electrolysis conditions, the electrocatalytic multicomponent transformation of barbituric acid **1**, 3-nitrobenzaldehyde **2b,** and 4-hydroxycumarin **3**

into corresponding chromeno-pyrano-pyrimidines **4b** in alcohol in an undivided cell containing an iron electrode as cathode and a Pt electrode as anode at constant current in the presence of tetrabutylammounium flouride as an electrolyte was studied. Also, the effect of current and solvent was also examined (Table 1). As for alcohol used as solvent, PrOH is preferable to MeOH and EtOH for this electrocatalytic transformation at room temperature.

As indicated in Table **1**, excellent conversions of starting compounds were obtained after 0.25 F/mol of electricity. The current density 4 mA/cm^2 (*I* = 20 mA, electrodes surface 5 cm^2) in n-PrOH at r.t.

Table 2. Electrocatalytic transformation of barbituric acid(**1**), aromatic aldehydes (**2a-g**) and 4-hydroxycoumarin (**3**) into chromeno-pyrano-pyrimidines **4a-g.**

Product	Ar	Current density (mAcm^{-2})	Time (min)	Electricity passed (F mol^{-1})	Yield (%)	Mp (ºC)	Mp (ºC) (lit. [14])
4a	C$_6$H$_5$	4	45	0.56	54	> 300 dec.	> 300 dec.
4b	3-NO$_2$ C$_6$H$_4$	4	20	0.25	92	> 300 dec.	> 300 dec.
4c	4-NO$_2$ C$_6$H$_4$	4	10	0.12	82	> 300 dec.	> 300 dec.
4d	2-Cl C$_6$H$_4$	4	25	0.16	88	> 300 dec.	> 300 dec.
4e	4-Cl C$_6$H$_4$	4	30	0.37	90	> 350 dec.	> 350 dec.
4f	3-BrC$_6$H$_4$	4	30	0.37	62	> 350 dec.	> 350 dec.
4g	4-BrC$_6$H$_4$	4	30	0.37	72	> 300 dec.	> 300 dec.

^{a}Reaction conditions: barbituric acid (2 mmol), aromatic aldehyde (2 mmol), 4-hydroxycoumarin (2 mmol), TBAF(0.2 mmol), n-PrOH/H$_2$O (15/5 mL), iron cathode (5 cm^2), platinum anode (5 cm^2), current density 4 mA/cm^2, room temperature.
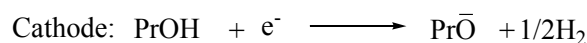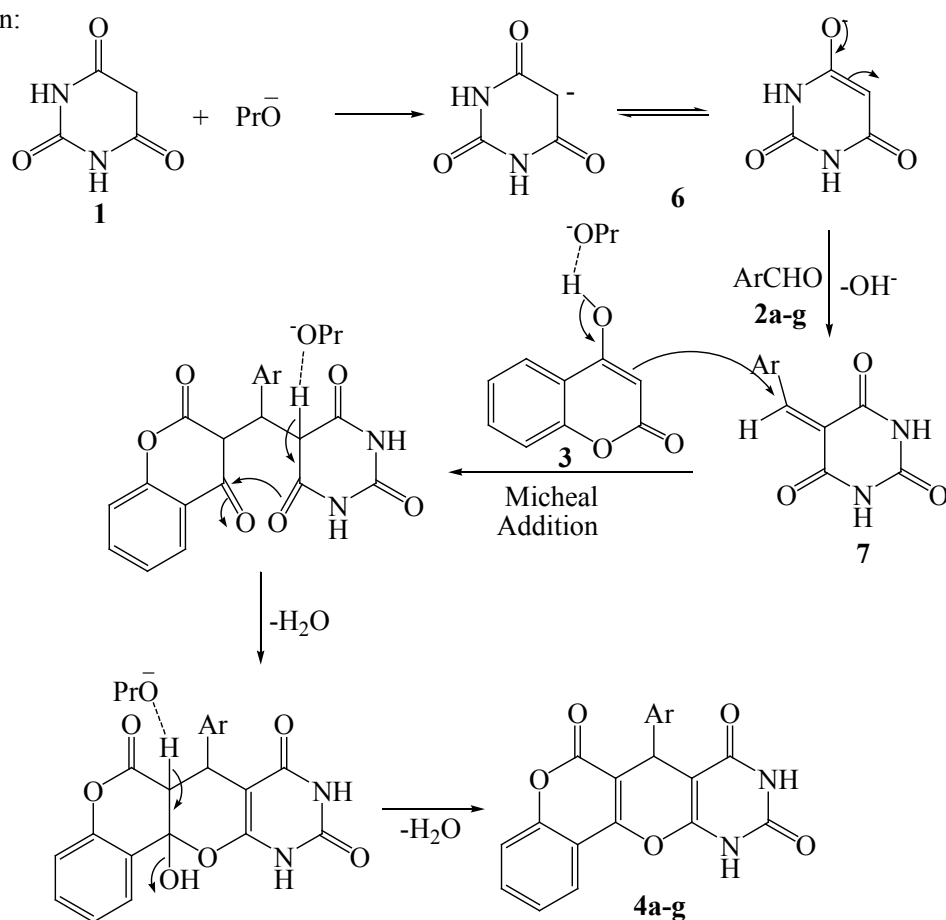
Scheme 2. A proposed mechanism for the electrocatalytic transformation of barbituric acid, aromatic aldehydes and 4-hydroxycumarin into chromeno-pyrano-pyrimidines **4a-g**

was found to be optimum for the electrochemically induced chain process and allowed for the highest yield (92%) of chromeno-pyrano-pyrimidines **4b**. The increase in the current density up to 10 mA/cm^2 ($I = 50$ mA) results in a slight decrease of the reaction yield, which may be connected with the activation of undesired direct electrochemical processes possible under these conditions and leading to oligomerization of starting material.

Under the optimal conditions (current density 4 mA/cm^2, 0.25 F/mol passed, n-PrOH as a solvent), the electrolysis of barbituric acid **1**, aromatic aldehydes **2a-g,** and 4-hydroxycumarin **3** in an undivided cell gives rise to the corresponding chromeno-pyrano-pyrimidines **4a-g** with 54-92 % yield at r.t. (Scheme 1, Table 2).

Taking into consideration the above results, the following mechanism for the electrocatalytic chain transformation of barbituric acid **1**, aromatic aldehydes **2a-g,** and 4-hydroxycumarin **3** into corresponding chromeno-pyrano-pyrimidines **4a-g** is proposed.

As the initiation step of the catalytic cycle, the deprotonation of an alcohol at the cathode leads to the formation of alkoxide anion. The subsequent reaction in solution between alkoxide anion **5** and barbituric acid **1** gives rise to enolate anion **6**. Then Knoevenagel condensation of enolate anion with aromatic aldehyde takes place in the solution with elimination of hydroxide anion and formation of arylidenebarbiturate **7**. Finally, the subsequent hydroxide-promoted Michael addition of 4-hydroxycumarin **3** to electron deficient Knoevenagel adduct **7** followed by intramolecular cyclization leads to corresponding chromeno[3',4':5,6]pyrano[2,3-*d*]pyrimidines **4a–g** (Scheme 2).

4. Conclusion

The electrocatalytic transformation of barbituric acid, aromatic aldehydes, and 4-hydroxycumarin in an undivided cell gives rise to the corresponding chromeno-pyrano-pyrimidines in comparison with conventional methods has advantages such as (i) in situ generation of base and avoidance of polluting or hazardous chemicals or the addition of base or probase, (ii) a fast one pot reaction in good to excellent yields at room temperature (iii). The procedure utilizes inexpensive reagents, green solvents, simple equipment, and an undivided cell (v). Moreover, it is easily carried out and is fully beneficial from the viewpoint of ecological organic synthesis and large-scale processes. Furthermore, this method can potentially used for determination of such molecules.

6. References

[1] J.B. Harbone (Ed.), The Flavonoids- Advances in Research, Chapman & Hall, London, 1988.

[2] G.A. Iacobucci, J.G. Sweeny, The chemistry of anthocyanins, anthocyanidins and related flavylium salts, Tetrahedron, 39 (1983) 3005-3038.

[3] B.A. Bohm, J.B. Choy, A.Y.-M. Lee, Flavonoids of *Balsamorhiza* and *Wyethia,* Phytochemistry, 28 (1989) 501-503.

[4] A. J. Moro, A. J. Parola, F. Pina, A-M Pana, V. Badea, I. Pausescu, S. Shova and L. Cseh, 2,2′-Spirobis[chromene] Derivatives Chemistry and Their Relation with the Multistate System of Anthocyanins, J. Org. Chem., 82, 10 (2017) 5301–5309.

[5] V.S. Parmar, S.C. Jain, K.S. Bisht, R. Jain, P. Taneja, A. Jha, O.D. Tyagi, A.K. Prasad, J. Wengel, C.E. Olsen, P.M. Boll, Phytochemistry of the genus *Piper,* Phytochemistry 46 (1997) 597-673.

[6] V.V. Polyakov, Chem. Nat. Compd. (Engl. Transl.) 1 (1999) 21.

[7] E. M. Grivsky and S. Lee, C.W. Sigel, D.S. Duch, and C.A. Nichol, Synthesis and antitumor activity of 2,4-diamino-6-(2,5-dimethoxybenzyl)-5-methylpyrido[2,3-d]pyrimidine, J. Med. Chem., 23 (1980) 327-329.

[8] J. A. Valderrama, P. Colonelli, D. Vásquez, M. F. González, J. A. Rodríguez and C. Theoduloz, Studies on quinones. Part 44: Novel angucyclinone N-heterocyclic analogues endowed with antitumoral activity, Bioorg. Med. Chem., 16 (2008) 10172-10181.

[9] D. Heber, C. Heers and U. Ravens, Positive inotropic activity of 5-amino-6-cyano 1,3dimethyl-1,2,3,4-tetrahydropyrido[2,3-d]pyrim idine-2,4-dione in cardiac muscle from guinea-pig and man. Part 6: Compounds with positive inotropic activity, Pharmazie, 48 (1993) 537-541.

[10] S. Furuya and T. Ohtaki, Eur. Pat. Appl. EP 608565, 1994.

[11] M. C. Bagley, D. D. Hughes, M. C. Lubinu, E. A. Merrit, P. H. Taylor and N. C. O. Tomkinson, Microwave-Assisted Synthesis of Pyrimidine Libraries, QSAR Comb. Sci., 23 (2004) 859-867.

[12] M. Debbabi, V. D. Nimbarte, S. Chekir, S. Chortani, A. Romdhane, H. B. jannet, Design and synthesis of novel potent anticoagulant and anti-tyrosinase pyranopyrimidines and pyranotriazolopyrimidines: Insights from molecular docking and SAR analysis, Bioorg. Chem., 82 (2019) 129-138.

[13] J. H. Lee, H. B. Bang, S. Y. Han, J. G. Jun, An efficient synthesis of (+)-decursinol from umbelliferone, Tetrahedron Lett. 48 (2007) 2889-2892.

[14] (a) Chen, Z.; Zhu, Q.; Su, W. A novel sulfonic acid functionalized ionic liquid catalyzed multicomponent synthesis of 10,11-dihydrochromeno[4,3-b]chromene-6,8(7H,9H)-dione derivatives in water, Tetrahedron Lett. 52 (2011) 2601-2604; (b) Pradhan, K.; Paul, S.; Das, A. R. Fe(DS)3, an efficient Lewis acid-surfactant-combined catalyst (LASC) for the one pot synthesis of chromeno[4,3-b]chromene derivatives by assembling the basic building blocks, Tetrahedron Lett. 54 (2013) 3105-3110.

[15] R. Kazemi-Rad, A. Azizian, H. kefayati, Electrogenerated acetonitrile anion/ tetrabutylammounium cation: An effective catalytic system for synthesis of novel chromeno[3',4':5,6] pyrano[2,3-d]pyrimidines, Tetrahedron Lett. 55 (2014) 6887–6890.

[16] S. Torii (Ed.), Novel Trends in Electroorganic Synthesis, Springer, Berlin (1998)

[17] H. Lund (Ed.), Organic Electrochemistry (fourth ed.), Marcel Dekker Inc., New York (2000)

[18] E. J. Horn, B. R. Rosen and P. S. Baran, Synthetic Organic Electrochemistry: An Enabling and Innately Sustainable Method, ACS Cent. Sci., 2, 5 (2016) 302-308.

[19] R. D. Little and K. D. Moeller, Introduction: Electrochemistry: Technology, Synthesis, Energy, and Materials, Chem. Rev. 118, 9 (2018) 4483-4484.

[20] C. Capello, U. Fischer, K. Hungerbuhle, What is a green solvent? A comprehensive framework for the environmental assessment of solvents, green chemistry, 9 (2007) 927-934.

[21] M. Tobiszewski, J. Namieśnik and F. Pena-Pereira, Environmental risk-based ranking of solvents using the combination of a multimedia model and multi-criteria decision analysis, Green Chem., 19 (2017) 1034-1042.

[22] H. kefayati, Sh. H. Amlashi, R. Kazemi-Rad, A. Delafrooz, Electrocatalytic multicomponent assembling of phthalhydrazide, aldehydes

and malononitrile: An efficient approach to 1H-pyrazolo[1,2-b]phthalazine-5,10-diones, C. R. Chimie 17 (2014) 894–898.

[23] R. Kazemi-Rad, A. Azizian, H. kefayati, Improved Synthesis of 2,2_ Arylmethylene Bis(3-hydroxy-5,5-dimethyl-2-cyclohexene-1-one) and 1,8 Dioxo-octahydroxanthene Derivatives Catalyzed by Electrogenerated Base and Sulfuric Acid, J. Chin.

Chem. Soc., 62(2015) 311-315.

[24] R. Kazemi-Rad, A. Azizian, H. kefayati, Electrocatalytic multicomponent assembling of aminouracils, aldehydes and malononitrile: An efficient approach to 7-aminopyrido[2,3-d] pyrimidine-6-carbonitrile derivatives, J. Serb. Chem. Soc., 81 (1) (2016) 29–34.

A magnetic graphitic carbon nitride as a new adsorbent for simple separation of Ni (II) ion from foodstuff by ultrasound-assisted magnetic dispersive-micro solid phase extraction method

Bahareh Fahimirad[a] and Alireza Asghari[a]*

[a] Department of Chemistry, Semnan University, Semnan, Iran

ABSTRACT

In this research, a magnetic graphitic carbon nitride (g-C_3N_4-$SnFe_2O_4$) was successfully synthesized and utilized as an efficient adsorbent for nickel (Ni^{2+}) separation/extraction from vegetable samples by ultrasound-assisted magnetic dispersive micro solid-phase extraction (UA-M-D-µSPE). After separation and preconcentration step, Ni ions were determined via micro-sampling flame atomic absorption spectrometry (MS-FAAS). A successful synthesis of g-C_3N_4-$SnFe_2O_4$ was investigated by Fourier transform infrared spectroscopy (FT-IR), X-ray diffraction (XRD), field emission scanning electron microscopy (FE-SEM), and vibrating sample magnetometer (VSM). The optimization of adsorption and desorption steps was effectively studied by the on-at-a time method. In addition, under the optimum experimental conditions, the limits of detection (LODs), the linear ranges (LR) and relative standard deviations (RSDs%, for n = 5) were obtained 1.0 µgL^{-1}, 4.0 ─ 500.0 µgL^{-1}, and 1.4 respectively.

1. Introduction

One of the important category of foodstuff is Vegetables. This category of foodstuff contain vitamins, anti-oxidants, minerals, and diverse beneficial phytochemicals[1, 2]. In presence of heavy metals in vegetables, even at trace levels, is one of health concern from industrial wastewater [3]. Among a variety of metal ions, nickel is toxic, even at trace levels [4-6]. Different methods use for determination of this metal ion such as flame atomic adsorption spectrometry (FAAS),

electrothermal atomic adsorption spectrometry (ETAAS), inductively coupled plasma-optical emission spectrometry (ICP-OES), and inductively coupled plasma-mass spectrometry (ICP-MS)[7]. But micro-sampling-FAAs (µ-FAAs) due to low cost which requires a low operational facility, and uses a small volume of the eluent, has recently been very much considered [7].

In any case, the use of these methods to measure low-nickel amounts is not suitable because of their low sensitivity. Therefore, the sample preparation step is required before the measurement by the µ-FAAs [8]. Among the various types of sample preparation

methods, solid phase extraction (SPE) is very much appreciated due to its simplicity, low cost, high speed; moreover, the solid phase extraction requires low amounts of reagents, a high recovery, environmentally friendly, and a low organic solvent consumption [9, 10]. The ultrasound-assisted dispersive magnetic solid-phase extraction (UA-DM-SPE) is a new form of SPE which leads to more rapidity and ease of operation compared with the conventional SPE. In this method, using ultrasonic waves, the contact surface of the adsorbent with the analyte is increased in a very short time, as well as due to the adsorbent magnetic property, the centrifuge step is removed and the process of separation and preconcentration is performed in short time [8]. As a result, in this method use a novel nanoadsorbents with a high adsorption efficiency and the easy separation is an important step. A graphitic carbon nitride (g-C_3N_4) is a new form of organic polymer-like material, and due to its quick and facile synthesis, special structure, and low cost has been a lot touched recently [11]. The g-C_3N_4 sheets can be used as SPE sorbents, but they have several problems, such as Re-aggregation of the nanosheets, and also their low surface area [12]. Therefore, to raise any of the characteristics of this compound and rapid separation of it from sample solution, nanomagnetic of $SnFe_2O_4$ was used for increasing of surface area and separation of g-C_3N_4 of the solution.

Therefore, in this work, the nanoadsorbent g-C_3N_4-$SnFe_2O_4$ with a very high absorption power as an efficient nanoadsorbent for ultrasound-assisted magnetic dispersive micro solid-phase extraction (UA-M-D-μSPE) was synthesized and applied for the separation and preconcentration of the Ni (II) ion and toxic metal ion was measured using the micro-sampling flame atomic adsorption spectrometry (μS-FAAS) technique.

2. Experimental Procedure

2.1. Materials

All the reagents used in this work including melamine, Ni (NO$_3$)$_2$.3H$_2$O, SnCl$_2$.2H$_2$O,

FeCl$_3$.6H$_2$O, HCl (37%), HNO$_3$, NaOH, H$_2$SO$_4$, and ethanol were of the highest available purity, supplied from Merck Company. Standard solution was prepared by dissolving appropriate amounts of Ni (NO$_3$)$_2$. In addition, 3H$_2$O in doubly distilled water at a concentration of 1000 mg L^{-1}. Working standard solutions with intermediate concentrations were prepared daily by dilution of the stock solutions.

2.2. Instrumentation

For determination of Ni(II) in the samples, an Agilent model 240 AA Shimadzu (USA) flame atomic adsorption spectrometer was used with the Ni hollow cathode lamps as the radiation sources. The pH values of the solutions were adjusted by a pH meter, PHS-3BWModel (Bell, Italy) with a glass combination electrode. An ultrasonic bath (SW3, Switzerland) was used at a frequency of 50/60 kHz to dissipate adsorbent in a sample solution.

Fourier transform-infrared (FT-IR) spectra using a Shimadzu 8400s spectrometer were determined in the range of 400-4000 cm^{-1}. Scanning electronmicroscopy (FE-SEM) analysis was carried out using a Tescanvega II XMU Digital Scanning Microscope. Energy-dispersive X-ray spectroscopy elemental analysis (EDX) of the samples was obtained using a Philips XL-30 energy-dispersiveX-ray spectroscope. X-ray diffraction (XRD) patterns were obtained on a Burker AXS (Model B8-Advance). The magnetic properties were analyzed using a vibrating sample magnetometer (VSM, Lakeshore7407) at room temperature.

2.3. Synthesis of g-C$_3$N$_4$-SnFe$_2$O$_4$

3 g of melamine was placed in a crucible and hated in 520 ^{0}C with a rate of 10 ^{0}C/min for 4 hours. Finally, yellow g-C_3N_4 precipitate was formed. In the next step, to synthesis of $SnFe_2O_4$ nanostructure, SnCl$_2$.2H$_2$O and FeCl$_3$.6H$_2$O with a stoichiometric ratio of 1:2 were mixed in 100 mL of distilled water

and was heated at 80 °C. Then pH of the solution was adjusted using NaOH solution in 10. After 3hours, a black precipitate of $SnFe_2O_4$ was formed. A black precipitate was collected by an external magnetic field, and repeatedly washed with ethanol and distilled water. Finally, the black precipitate was dried at 120 ° C for 24 h. To synthesis of the g-C_3N_4-$SnFe_2O_4$ nanoadsorbent, 0.13 g of g-C_3N_4 whit 0.2 g of the $SnFe_2O_4$ nanostructure was homogeneously mixed by grinding in an agate mortar for 30 min and then the powder was calcined in a furnace at 400 °C for 4 hours [13].

2.4. Preparation of real samples

The vegetable were provided from Tehran markets in Iran. The vegetables were cut into small pieces, washed with deionized water. Then, the samples were dried in an oven for 24 hours. 25 mL of HNO_3 (65%) was added to 1.2 gr of each sample and placed in acid overnight. Then the samples were heated at 250 °C, until their liquid contents were evaporated, and they became almost dried. In order to complete the digestive process, 5 mL of H_2O_2 (30%) was added to the samples and then heated to vaporize their liquid contents. Afterwards, the samples were washed with deionized water and heated to boil the solutions. Then the contents were cooled and transferred to sample flask of 25 mL, and diluted with deionized water to 25 mL. Finally, the pH values for the solutions were adjusted, and certain amounts of the metal ions were spiked.

2.5. Procedure for magnetic dispersive micro solid-phase extraction

10.0 mg nanoadsorbent was added to 10.0 mL of sample solution in a glass vial containing containing 50.0 μgL^{-1} of Ni (II) at a pH value of 6.0. The solution was sonicated for 5 min at 25±3 °C, and then the nanoadsorbent was separated from the solution by a magnetic field within 2 min. In the desorption step, 250 μL of HNO_3 (3 $molL^{-1}$) was added to the sample solution, and sonicated

for 4 min. Then, HNO_3 solution as the eluent was collected and then injected into FFAS by means of a micro-sampler for determining the metal ions. The extraction recovery (ER), and relative recovery (RR) for each metal ion were calculated as:

$$ER = \frac{n_{inj}}{n_0} \qquad (1)$$

where C_{inj} is the concentration of the metal ions in 200 μl eluent (in the desorption step), and c_0 is the initial concentration of the metal ions.

$$RR = \frac{C_{found} - C_{real}}{C_{added}} \times 100 \qquad (2)$$

where c_{found}, c_{real}, and c_{added} are the concentration of the analyte after adding the standard to the real sample, concentration of the real sample, and concentration of the standard solution which was injected to the real sample, respectively[14].

3. Results and discussions

3.1. Characterization of synthesized nanoadsorbent

The crystalline structures of g-C_3N_4, $SnFe_2O_4$, and g-C_3N_4-$SnFe_2O_4$ were determined by XRD. In Fig.1a, two typical diffraction peaks can be observed at $2\Theta= 27.47$ and 13.51^0 for pure g-C_3N_4, which represent the inter-planar graphitic stacking; these peaks well-agreed with the values in the standard card (JCPDF 87-1526). Also, in Fig 1b, the peaks at $2\Theta=20.18$, 23.31, 33.23, 37.26, 39.2, 40.98, 47.71, 53.75, and 59.38 confirm $SnFe_2O_4$. Also Fig. 1c confirms the formation of the g-C_3N_4-$SnFe_2O_4$ composite according to reference[8]. The FT-IR spectra in Fig 2a shows the peaks for pure g-C_3N_4 at 1241,1319, and 1409 cm^{-1} can be attributed to aromatic C-N stretching and the peak at 810 cm^{-1} can be attributed to triazine units and also, the peaks at 1568 and 1650 cm^{-1} can be related to C=N stretching [15, 16]. The adsorption peak in Fig. 2 b at 570 cm^{-1} can be attributed to the stretching vibrations of the Sn–O and Fe–O bonds [17]. Finally, the index peaks in Fig. 2c confirm
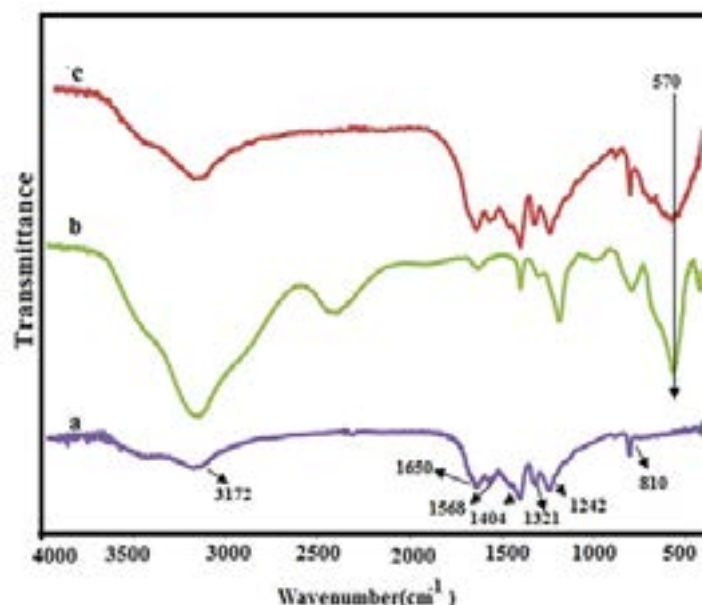
Fig. 1. FT-IR spectra of (a) g-C$_3$N$_4$, (b) SnFe$_2$O$_4$, and (c) g-C$_3$N$_4$- SnFe$_2$O$_4$.

the formation of the g-C$_3$N$_4$-SnFe$_2$O$_4$ compound. The FE-SEM micrographs for the nanostructures g-C$_3$N$_4$ and g-C$_3$N$_4$-SnFe$_2$O$_4$ are shown in Figs. 3a and b. According to these figures, the SnFe$_2$O$_4$ nanostructure is cubic with a quite uniform size of about 60-120 nm. The Fig 3b shows that the cubic particles of SnFe$_2$O$_4$ are uniformly distributed on the g-C$_3$N$_4$ surface. The magnetic properties of the synthesized nanoadsorbent was investigated through a vibrating sample magnetometer (VSM) at room temperature. Fig. 4 show the magnetic hysteresis curve for SnFe$_2$O$_4$ and g-C$_3$N$_4$-SnFe$_2$O$_4$ in an applied magnetic field. The maximum saturation magnetization (Ms) values of SnFe$_2$O$_4$ and g-C$_3$N$_4$-SnFe$_2$O$_4$ were found to be 4.87 and 3.14 emu g^{-1} respectively. The results of this analysis show that synthesized nanoadsorbent has a good magnetic strength, and that it can be separated easily from the aqueous solution with the help of an applied magnetic field.
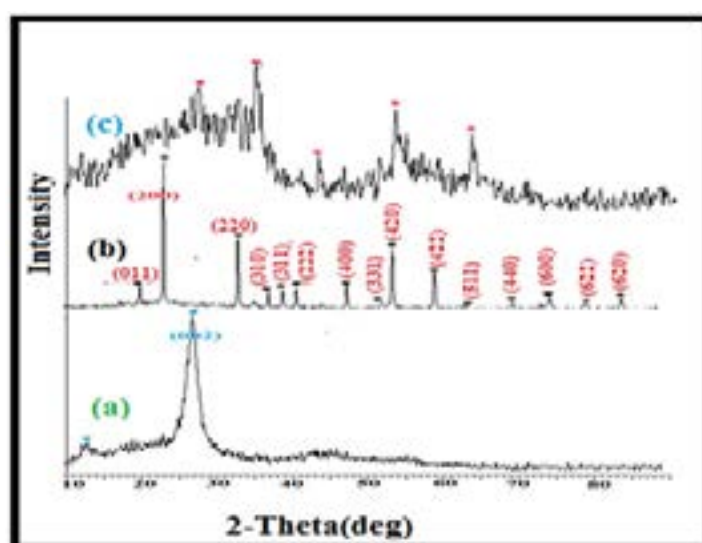
Fig. 2. XRD pattern of (a) g-C$_3$N$_4$ (b) SnFe$_2$O$_4$ and (c) g-C$_3$N$_4$- SnFe$_2$O$_4$.
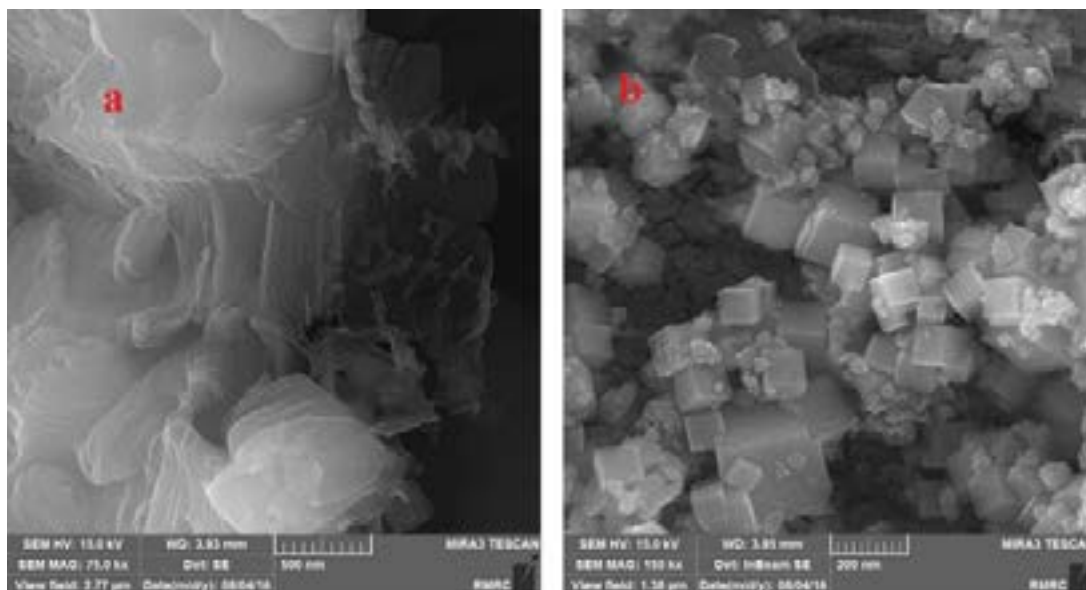
Fig. 3. SEM image of (a), g-C$_3$N$_4$ and (b) g-C$_3$N$_4$- SnFe$_2$O$_4$.

3.2 Optimization of experimental conditions

To investigation of effective parameters, in adsorption step, first 10 mL of solutions containing metal ions with concentration of 10 µgL^{-1} were prepared and a certain amount of adsorbent was added to it. Then, pH of solutions was set using HCl or NaOH solutions (0.1 molL^{-1}) and the solution was ultrasound for a specific time. Then adsorbent was separated by using magnetic field. In desorption step, the certain volume of eluent was added to

adsorbent, and the solution was ultrasound for a specific time. In this step, Ni (II) was desorb in to eluent, and finally was injected to FAAs by using micro-sampling device.

3.2.1 Effect of solution pH, adsorbent amounts, and ultrasonic time in adsorption step

The solution pH was investigated in the range of 3 to 8. The results in Fig. 5a show that in pH 6, the most recovery is achieved. In acidic pH values, there is a strong competition
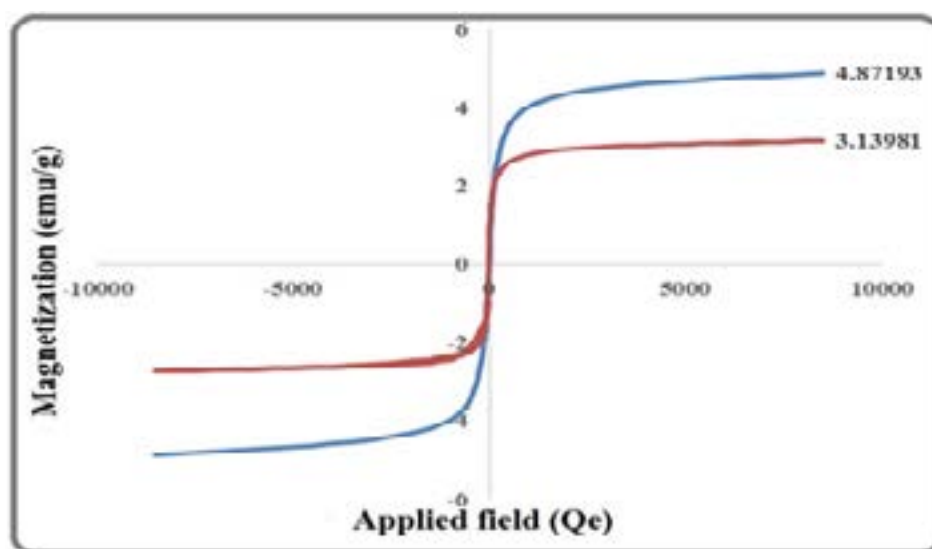

Fig. 4. Magnetization curves of (a), SnFe$_2$O$_4$ and (b) g-C$_3$N$_4$- SnFe$_2$O$_4$.
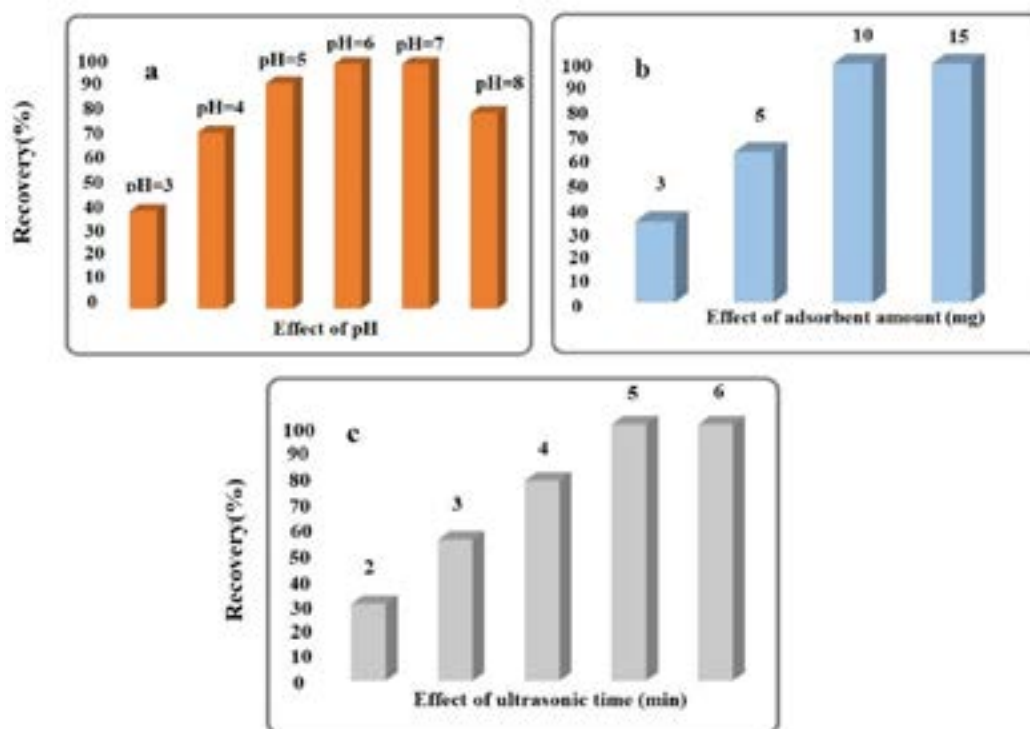
Fig. 5. The effect of effective parameters on the recovery percentage of Ni(II) ion in adsorption step.

between H^+ ions and metal ion, as the result in pH less than pH of 6, the recovery of metal ion adsorption decrease. On the other hand, in basic pH values, by increasing of OH concentration in sample solution, 1) the active sits on the adsorbent surface (OH and NH groups), due to the formation of the hydrogen bond, deactivated and as a result the recovery reduce; 2) the reduction in recovery can be attributed to the formation of the precipitation of some ion in the form of hydroxides [8]. The adsorbent amounts was investigated in range of 3 to 15 mg. The results in Fig 5b shows that an absorbent amount of 10 mg of nano adsorbent for the metal ion lead to most recovery. The effect of ultrasonic time was investigated on the recovery of metal ions in rang 2 to 6 min. According to the results shown in figure 5c, the time of 5 min was selected as optimum time.

3.2.2 Effects of type, concentration, and volume of eluent, and ultrasonic time at the desorption step
The eluents including HCl, HNO_3 and H_2SO_4 were investigated on the recovery. The results in Fig 6a show that HNO_3 for metal ion has as better eluent. The concentration of eluent and the volume of eluent were investigated in rang 1 to 4 $mol.L^{-1}$ and in rang of 100 to 300 μL, respectively. According to figure 6b and 6c the optimum concentration and volume of eluent were obtained 3 $mol.L^{-1}$ and 250 μL of the eluent. The effect of ultrasonic time was investigated in rang 2 to 5 min. The results in Fig 6d show that by increasing of ultrasonic time to 4 min the recovery of metal ion increase and then the recovery is stationary. The result indicates that the best time for this step was 4 minutes.

3.3. Analytical validation
Under the optimized experimental conditions, the linear ranges with determination coefficient (r^2) of
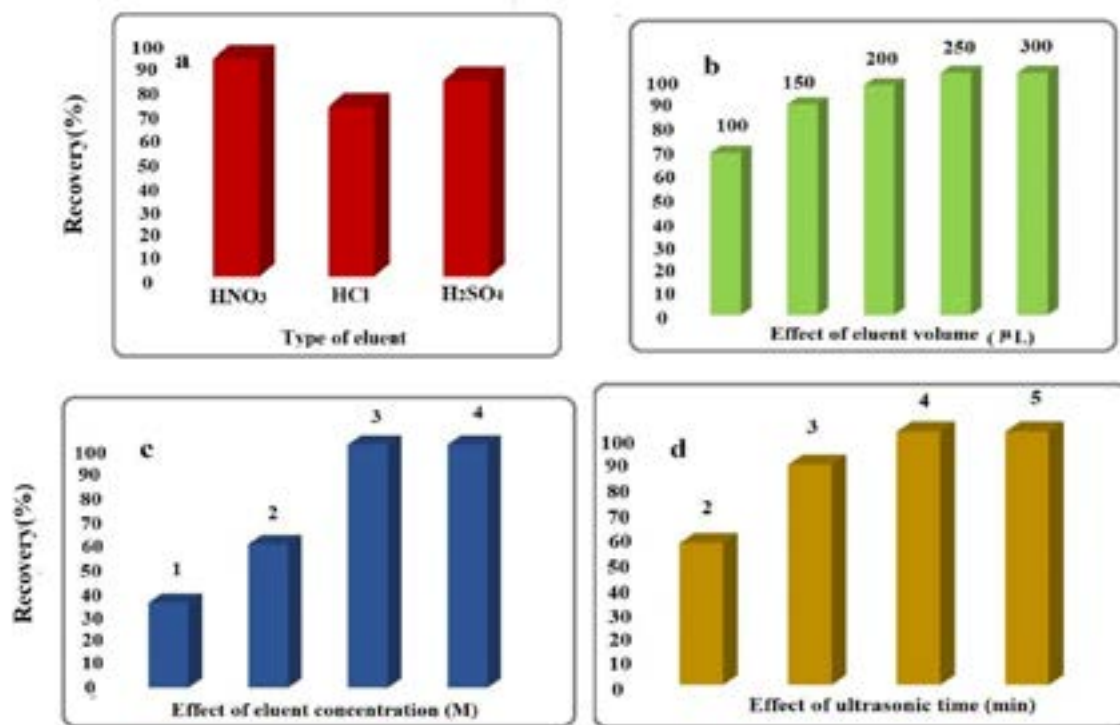
Fig. 6. The effect of effective parameters on the recovery percentage of Ni(II) ion in desorption step.

calibration 0.996 were obtained between 4.0-500.0 µg L^{-1}. Limit of detection (LOD) for five replicates were calculated 1.0 µg L^{-1}.

Also, the relative standard deviations (RSDs) were obtained for 5 repetitions, and were 1.4%. Finally, the results indicate that the proposed method has a good precision for the separation and preconcentration of trace amounts of Ni (II) ions.

3.4. Application of method in real samples
Considering the importance of measuring of heavy

metals such as Ni(II) ion in vegetables, hence in the present work, the proposed method was used to determination and extraction of Ni ion in the samples of Leek, Lettuce, Parsley, and Radish. For this purpose, in the obtained optimum condition, the method was done in real samples, and relative recovery (RR) was calculated for Ni (II) ions according to the equation (2). The results in Table 1 show that measured amounts are in good agreement with added amounts of Ni (II) ions. Finally, the obtained results confirm the good high ability of

Table 1. Levels of metal ions in real samples.

Sample	[a]Ni (II)		
	Added (µg L^{-1})	(found-real) (µg L^{-1})	[b]RR (%)
Leek		BDL	
	50	49.0±1.5	98.0
Parsley		BDL	
	50	49.5±1.3	99.0
Radish		BDL	
	50	50.0±1.5	100.0
Lettuce		BDL	
	50	48.8±4.0	97.6

[a] Mean of three determinations ± confidence interval (P = 0.95, n =5)
[b] Relative Recovery

Table 2. Effect of potentially interfering ions on recovery of metal ions.

Potentially interfering ions	Tolerance limit[a] (C_i/C_a)	Recovery%
		Ni(II)
Na^+	1000	99.00
Mg^{2+}	1000	100.00
NO^{3-}	1000	99.00
Cl^-	1000	99.40
Zn^{2+}	600	98.83
Al^{3+}	500	98.50

[a] Concentration ratio of potentially interfering and analyte ions. Adsorption conditions: 10 mg of adsorbent, pH=6. Desorption conditions: 250 μL of HNO_3 with concentration of 3 mol L^{-1}.

the method for determination trace concentration of Ni ion in real samples.

3.5. Effect of foreign species on the recovery

In the optimum condition, the effects of the foreign ions was investigated on the UA-M-D-μSPE method. The tolerance limit is defined as the concentration that results in a change of ±5% in the recoveries. Accordingly, the results in Table 2 indicate that the common ions with high concentrations in real samples do not have a considerable interference effect on the recovery, and the adsorbent can be used for this method without significant matrix effects.

3.6. Comparison methods with other methods of SPE for separation Ni(II).

In order to demonstrate the efficiency of the method, a comparison was done between the proposed method and the other methods. Table 3 shows the type of nanoadsorbent, method, amount of nanoadsorbent, LOD, RSD, and volume of eluent for the extraction and preconcentration of the Ni (II) ions. The results in Table 3 show that maximum recovery in proposed method in compared with the other method was obtained with the least amount of nanoadsorbent. Also, this method is environmentally friendly due to the low use of an elution solvent. This method is also simple and fast. In addition to, compared with the same methods, our method has a low RSD and also the limit of detection this method is comparable to the other methods presented in Table3 .

4. Conclusions

In this work, g-C_3N_4-$SnFe_2O_4$ adsorbent with a

Table 3. Comparison between EA-DM-μSPE and other published methods.

Adsorbent	Metal	Method	Amount of adsorbent (mg)	LOD (ng.mL^{-1})	RSD (ng.mL^{-1})	Final volume of eluent	Ref.
GO–H_2NP^1	Ni(II))	SPE column /FAAS	40	5.4×10^{-3}	-	5.0 mL	[18]
Ion-imprinted polymers	Ni(II)	SPE column /FAAS	200	0.2	2.5	5.0 mL	[19]
DMG/SDS-ACMNPs^2	Ni(II)	SPE /FAAS	200	4.6	1.9	2.0 mL	[20]
Molecularly imprinted polymers	Ni(II)	SPE column /FAAS	575	0.3	5.0	5.0 mL	[21]
g-C_3N_4-$SnFe_2O_4$	Ni(II)	UA-M-D-μSPE /MS-FAAS	10	1.0	1.4	250 μL	This work

[1] Graphene oxide with covalently linked porphyrin
[2] Dimethylglyoxim/sodium dodecyl sulfate-immobilized on alumina-coated magnetite nanoparticles

good activity was successfully synthesized, and its application was investigated for extraction and preconcentration of the Ni (II) ion using ultrasound-assisted magnetic dispersive micro solid-phase extraction method. Preconcentrated nickel ion was measured with micro sampling flame atomic adsorption spectroscopy.

The most important benefits of this method are: low time (9 min), low volume of eluent (250 µL), and low amount of adsorbent (10 mg). Finally, the results obtained showed that the method had low LODs, a high recovery in a short time, and a good preconcentration factor due to the use of a low amount of eluent for trace amounts of the understudied ions.

5. Acknowledgment

6. Nomenclature

FAAS: flame atomic adsorption spectrometry

ETAAS: electro-thermal atomic adsorption spectrometry

ICP-OES: inductively coupled plasma-optical emission spectrometry

7. References

[1] B. Demmig-Adams, W.W. Adams, Antioxidants in photosynthesis and human nutrition, Science, 298 (2002) 2149-2153.

[2] L. Ren, Y. Hemar, C.O. Perera, G. Lewis, G.W. Krissansen, P.K. Buchanan, Antibacterial and antioxidant activities of aqueous extracts of eight edible mushrooms, Bioact. Carbohydr. Dietary Fibre., 3 (2014) 41-51.

[3] A. Wilkowska, M. Biziuk, Determination of pesticide residues in food matrices using the QuEChERS methodology, Food. Chem, 125 (2011) 803-812.

[4] M. Ghazaghi, H.Z. Mousavi, A.M. Rashidi, H. Shirkhanloo, R. Rahighi, Innovative separation and preconcentration technique of coagulating homogenous dispersive micro solid phase extraction exploiting graphene oxide nanosheets, Anal. chim. acta, 902 (2016) 33-42.

[5] L. Zhang, V. Hessel, J. Peng, Q. Wang, L. Zhang, Co and Ni extraction and separation in segmented micro-flow using a coiled flow inverter, Chem. Eng. J, 307 (2017) 1-8.

[6] A.A. Gouda, S.M. Al Ghannam, Impregnated multiwalled carbon nanotubes as efficient sorbent for the solid phase extraction of trace amounts of heavy metal ions in food and water samples, Food. Chem, 202 (2016) 409-416.

[7] B. Barfi, A. Asghari, M. Rajabi, S. Sabzalian, F. Khanalipoor, M. Behzad, Optimized syringe-assisted dispersive micro solid phase extraction coupled with microsampling flame atomic absorption spectrometry for the simple and fast determination of potentially toxic metals in fruit juice and bio-fluid samples, RSC. Adv, 5 (2015) 31930-31941.

[8] B. Fahimirad, A. Asghari, M. Rajabi, A novel nanoadsorbent consisting of covalently functionalized melamine onto $MWCNT/Fe_3O_4$ nanoparticles for efficient microextraction of highly adverse metal ions from organic and inorganic vegetables: Optimization by multivariate analysis, J. Mol. Liq, 252 (2018) 383-391.

[9] A. Safavi, N. Iranpoor, N. Saghir, S. Momeni, Glycerol–silica gel: a new solid sorbent for preconcentration and determination of traces of cobalt (II) ion, Anal. Chim. Acta, 569 (2006) 139-144.

[10] M. Tuzen, K.O. Saygi, M. Soylak, Novel solid phase extraction procedure for gold (III) on Dowex M 4195 prior to its flame atomic absorption spectrometric determination, J. Hazard. Mater, 156 (2008) 591-595.

[11] K. Vignesh, M. Kang, Facile synthesis, characterization and recyclable photocatalytic activity of $Ag_2WO_4@$ g-C_3N_4, Mater. Sci. Eng. B, 199 (2015) 30-36.

[12] H.-J. Li, B.-W. Sun, L. Sui, D.-J. Qian, M. Chen, Preparation of water-dispersible porous gC 3 N 4 with improved photocatalytic activity by chemical oxidation, Phys. Chem. Chem. Phys, 17 (2015) 3309-3315.

[13] B. Fahimirad, A. Asghari, M. Rajabi, Magnetic graphitic carbon nitride nanoparticles covalently modified with an ethylenediamine for dispersive

solid-phase extraction of lead (II) and cadmium (II) prior to their quantitation by FAAS, Micro, Chim. Acta, 184 (2017) 3027-3035.

[14] M.R. Sohrabi, Z. Matbouie, A.A. Asgharinezhad, A. Dehghani, Solid phase extraction of Cd (II) and Pb (II) using a magnetic metal-organic framework, and their determination by FAAS, Micro. Chim. Acta, 180 (2013) 589-597.

[15] J. Liu, T. Zhang, Z. Wang, G. Dawson, W. Chen, Simple pyrolysis of urea into graphitic carbon nitride with recyclable adsorption and photocatalytic activity, J. Mater. Chem, 21 (2011) 14398-14401.

[16] G. Li, N. Yang, W. Wang, W. Zhang, Synthesis, photophysical and photocatalytic properties of N-doped sodium niobate sensitized by carbon nitride, J. Phys. Chem. C, 113 (2009) 14829-14833.

[17] Y. Jia, D.-H. Kim, T. Lee, S. Kang, B. Lee, S. Rhee, C. Liu, One-pot solvothermal synthesis of magnetic SnFe 2 O 4 nanoparticles and their performance in the photocatalytic degradation of chlortetracycline

with visible light radiation, RSC. Adv, 6 (2016) 76542-76550.

[18] A. Moghimi, M. Alijanianzadeh, R. Pourahmad, Extraction and separation of Ni (II) from by functionalized graphene oxide with covalently linked porphyrin (GOH$_2$NP) adsorbed on surfactant coated C18, Afr. J. Pure Appl. Chem, 7 (2013) 360-369.

[19] M. Saraji, H. Yousefi, Selective solid-phase extraction of Ni (II) by an ion-imprinted polymer from water samples, J. hazard. mater, 167 (2009) 1152-1157.

[20] M.A. Karimi, M. Kafi, Removal, preconcentration and determination of Ni (II) from different environmental samples using modified magnetite nanoparticles prior to flame atomic absorption spectrometry, Arab. J. Chem, 8 (2015) 812-820.

[21] A. Ersöz, R. Say, A. Denizli, Ni (II) ion-imprinted solid-phase extraction and preconcentration in aqueous solutions by packed-bed columns, Anal. Chim. Acta, 502 (2004) 91-97.

Dispersive solid phase microextraction based on amine-functionalized bimodal mesoporous silica nanoparticles for separation and determination of calcium ions in chronic kidney disease

Sara Davari [a], Farnaz Hosseini [a], and Hamid Shirkhanloo [b,*]

[a] *Islamic Azad University of Pharmaceutical Sciences (IAUPS), Medical Nano Technology Tehran, Iran*
[b] *Research Institute of Petroleum Industry (RIPI), West Entrance Blvd., Olympic Village, P.O. Box: 14857-33111, Tehran, Iran*

A B S T R A C T

The ultrasound assisted- dispersive solid phase microextraction method (USA-SPME) was used for in-vitro study on separation/extraction of calcium ions in human blood of chronic kidney disease (CKD). In this procedure, amine-functionalized bimodal mesoporous silica nanoparticle (NH_2-UVM_7) as a solid phase was used for in-vitro separation/extraction of calcium from blood/serum samples. Moreover, a mixture of NH_2-UVM_7 with ionic liquid and acetone (S/IL/Ac) was added to serum/blood sample containing of Ca (II) at pH of 7.3. After ultrasonic bath and centrifuging, NH_2-UVM_7/ IL settled down in bottom of tube, which was extracted Ca (II) ions by binding to amine group ($[Ca]^{2+} \rightarrow : NH_2 - UVM_7$). The concentration of Ca (II) was determined by flame atomic absorption spectrometry (F-AAS, N_2O, C_2H_2) after back extraction remained adsorbent in IL by 0.5 mL of HNO_3 (0.5 M). The results showed us, the NH_2-UVM_7 is a powerful adsorbent for decreasing and controlling of high level calcium concentration in human body and can be used for in vivo study on decreasing calcium concentration in hypercalcemia patient with CKD. The capacity absorption of NH_2- UVM_7 in blood and water samples was obtained 258.5 mg g^{-1} and 267.2 mg g^{-1} at room temperature (25°C). The characterization of NH_2-UVM_7 (SEM, TEM, FTIR and XRD) and comparisons between proposed method and previous methods showed us, the NH_2-UVM_7 as effectiveness sorbent for decreasing calcium concentration level in blood of hypercalcemia patients. Validation of methodology was confirmed using standard reference material (NIST, SRM). Finally, the LOD and %RSD was obtained 3.0 mg L^{-1} and 3.6, respectively.

1. Introduction

Calcium is essential element for bones and teeth in body. It is also important role in heart function, blood clotting, and muscle functioning. Calcium levels increase in patients with kidney disease. Raised calcium levels cause headaches, nausea, sore eyes, aching teeth, itchy skin, and confusion. Calcium (Ca) as a mineral has important role in human body such as; bones, teeth, and nerves. The kidneys keep calcium at normal levels in blood.

Also, the vitamin D is important factor for calcium balance in blood serum and kidneys help to activate vitamin D. Chronic kidney disease (CKD) caused to renal failure and hypercalcemia in human. (Normal range: 84–102 mg/L or 2.2–2.5 mmol/L). Hypercalcemia has a positive chronotropic effect on decreasing of heart rate and a positive inotropic effect on increasing of contractility [1, 2]. In CKD, the kidneys are not able to keep the levels of calcium at healthy levels, start to failure and increase parathyroid hormone. So, it is very important that blood calcium level determined

correctly. In parathyroid surgery for removal of glands, blood calcium and phosphate levels must be checked [3-7]. Different techniques, including spectrophotometry, flame atomic absorption spectrometry (F-AAS), inductively coupled plasma (ICP), inductively coupled plasma mass spectrometry (ICP-MS), inductively coupled plasma optical emission spectrometry (ICP-OES), and other spectrometry methods were used for determination calcium in human biological samples [8-12]. In recent years, many methods have been used for sample preparation in biological samples, such as microwave digestion coupled with ICP-MS, liquid liquid microextraction (LLME), micro solid phase extraction (MSPE) based on nanomaterials, and ionic liquid-solid phase extraction (IL-SPE) for improving of metal extraction[13-16]. Nowadays, IL-SPE has efficient recovery for metal extraction in blood samples. In addition, many carbonaceous materials such as activated carbons [17], natural Adsorbents [18], fullerenes [19], carbon nanotubes [20], and graphene [21, 22] have used for extraction/separation due to their unique properties, such as nano particle size, high surface area, and adsorption capacity [23].

The mesoporous silicate nanoparticles (MSNPs) have been used for a large reactants inside the pores. The properties of MSNPs have simply accessed to sulfur/amine/carboxylate functional groups on surface structure. The Nano mesoporous silica have high surface area and physical adsorption as compared to MSM. The properties of MSNPs have been investigated in metal extraction/separation in biological and water samples by biotechnology. In addition, MSNPs as adsorbents have large surface area and high adsorption capacity for removal of metals from human body such as urine, blood, and plasma. The bimodal of mesoporous silica nanoparticles (UVM$_7$) are an interesting material which can be considered as an special sorbent for extraction of metals in blood samples[24-28]. In

this work, a new applied method based on NH$_2$-UVM$_7$ as a nano adsorbent was used for calcium extraction/separation in human blood samples by USA-SPME. To the best of our knowledge, there are no reports on decreasing calcium concentration level in patient with renal failure and hypercalcemia.

2. Experimental

2.1. Reagents and Instrumental

The experiments were performed using a GBC-932 flame atomic absorption spectrometer equipped with an auto-sampler instrument (F-AAS, Dandenong, Victoria, Australia). A hollow cathode lamp of calcium operated at a current of 15 mA and a wavelength of 239.9 nm with a spectral band width of 0.5 nm and deuterium background corrector was applied (100-760 mg L^{-1}). Chemical interferences were seen for air acetylene for calcium determination. For improving of interferences strontium/lanthanum (2000 mgL^{-1}) was added to solution samples. All analytical grade of reagents such as HNO3, Hcl, H2SO43, NaOH, buffers, lanthanum solution (0.5 %), tetraethyl ortho-silicate, triethanolamine , cetyltrimethylammonium bromide and triethoxysililpropylamine were purchased from Merck Company (Germany). In a 1000 mL volumetric flask, add 50 mL deionized water to 1.249 g anhydrous calcium carbonate (CaCO$_3$). Dissolve by adding dropwise 10 mL concentrated hydrochloric acid (HCl). Dilute to 1 liter with deionized water. This standard stock solution is 1000 mg Ca^{2+}/L.

2.2. Synthesis of NH$_2$-UVM$_7$

The general procedure for synthesis of bimodal mesoporous silica nanoparticle (UVM$_7$) is the atrane route, in which the presence of the polyalcohol is the key to balancing the hydrolysis and condensation reaction rates. In a typical synthesis, TEOS (tetraethyl ortho-silicate) was added to predetermine amounts of TEAH^3 (triethanolamine). The solution was heated up to 140 °C under

vigorous stirring. After cooling down to 90 °C, CTAB (cetyltrimethylammonium bromide) was added to this solution. For the functionalization of calcined UVM_7 with amine groups, 1.2 g of triethoxysililpropylamine ($C_9H_{23}NO_3Si$) and 2 g of calcined UVM_7 were added to appropriate amount of toluene and refluxed for 24 h at 80 °C [14]. The amine-functionalized bimodal mesoporous silica nanoparticle (NH_2-UVM_7) was used for extraction calcium ions from blood and serum samples.

2.3. Human Sample preparation
For sample preparation of blood/serum samples, only 0.2 mL of samples diluted with DW up to 10 mL and used as real sample. The people of this study selected in two groups: the biological samples from normal men (control groups, 20 N) and renal failure with hypercalcemia as a subject men (n=20). The subject and control groups was selected from men which was matched from people of the same age. For sampling, all glass tubes were washed with a 1.0 mol L^{-1} of HNO_3 solution for at least 24 h and thoroughly rinsed 15 times with ultrapure water before we use. The calcium concentrations in healthy human such as, whole blood / serum have a range from 8.4 to 10.2 mg dL^{-1}. Even minor contamination at any stage of sampling, sample

storage and handling, or analysis has the potential to affect the accuracy of the results. In this study, only 0.2 mL of blood/serum samples were collected from dialysis patients and healthy matched controls which were aged between 30 to 60 years. Separate and disposable sterilized plastic syringes were used for human blood sampling. Based on world medical association declaration of Helsinki and recommendations guiding physicians in biomedical research and human Laboratory, the sample storage and blood/urine sampling was prepared based on principles of Helsinki law and absolutely protect the life and health of the human subject. [29]. For analysis of whole blood samples, 10 μL of pure heparin liquid (free Ca, Germany) is added to 10 mL of sample by auto sampler and used 0.2 mL for proposed procedure. By proposed method, the analysis of blood samples can be obtained with minimum of sample (0.2 mL) which was diluted by DW up to 10 mL(DF=50). The human blood/urine sample was maintained at –20 °C in a cleaned glass tube without any reagents.

2.4. Characterizations of NH_2-UVM_7
The SEM was performed to illustrate the morphology and particle size distribution of the calcined NH_2- UVM_7. TEM image also illustrates
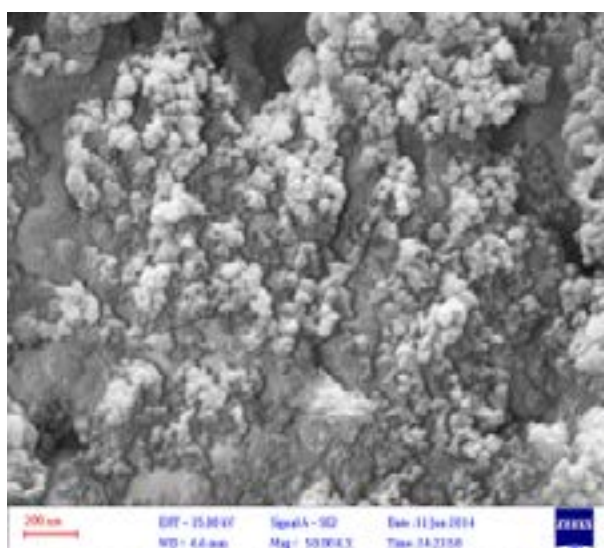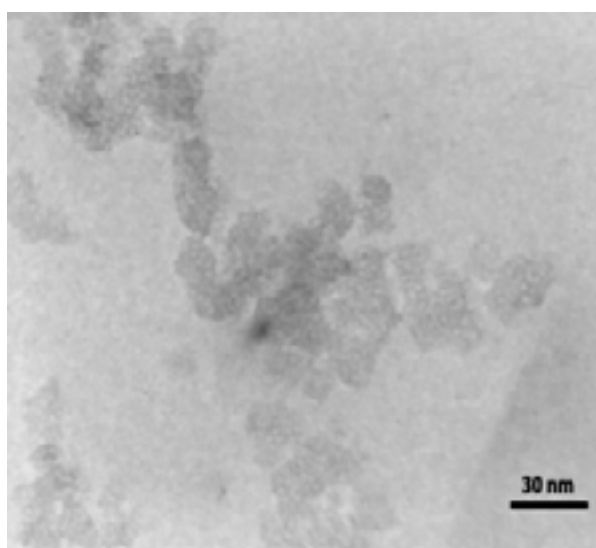

Fig. 1a. SEM of NH_2-UVM_7

Fig. 1b. TEM of NH_2-UVM_7
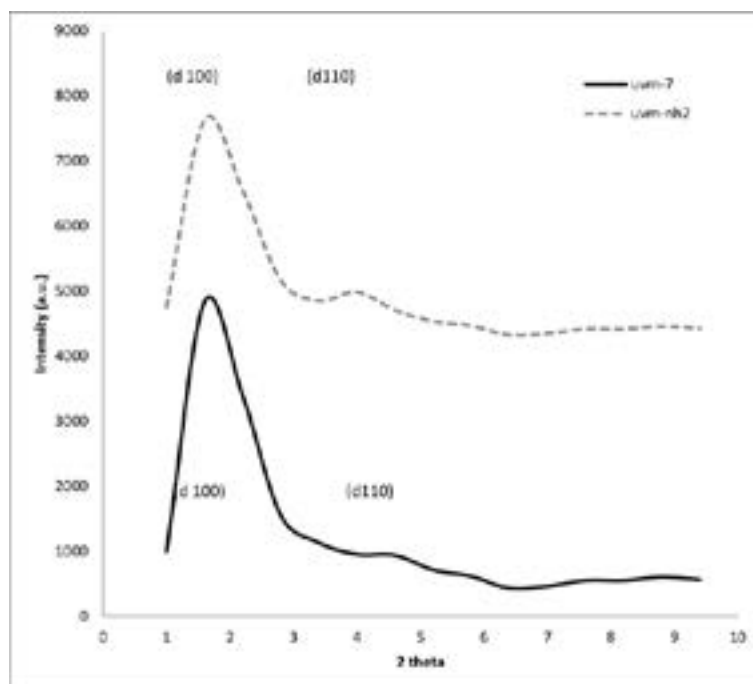
Fig. 2. XRD of UVM$_7$ and NH$_2$-UVM$_7$

pore structure of NH$_2$- UVM$_7$ (Fig 1a and 1b). XRD patterns of calcined UVM$_7$ and NH$_2$-UVM$_7$ are shown in figure 2. There are three resolved diffraction peaks in XRD patterns of NH$_2$-UVM$_7$ and UVM7, which can be indexed as the (100), (110), (200) and (210) reflections associated with hexagonal symmetry (Fig.2). The nitrogen adsorption-desorption isotherms of UVM$_7$ and NH$_2$-UVM$_7$ were determined and displayed. The corresponding isotherm of both samples displays two distinct regions at medium and high relative pressure which can be attributed to the presence of bimodal pore system. The first is related to the presence of small mesopores (IUPAC clacification), and the second is related to the large mesopores (Fig.3).

2.5. General procedure

In this procedure, 10 mL of standard solution and human blood /serum sample containing calcium ions was used for extraction/separation of calcium. The pH was adjusted to 7.5 with buffer solutions. The amine group of NH$_2$-UVM$_7$ (5 mg) as a complexing agent was dispersed in 1-Butyl-4-methylpyridinium hexafluorophosphate [BMPy]

[PF$_6$] (IL/Ac, 0.2 mL) and injected to human serum samples for separation/extraction of Ca ions. The solution place in ultrasound bath for 5 min and Ca^{2+} were complexed and efficient preconcentrated/ extraction by amine group of NH$_2$-UVM$_7$ at optimized pH. After shaking, the sample was centrifuged for 5 min and S/IL/Ac settled down in bottom of tube, which was extracted Ca (II) ions by binding to amine group ([Ca]$^{2+}$ →: NH$_2$ — UVM$_7$). Finally, the settled phase was back extracted by 0.5 mL of HNO3 (0.5 M), diluted up to 1 mL with DW and determined by F-AAS. In addition in 1-Butyl-4-methylpyridinium hexafluorophosphate [BMPy] [PF$_6$] (IL/Ac, 0.2 mL) can be extracted calcium from blood samples up to 6.8% (Fig.4). Extraction conditions of calcium with proposed method was shown in table 1.

4. Results and Discussions:

4.1. Effect of pH

In this work, the influence of sample pH on absorption of Ca (II) has been investigated using different pH from 2 to 12 for 10-75 mg L^{-1} of calcium standard and 0.2 mL of blood samples.
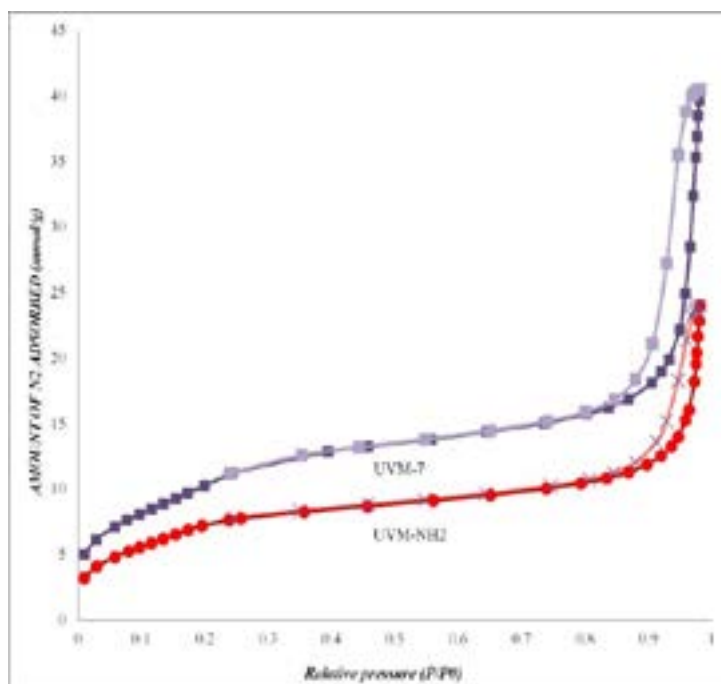
Fig. 3. The isotherms of UVM_7 and NH_2-UVM_7

Table 1. Extraction conditions of calcium with proposed method

Parameter	Value
Working pH	7.50
Amount of NH_2-UVM_7	5.00 mg
Sample volume of blood and serum	0.20 mL
Volume of sample injection	1.00 mL
working range (blood)	9.80-75.90 mg L^{-1}
Linear range (Urine)	10- 50 mg L^{-1}
Intra-day precision (RSD %, n=10)	3.60
Inter-day precision (RSD %, n=10)	4.20
Limit of detection of blood (LOD)	3.00 mg L^{-1}
Preconcentration factor blood (PF)	10.20
Buffer concentration	0.03 mol L^{-1}
Volume and concentration of back-extraction solvent (HNO_3)	500 μL and 0.50 mol L^{-1}
Correlation coefficient	$R^2 = 0.9995$
Ionic liquid/acetone	0.20 mL

The buffer were used for adjusting between pH=7 to 7.7. The complexation was strongly conditioned by the pH of solutions and subsequently affects extraction efficiency of the complex. The result shows that the highest extraction efficiency for Ca (II) was achieved from pH 7.5 (Fig. 5).

4.2. Effect of sample volume

Sample volume one of the most important parameters to be studied. The effect of sample volume was examined in the range of 1-50 mL for 10-50 mg L^{-1} of Ca (II). Quantitative extraction was observed between 1 - 15 mL. At higher
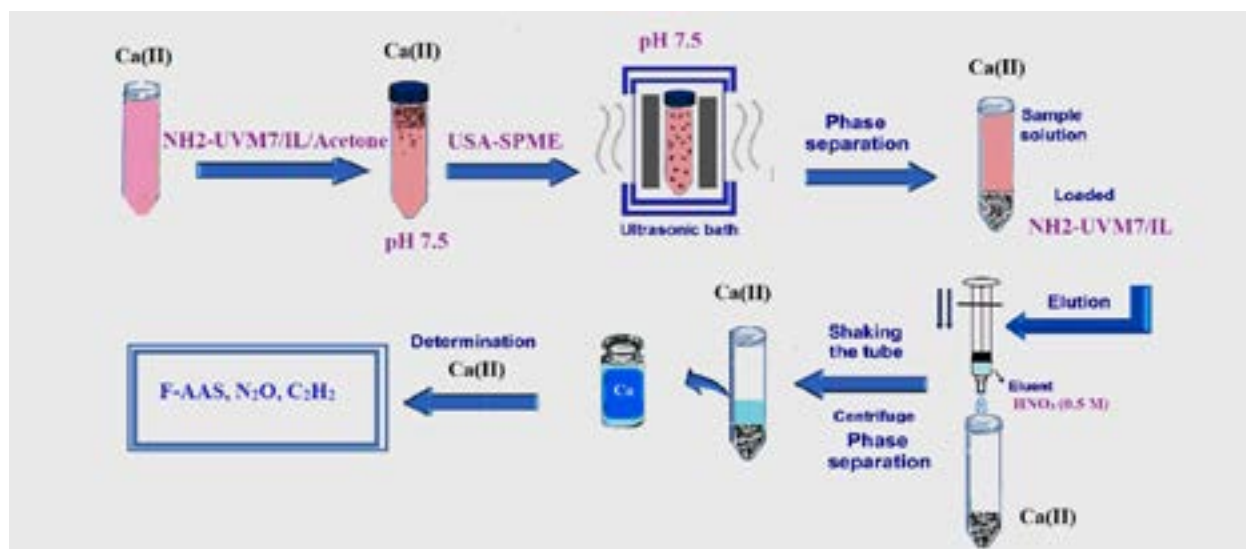
Fig. 4. The procedure of extraction/separation of calcium by USA-SPME

volumes the recoveries are decreased. Therefore, a sample volume of 10 mL was selected for further experiments of USA-SPME in standard and blood samples (Fig. 6). As a consequence, the volume required to back extraction of Ca (II) ions from NH_2-UVM_7 depends on the strength of Ca (II) retention and amount of NH_2-UVM_7 were used in USA-SPME.

4.3. Effect of amount of adsorbent

In optimized conditions, 0.2 mL of blood samples, pH of 7.5 for 10 mL of sample volume, the effect of amount of sorbent was evaluated. It was observed that extraction efficiency of the system was remarkably affected by NH_2-UVM_7 amount in blood samples, so it was examined within the range of 1–15 mg. Quantitative extraction was observed at higher than 4 mg by USA-SPME. Therefore, in order to achieve a suitable preconcentration, 5 mg of NH_2-UVM_7 was chosen as optimum leading to a final adsorbent (Fig. 7). Because of high surface of nano-adsorbent (S/V) a very little amount of NH_2-UVM_7 were used.
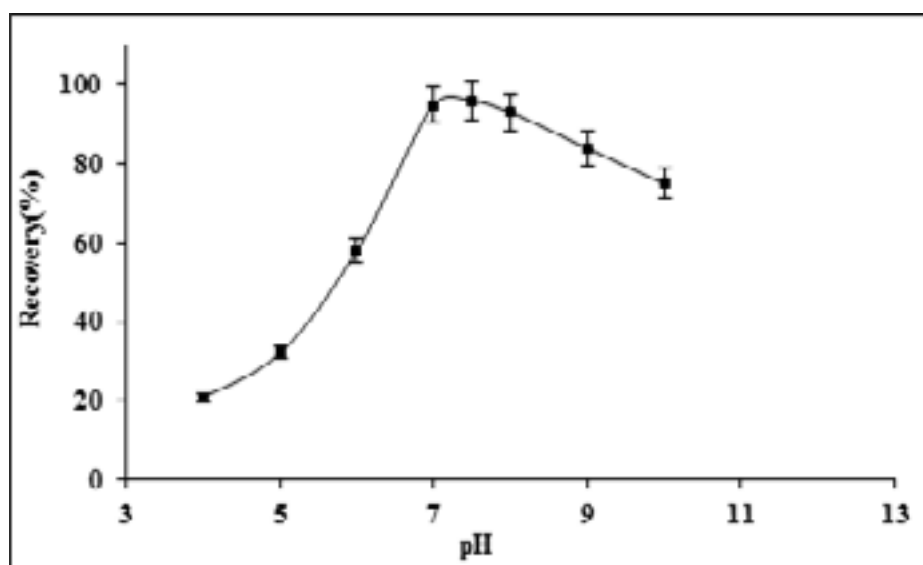
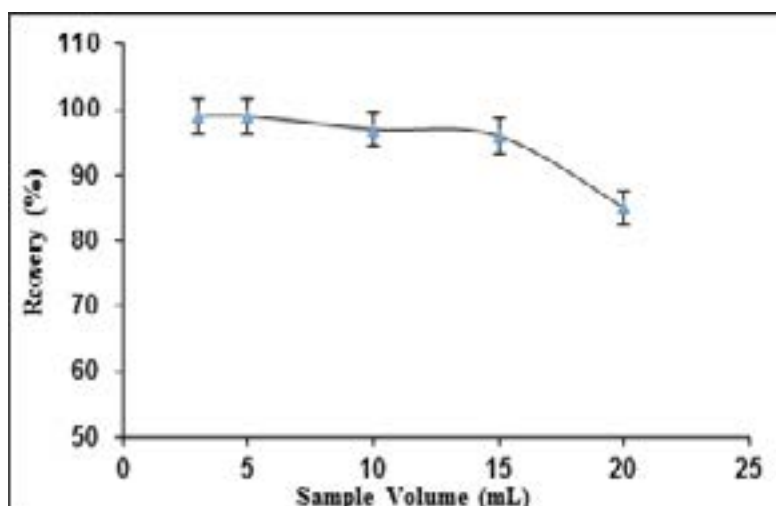**Fig. 5.** The influence of sample pH on absorption of Ca (II) by USA-SPME

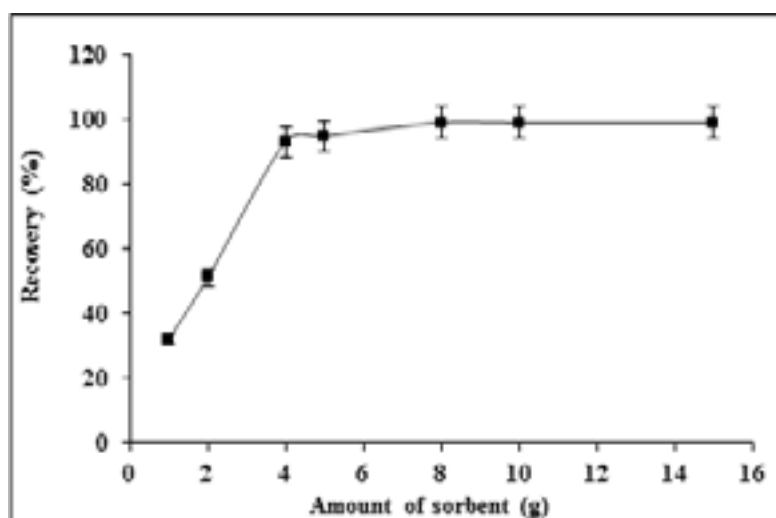**Fig. 6.** The influence of sample volume on absorption of Ca (II) by USA-SPME

Fig. 7. The influence of amount of sorbent on absorption of Ca (II) by USA-SPME

4-4 Effect of matrix

FAAS is a very simple method with low interference for determination calcium in human body. By USA-SPME, the interference of some coexisting ions in blood and serum samples on the recovery of Ca (II) ions was evaluated for optimized parameters. The interference of coexisting ions effected on pre-concentration step by proposed method. The typical ions in blood and serum samples such as cofactors of Mg, Cu, Zn, Fe, Mn, Cr, Na, K, and Co which was interfered on calcium extraction were investigated. The proposed procedure was performed using a 10 mL sample containing 10-50 mg L^{-1} of analyte and 1— 5 g L^{-1} of different

concentration of matrix ions. The tolerate amounts of each ion were tested that caused less than 7% of the absorbance alteration. In optimized conditions, the ions such as, Zn^{2+}, Cu^{2+}, Cr^{3+}, Co^{2+}, Mn^{2+}, Mg^{2+}, Na^+, K^+, Fe^{2+} and Mg^{2+} do not interfere to lead extraction by USA-SPME procedure (less than 7%). On the other hand, tolerable concentration ratio of interfering ions versus Ca(II) ions for Ni^{2+}, HCO_3^-, SO_4^{2-} and CO_3^{2-}, NO_3^- , PO_4^{3-} , Br, Cl^- , F^- was less than 360 and 520, separately. The tolerable concentration ratio of interfering ions versus Ca(II) ions for Hg and Ag was obtained less than 45. The results showed us, the most of the probable concomitant cations and anions have no

Table 2. Effect interfering ions on the recovery of Ca (II) ions by USA-SPME procedure

Foreign Ions	Concentration ratio ($C_{interferent\ ions}/C_{Ca^{2+}}$)			Mean of Recovery (%)		
	Standard	Blood	serum	Standard	Blood	Plasma
Zn^{2+}, Cu^{2+}, Cr^{3+}, Co^{2+}, Mn^{2+}	1100	950	900	97.2	95.1	96.8
Mg^{2+}, Na^+, K^+, Fe^{2+}, Mg^{2+}	1200	1000	800	98.4	97.1	99.5
CO_3^{2-}, NO_3^-, PO_4^{3-}, Br^-, Cl^-, F^-	700	520	470	97.7	98.2	98.9
Ni^{2+}, HCO_3^-, SO_4^{2-}	450	360	320	96.2	95.0	97.3
Hg^{2+}, Ag^+	60	45	40	95.4	96.2	95.8

considerable effect on the recovery efficiencies of lead ions (Table 2).

4.5 Method Validation

The USA-SPME method based on NH_2-UVM_7, were applied to determine Ca (II) in water samples. The spiked samples were prepared to demonstrate the reliability of the method for determination of Ca (II). The remaining aliquots were spiked with increasing quantities of Ca (II) and then analyzed by the proposed method (Table 3). The recoveries of spiked samples are satisfactorily reasonable and were confirmed by using the additional method, which indicates the capability of the system in the determination of Ca (II) in standard and human blood samples (0.2 mL). Also, the results showed that the Ca (II) concentrations in blood samples ranged from 11.63- 15.17 mg L^{-1} and 8.58 − 10.76 µg L^{-1} in the renal failure subjects and control samples, respectively (Table 4). The intra mean concentration of Ca (II) in serum of hypercalcemia subjects (12.45 ± 0.59 µg L^{-1}) was significantly higher than healthy men controls (8.95 ± 0.44 µg L^{-1}) (P< 0.001). Also, total value of calcium in blood of hypercalcemia subjects is higher than the normal groups which were recommended by standard value of human biochemistry. The results showed that the Ca (II) concentrations in blood samples of hypercalcemia subjects (20N) were higher than in controls groups. There is no correlation between control and subject groups were achieved (r ≈ 0.1).

5. Conclusions:

In this method, NH_2-UVM_7 nano-particles were

Table 3. Validation of calcium determination with FAAS by Ca (II) standard addition in human blood and water samples (mg L^{-1})

Sample	Added	Found [*]	Recovery (%)
[a]Blood	---	15.2± 0.6	---
	15.0	29.8 ± 0.7	98.0
[a]Blood	---	19.4 ± 0.8	---
	20.0	40.1 ± 1.7	103.3
[a]Blood	---	14.3 ± 0.6	---
	15.0	28.8 ± 0.8	96.6
wastewater	---	6.3 ± 0.3	---
	5.0	11.1 ± 0.5	96.0
Water	---	2.2 ± 0.1	---
	2.0	4.3 ± 0.3	105
Waste water	---	10.6 ± 0.1	---
	10.0	20.3 ± 0.1	97.0

[*]Mean of three determinations ± confidence interval (P = 0.95, n =5)
[a] 0.2 mL of blood samples diluted with DW up to 10 mL (DF:50)

Table 4. determination of calcium in serum, blood and urine by USA-SPME method (intra –day and inter day) (mg dL^{-1})

Sample	Hypercalcemia Men (n=20)		Healthy Men (n=20)		Hypercalcemia	
	Intra-day	Inter day	Intra-day	Inter day	r	*P value*
Serum	12.45 ± 0.59	12.62 ± 0.64	8.95 ± 0.44	9.08 ± 0.51	0.113	*<0.001*
Plasma	7.94 ± 0.46	8.02 ± 0.52	6.32 ± 0.32	6.53 ± 0.48	0.102	*<0.001*
Blood	13.04 ± 0.63	13. 27 ± 0.68	10.06 ± 0.48	9.87 ± 0.55	0.117	*<0.001*

*Correlations are based on Pearson coefficients (r). Statistical significance will be observed if $P < 0.001$
Mean of three determinations of samples ± confidence interval (P = 0.95, n =10)

used as a solid phase for extraction and separation of Ca (II) by USA-SPME. The developed method has the advantages of simplicity, relative selectivity, and high preconcentraion factor for Ca (II). A small amount of adsorbent, low volume of sample (0.2 mL) is employed in this procedure. The determination of Ca (II) in blood and environmental samples was successfully performed. The LOD, preconcentration factor, working range, and dilution factor for human samples was obtained 3.0 mg L^{-1}, 10.2, 9.8-75.9 mg L^{-1} and 50 respectively.

6. Acknowledgment

7. References:

[1] K.M. Gallant, D.M. Spiegel, Calcium balance in chronic kidney disease, Curr. Osteoporos. Rep., 15 (2017) 214-221.

[2] P.H.F. Gois, D. Ranganathan, A. C. segura, Vitamin D deficiency in chronic kidney Disease: recent evidence and controversies, Int .J. Environ. Res. Public Health, 15 (2018) 1773-1780.

[3] P.H.F. Gois, D Ferreira, S. Olenski, A.C. Seguro, Vitamin D and infectious diseases: simple bystander or contributing factor, Nutrients, 9 (2017) 651.

[4] G. Jean, J.C. Souberbielle, C. Chazot, Vitamin D in chronic kidney disease and dialysis patients, Nutrients, 9 (2017) 328.

[5] J. Blaine, M. Chonchol, M. Levi, Renal control of calcium, phosphate, and magnesium homeostasis, Clin. J. Am. Soc. Nephrol., 10 (2015) 1257-1272.

[6] M. Brini, D. Ottolini, T. Calì, E. Carafoli, Calcium in Health and Disease: Interrelations between essential metal ions and human diseases, Metal ions in life sciences, Chapter 4, Springer Netherlands (2013).

[7] J. Lappe, P. Watson, D. Travers-Gustafson, Effect of vitamin D and calcium supplementation on cancer incidence in older women: a randomized clinical trial, JAMA, 317.12 (2017) 1234-1243.

[8] B. S. F. Alves, F. I. M. Carvalho, A.S. Cruz, K. G. F. Dantas, Determination of Ca, Mg, Na, and K in biodiesel of oilseed from northern Brazil, Revista Virtual de Quimica, 10 (2018) 542-550.

[9] L. Poirier, J. Nelson, D. Leong, L. Berhane, P. Hajdu, F. Lopez-Linares, Application of ICP-MS and ICP-OES on the determination of nickel, vanadium, iron, and calcium in petroleum crude oils via direct dilution, Energy and Fuels, 30 (2016) 3783-3790.

[10] B. Han, M. Ge, H. Zhao, Y. Yan, J. Zeng, T. Zhang, W. Zhou, J. Zhang, J. Wang, C. Zhang, Determination of serum calcium levels by 42Ca isotope dilution inductively coupled plasma mass spectrometry, Clin. Chem. Lab. Med., 56 (2017) 51-58.

[11] Y. Yan, M. Ge, R. Ma, H. Zhao, D. Wang, C. Hu, et al, A candidate reference method for serum calcium measurement by inductively coupled plasma mass spectrometry, Clin. Chim. Acta, ٤٦١ (٢٠١٦) ١٤١- ١٤٥.

[12] S. Li, J. Wang, Measurement of Calcium in human serum by dynamic reaction cell and two-way ID–ICP–MS, Chem. Anal. Meter., 24 (2015).

[13] J. Płotka-Wasylka, M. Frankowski, V. Simeonov, Ż. Polkowska, J. Namieśnik, Determination of metals content in wine samples by inductively coupled plasma-mass spectrometry, Molecules, 23 (2018) 2886.

[14] H. Shirkhanloo, M. Ghazaghi, A. Rashidi, A. Vahid, Arsenic speciation based on amine-functionalized bimodal mesoporous silica nanoparticles by ultrasound assisted-dispersive solid-liquid multiple phase microextraction, Microchem. J., 130 (2017) 137-146.

[15] H. Zhang, Y. Yuan, Y. Sun, C. Niu, F. Qiao, H. Yan, An ionic liquid-magnetic graphene composite for magnet dispersive solid-phase extraction of triazine herbicides in surface water followed by high performance liquid chromatography, Analyst, 143 (2018) 175-181.

[16] A.C. Sotolongo, E.M. Martinis, R.G. Wuilloud, An easily prepared graphene oxide–ionic liquid hybrid nanomaterial for micro-solid phase extraction and preconcentration of Hg in water samples, Anal. Method., 10.3 (2018) 338-346.

[17] I. García-Díaz, F. López, F. Alguacil, Carbon Nanofibers: A New Adsorbent for Copper Removal from Wastewater, Metals, Metals, ٨ (٢٠١٨) ٩١٤.

[18] R. Pournima, M. Shrikant, A short overview: Heavy metal toxicity, health hazards and their removal technique by natural adsorbents, Inter. J. Curr. Eng. Technol., 8 (2018) 400-406.

[19] E. Ciotta, P. Prosposito, P. Tagliatesta, C. Lorecchio, L. Stella, S. Kaciulis, P. Soltani, E. Placidi, R. Pizzoferrato, Discriminating between different heavy metal ions with fullerene-derived nanoparticles, Sensors, 18 (2018) 1496.

[20] Z.A. Alothman, S.M. Wabaidur, Application of carbon nanotubes in extraction and chromatographic analysis: A review, Arab. J. Chem. (in press 2018). https://doi.org/10.1016/j.arabjc.2018.05.012

[21] M. Rosillo Lopez, C.G. Salzmann, Highly efficient heavy-metal extraction from water with carboxylated graphene nanoflakes, RSC. Adv., 8 (2018) 11043-11050.

[22] K.C.M.S. Lima, A.C.F. Santos, R.N. Fernandes, F.S. Damos, R.D, Luz, *Development* of a *novel sensor* for isoniazid based on ٢,٣-dichloro-٥,٦-dicyano-p-benzoquinone, Microchem. J., 128 (2016) 226-234.

[23] D.R. Dreyer, S. Park, C.W. Bielawski, R.S. Ruoff, The chemistry of graphene oxide, Chem. Soc. Rev., 39 (2010) 228-240.

[24] J.P. Thielemann, F. Girgsdies, R. Schlögl, C. Hess, Pore structure and surface area of silica SBA-15: influence of washing and scale-up, Beilstein. j.

nanotechnol., 2 (2011) 110-118.

[25] X. Xue, F. Li, Removal of Cu (II) from aqueous solution by adsorption onto functionalized SBA-16 mesoporous silica, Micropor. Mesopor. Mater., 116 (2008) 116-122.

[26] J. El Haskouri, J.M. Morales, D. Ortiz de Zárate, L. Fernández, J. Latorre, C. Guillem, A. Beltrán, D. Beltrán, P. Amorós, Nanoparticulated silicas with bimodal porosity: chemical control of the pore sizes, Chem., 47 (2008) 8267-8277.

[27] J. Mo, L. Zhou, X. Li, Q. Li, L. Wang, Z. Wang, On-line separation and pre-concentration on a mesoporous silica-grafted graphene oxide adsorbent coupled with solution cathode glow discharge-atomic emission spectrometry for the determination of lead, Microchem. J., 130 (2017) 353-359.

[28] S. Bayir, A. Barras, R. Boukherroub, S. Szunerits, L. Raehm, S. Richeter, J.O. Durand, Mesoporous silica nanoparticles in recent photodynamic therapy applications, Photochem. Photobiol. Sci., 17.11 (2018): 1651-1674.

[29] World medical association declaration of Helsinki, Ethical Principles for Medical Research Involving Human Subjects, Adopted by the 18th WMA General Assembly, Helsinki, Finland, June (1964). http://www.wma.net/en/30publications/10policies/b3

Analytical Methods: Electrochemical azido-selenenylation of some olefins by cyclic voltammetry and controlled-potential coulometry

Ahmad Rouhollahi [a],*, Zeenat Asghari[a], and Barahman Movassagh[a]

[a]*Chemistry Department, Faculty of Science, K.N. Toosi University of Technology, Tehran 15418, Iran.*

A B S T R A C T

Electrochemical azido-phenylselenenylation of some olefins was studied with the oxidation of diphenyl diselenide in the presence of some olefins and sodium azide in dimethyl formamide containing tetra butyl ammonium perchlorate as supporting electrolyte in an H-type cell. The electrochemical oxidation of the mixture of $(PhSe)_2$, olefins, and NaN_3 was studied by cyclic voltammetry and controlled-potential coulometry. Anti product can be obtained with Markovnikov orientation. This product was characterized by ^1H, ^{13}C NMR, and IR spectroscopy.

1. Introduction

Selenium is a biologically essential element for all vertebrates. A number of organoselenium compounds have been found in living tissue: Selenocoenzyme A, Selenobiotine, Se-methyl Selenomethionine, Selenosystathione, Selenohomocystine, Selenocystine, Selenomethionine, etc. Moreover, Selenium is also known to help prevent cancer and cardio-vascular diseases [1-7]. Despite the similarities between sulfur containing molecules and their selenium congeners, there are several unique features of organoselenium compounds. They can be used in nucleophilic, in electrophilic, as well as in radical reactions [8]. Organoselenium compounds have found applications as oxygen transfer reagents in organic and organometallic synthesis and as oxygendonor ligands in main and transition metal complexes [9]. Also, diselenides are known as mediators, redox catalyst and important precursors in organic electrosynthesis. It is evident that investigations of reactivity and redox mechanisms of organic Selenium compounds are of great importance today. Diaryl diselenide themselves can serve in electrosynthesis

as mediators in indirect electrolyses of organic compounds, as redox catalysts for reduction of protons, oxidation of water or derivatization of olefins, as a trap for new complexes [1]. The chemistry of organoselenium compounds has been extensively investigated because of their utility in organic synthesis [2, 10-12]. The reaction of carbon-carbon double bonds with selenium electrophiles is performed under mild reaction conditions and the reaction products can be used in a variety of subsequent functionalizations [12]. It is well established that addition to unsymmetrical olefins initiated by electrophilic phenylselenium species proceeds through the formation of seleniranium intermediates which, in the presence of external or internal nucleophiles, usually affords anti adducts with prevalent Markovnikov orientation [13]. In addition, the phenylseleno group is an important functionality in organic synthesis because it can be easily introduced into and removed from unsaturated compounds [2, 14]. The products obtained from the azido-selenenylation of alkenes contain the phenylseleno and azido groups which can be used for several conversions [15]. Electrosynthesis is the optimal method for carrying out redox reactions, because it works at normal temperature and has the following advantages [16, 17]. Also, organic electrosynthesis is not a new technique, and there is considerable knowledge of the types of reactions which take place at cathodes and anodes. One view of organic electrochemistry is that it is a unique non-thermal method for activating molecules .Since the rate of reaction can normally be increased by raising the electrode potential, it is possible to carry out reactions with high activation energy at low temperature. Another view is that electrochemistry is an alternative to chemical redox methods [18]. There are several works of phenylseleno group›s versatility, including the alkoxylation of alkenes [19], carbonyl compounds [20], and fluoriation of alkenes [21]. Electrochemical cyclization of unsaturated hydroxyl compounds containing phenylselenoetherification and phenylselenolactonization have been reported [22]. In several papers, diphenyl diselenide is used as a catalyst for electrosynthesis of many organic compounds [12, 14].

In the present work, the electrochemical oxidation of diphenyl diselenide in the presence of some olefins and NaN_3 was examined by cyclic voltammetry and controlled-potential coulometry. The electrochemical generation of phenylselenenyl cation followed the formation of anti adduct by a Markovnikov reaction. The final product was purified by preparative thin layer chromatography and characterized by ^{1}H NMR, ^{13}C NMR, and IR spectroscopy.

2. Experimental Procedure

2.1. Instruments

Cyclic voltammetry and controlled-potential coulometry was performed with an Autolab potentiostat/galvanostat, PGSTAT 30 (Eco Chemie, Utrecht, The Netherlands).

The set-up was used a three-electrode cell with a platinum disc (2 mm diameter) as the working electrode, a saturated Ag/AgCl double junction reference electrode, and a platinum wire as the auxiliary electrode. A platinum rod with a diameter (mm) and length (cm) as working electrode was used in controlled-potential coulometry. The working electrode potential was followed vs. Ag/AgCl double junction reference electrode (from Azar electrode, Iran). Electrosyntheses have been carried out both undivided and divided cells. NMR spectra were recorded on a Bruker AQS-300 Avance Instruments. Thin layer chromatography (TLC) was performed on plastic sheets pre-coated with silica-gel (Merck), and spots were visualized with UV light and iodine tank.

2.2. Chemicals and reagents

Diphenyl diselenide, cyclohexene, 1-octene, 1-heptene, styrene, and sodium azide were obtained

from Merck. Tetra butyl ammonium per chlorate (TBAP) and cyclooctene were purchased from Fluka. Dimethyl formamide was prepared from Aldrich.

2.3. Experimental procedure

The $(PhSe)_2$ (0.3 mmol) and excess of olefins and NaN_3 are dissolved in 20 ml dimethyl formamide. Organic solution is contained 1.5 mmol of TBAP as supporting electrolyte. Constant potential electrolysis of the solution was performed in an H-type divided cell under an air atmosphere at room temperature. Constant potential was chosen 1.96 mV (Vs. Ag/AgCl). The electrolysis was terminated when the current decayed to 90% of initiated current. The progress was monitored by cyclic voltammograms and TLC in different times of reaction. At the end of electrolysis, extraction of the cell solution, afforded an organic phase which its solvent is evaporated. Then, the residue purified by preparative thin layer chromatography over silica gel (eluent was a mixture of n-hexane/ ethyl acetate). The product was characterized by ^{1}H NMR, ^{13}C NMR, and IR spectroscopy.

2.4. Characteristics of products

2.4.1. 1-phenylseleno -2-(azido)cyclohexane

IR (neat) (v_{max},cm[-1]) : 2095 (N=N-N-), 1576, 1468, 1263 (=C-H aromatic), 982, 860, 835 and 754 cm^{-1}. ^{1}H NMR, δ (300 MHz, $CDCl_3$): 7.63-7.5 (m,2H), 7.33-7.25(m, 3H), 3.3(dd, 1H, J=7.9 and 12.6Hz), 3.08(dd, 1H, J=6.5 and 12.6Hz), 2.15-1.26(m, 8H). ^{13}C –NMR, δ (75 MHz, $CDCl_3$): 135.8, 134.7, 129.1, 128.0, 127.7, 127.5, 64.5, 33.0, 31.8, 29.7, 25.8, 21.6.

2.4.2. 1-azido-1-phenyl-2-(phenylseleno)ethane

IR (neat) (v_{max}, cm[-1]) : 2103(N=N-N-), 1660(C=C), 1585, 1476, 1268 (=C-H aromatic), 985, 872, 841 and 764 cm^{-1}. ^{1}H NMR, δ (300 MHz, $CDCl_3$): 7.60-7.40 (m, 2H), 7.40-7.15(m, 8H), 4.26(dd, 1H, J=6.5 and 7.9 Hz), 3.23(dd, 1H, J=7.9 and 12.6 Hz),

3.18(dd, 1H, J=6.5 and 12.6 Hz). ^{13}C NMR, δ (75 MHz, $CDCl_3$): 138.7, 133.3, 129.2, 128.8, 126.8, 127.4, 126.8, 66.0, 33.9.

2.4.3 1-phenylseleno-2-(azido)octane

IR (neat) (v_{max},cm[-1]) : 2094(N=N-N-), 1570, 1465, 1259 (=C-H aromatic), 979, 858, 833 and 752 cm^{-1}. ^{1}H NMR, δ (300 MHz, $CDCl_3$): 7.61-7.55(m, 2H), 7.38-7.32(m, 3H), 3.41(dd, 1H, J=4.0 and 16.0Hz), 3.37(dd, 1H, J=8.0 and 16.0Hz), 3.04-2.94(m, 1H), 1.68-0.83(m, 13H). ^{13}C NMR, δ (75 MHz, $CDCl_3$): 135.2, 133.0, 129.0, 127.9, 55.9, 44.6, 32.4, 31.5, 28.9, 27.4, 22.5, 13.9.

2.4.4. 1-phenylseleno-2-(azido)cyclooctane

IR (neat) (v_{max}, cm[-1]): 2094(N=N-N-), 1572, 1468, 1261 (=C-H aromatic), 984, 863, 835 and 753 cm^{-1}. ^{1}H NMR, δ (300 MHz, $CDCl_3$): 7.8-7.77(m, 2H), 7.3-7.25(m, 3H), 3.70(dd, 1H, J=4.0 and 16.0Hz), 3.15(dd, 1H, J=8.0 and 16.0Hz), 2.18-1.25(m, 12H). ^{13}C NMR, δ (75 MHz, $CDCl_3$): 133.3, 129.4, 128.0, 124.4, 124.1, 123.5, 34.9, 34.4, 31.9, 31.6, 30.2, 28.9, 27.1, 22.7.

2.4.5. 1-phenylseleno-2-(azido)heptane

IR (neat) (v_{max} , cm[-1]): 2094(N=N-N-), 1573, 1470, 1265 (=C-H aromatic), 986, 864, 838 and 756 cm^{-1}. ^{1}H NMR, δ (300 MHz, $CDCl_3$): 7.61-7.58(m, 2H), 7.39-7.34(m, 3H), 3.37(dd, 1H, J=7.9 and 12.6 Hz), 3.25(dd, 1H, J=6.5 and 12.6 Hz), 2.04-0.83(m, 11H). ^{13}C NMR, δ (75 MHz, $CDCl_3$): 143.4, 137.3, 132.9, 129.6, 128.9, 127.3, 62.1, 58.6, 34.8, 32.4, 24.3, 23.4, 21.6.

3. Results and discussions

3.1. Cyclic voltammetry

Cyclic voltammogram of a platinum electrode to $(PhSe)_2$ in anhydrous dimethyl formamide containing M TBAP at a sweep rate of 100 mv s[-1] in the absence and presence of cyclohexene and sodium azide (excess amount) is shown in Figure 1. This figure shows an oxidative peak (1a) at 1.75

V (vs. Ag/AgCl), which is consisted with oxidation of $(PhSe)_2$ to the phenylselenenyl cation. Cyclic voltammogram of $(PhSe)_2$ in the presence of C_6H_{10} and NaN_3 shows two oxidative peaks (2a, 3a) at 1 V and 1.96 V. The cyclic voltammetry experiments of the mixture of $(PhSe)_2$, C_6H_{10}, and NaN_3 were performed in different potential sweep rates of 40-700 mv s^{-1}(Fig. 2). The results of cyclic voltammogram of figure 2 show an increase in the height of anodic peak and oxidation potential. The linear relation of the peak current of 1V vs. square root of sweep rate obtained with data of figure 2 confirms the departure from diffusion control. The multi-cyclic voltammograms of 4mM $(PhSe)_2$ and excess amount of C_6H_{10} and NaN_3 show a decrease in second scan of anodic peak. After second scan, anodic peak becomes constant (Fig. 3). We seached several conditions for finding optimum results. Firstly, different solvents are used in the experiments. Acetonitryl was not suitable solvent because of reaction with phenylselenyl cation. The second oxidation peak shows it in figure 4. Kunai et al. postulated a reaction between PhSe$^+$, CH$_3$CN in the presence cyclohexene [9]. So we abandoned this solvent. Dimethyl formamide was very suitable solvent for this reaction. Cyclic voltammetry

confirmed this well. In addition to solving well all reactants, it did not show any oxidation peaks in the potential limit.

By supporting the electrolyte which was optimized for this reaction, it is suggested by a method for increasing yield with bromide ion of electrolyte Torii et al. This anion obtained the reactive mediator as PhSeBr with PhSe$^+$ [17]. Tetrabutylammonium bromide (TBAB) as supporting electrolyte could not prepare the expectant results. In figure 5, cyclovoltammograms confirmed it, and difference of oxidation peak of TBAB and tetrabutylammonium perchlorate (TBAP) is absolutely. Table 1 shows the synthesized products of different alkenes and their yields.

3.2. Constant voltage electrolysis

The controlled-potential coulometry was performed in organic solution which is contained 0.3 mmol of $(PhSe)_2$ and excess amount of C_6H_{10} and NaN_3 at constant anodic potential of 1.96 V (vs. Ag/AgCl) with an H-type divided cell. Poor results received with undivided cell. The electrolysis was performed between 3-5 h, depending on the passed charge for the reaction. The monitoring of electrolysis was performed by TLC and cyclic voltammetry.
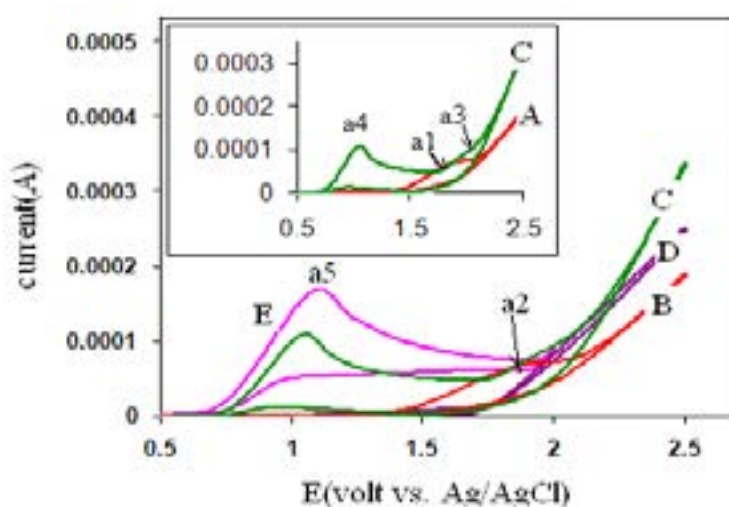

Fig. 1. Cyclic voltammogram of 4 mM $(phSe)_2$ (A) , 4 mM $(phSe)_2$ in the presence of C_6H_{10} (B), 4 mM $(phSe)_2$ in the presence of C_6H_{10} and NaN_3 (C), C_6H_{10} (D) , NaN_3 (E) with 0.2 M TBAP at a platinum electrode. Potential sweep rate was 100 mVs^{-1}.
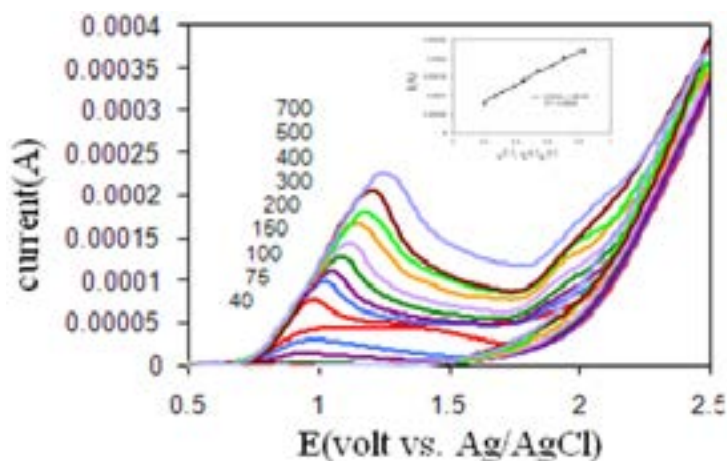
Fig. 2. Cyclic voltammograms of 4 mM (phSe)$_2$ and 0.2 M TBAP in the presence of excess amounts of C$_6$H$_{10}$ and NaN$_3$ at a platinum electrode and at different potential sweep rates (40-700 mVs^{-1}).
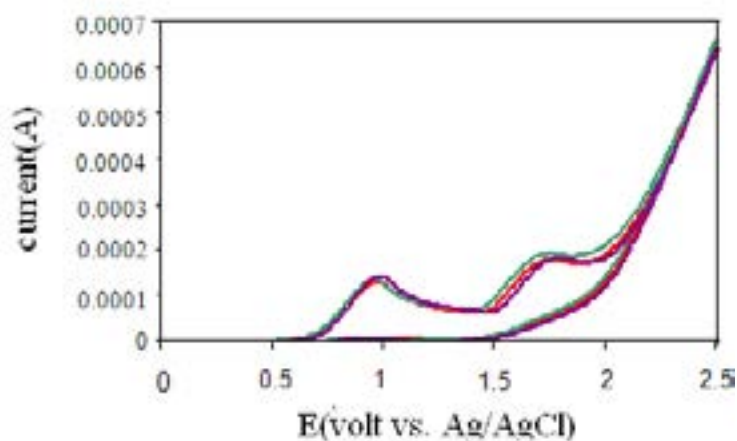

Fig. 3. Multi-cyclic voltammograms of 4 mM (phSe)$_2$ and 0.2 M TBAP in the presence of excess amounts of C$_6$H$_{10}$ and NaN$_3$ at a platinum electrode. Potential sweep rate was 100 mV.s^{-1}.
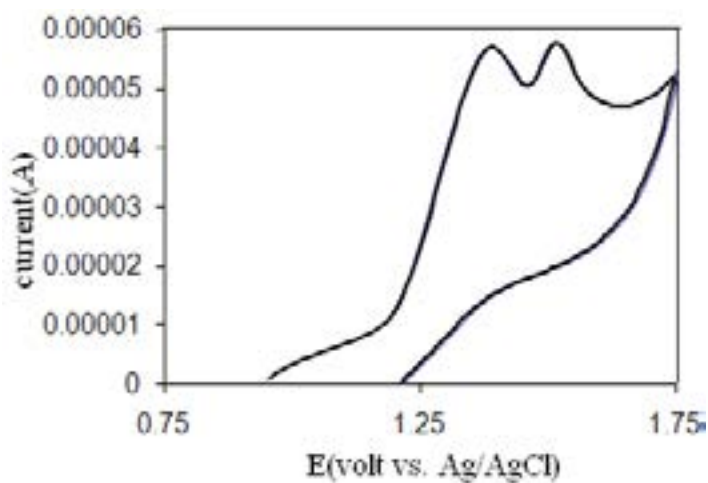

Fig. 4. Cyclic voltammogram of 4 mM (phSe)$_2$ and 0.2 M TBAP in CH$_3$CN at a platinum electrode. Potential sweep rate was 100mVs^{-1}.
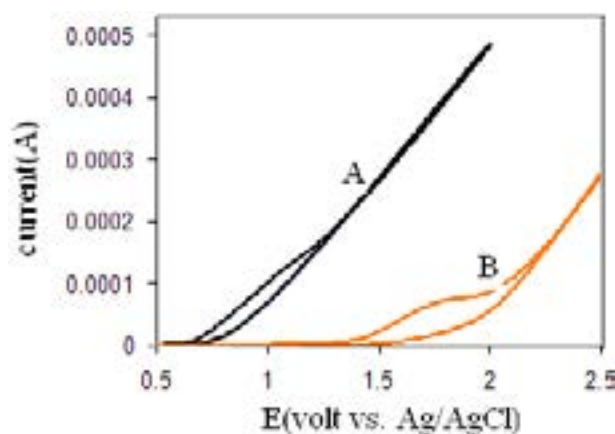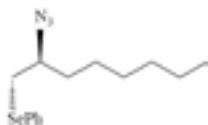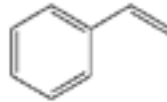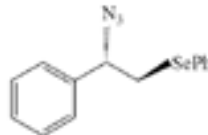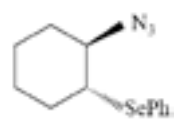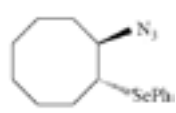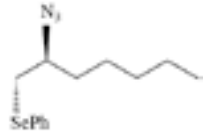
Fig. 5. Cyclic voltammograms of 4 mM (phSe)$_2$ in the presence of excess amounts of C$_6$H$_{10}$ and NaN$_3$ at a platinum electrode. Supporting electrolytes were tetrabutylammonium bromide (A), tetrabutylammonium Perchlorate (B). Potential sweep rate was 100 mV.s^{-1}.

Table 1. The synthesized products of different alkenes and their yields.

Entry	Alkene	Product	Time (h)	Isolated yield (%)	Theoriticalyield (%)	Current efficiency (%)
1			3	57	68	90
2			3.5	60	70	90
3			3	54	63.5	84
4			4	53	62	86
5			3	58	69	84

Moreover, it was shown a decrease in the anodic peak current of the product during various times of the electrolysis progressing (Fig. 6).
N-value of about 2 electrons calculated for controlled-potential coulometry at the potential of 1.96 V. The mechanism of electrochemical azido-selenenylation of olefins proposed EC reaction which the olefins react with the phenylselenenyl cation of the oxidative (PhSe)$_2$ in a nucleophilic addition fashion. This reaction generated the intermediate of selenyranium cation which was reacted with Sodium azide for synthesis of the
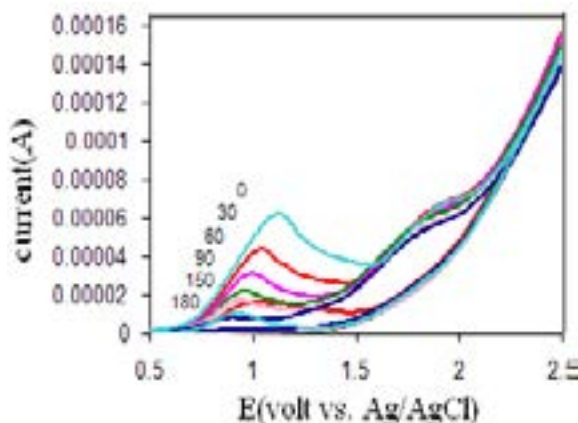
Fig. 6. Cyclic voltammograms of 4 mM $(phSe)_2$ and 0.2 M TBAP in the presence of excess amounts of C_6H_{10} and NaN_3 at a platinum electrode during controlled potential coulometry versus Ag/AgCl. Potential sweep rate was 100 mV.s^{-1}.

product (scheme 1). The results of IR spectroscopy of the final product show removal of C=C band for vinylil group in 1662 cm^{-1}. A relatively strong adsorption band disappeared for N-N=N group of NaN_3 in 2095 cm^{-1}.

4. Conclusions

In this paper, olefins and Sodium azide as nucleophile reacted with phenylselenenyl cation derived from electrochemical oxidation of $(PhSe)_2$. This progress was leading to the formation of azido-phenylselenenyl functionalized product with Markovnikov reaction. The final product was received a relatively good yield (60%). Like prior papers [4], regeneration of diphenyl diselenide was caused low yield of the product. The study of cyclic voltammograms and coulometric data was confirmed EC mechanism for electrochemical azido-selenenylation of olefins. The results and conditions of this project are better of the organic azido-selenenylation reactions [13, 20].

In comparison of organic reactions, the present electrochemical method considers being ineffective because of easier conditions (room temperature and atmosphere pressure), using lower amounts of reactants, not used catalysts, relatively short reaction times, high purity, and selectivity.

5. References

[1] L. Prashanth, K. K. Kattapagari, R. T. Chitturi, V. R. Reddy Baddam, L. K. Prasa, A review on role of essential trace elements in health and disease, J. Dr. NTR Un. Health Sci., 4 (2015) 75-85.

[2] V. Gandin, P. Khalkar, J. Braude, A. P. Fernandes, Organic selenium compounds as potential chemotherapeutic agents for improved cancer treatment, Free Radical Biol. Med.,127 (2018) 80-97.

[3] R. L. Quispe, M. L. Jaramillo, L. S. Galant, D. Engel, A. L. Dafre, J. B. Teixeira da Rocha, R. Radi, M. Farina, A. F. de Bem, Diphenyl diselenide protects neuronal cells against oxidative stress and
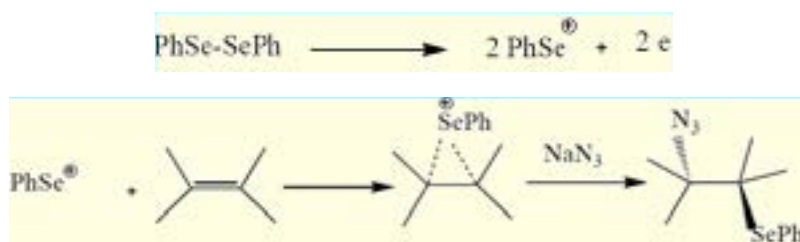
Scheme 1. Mechanism of Reaction.

mitochondrial dysfunction: Involvement of the glutathione-dependent antioxidant system, Redox Biol., 20 (2019) 118-129.

[4] A. R. Patra, S. Singha Roy, A. Basu, A. Bhuniya, A. Bhattacharjee, S. Hajra, U. Hossain Sk, R.Baral, S. Bhattacharya, Design and synthesis of coumarin-based organoselenium as a new hit for myeloprotection and synergistic therapeutic efficacy in adjuvant therapy Scientific Reportsvolume 8, Article number: 2194 (2018)

[5] C. Narajji, M. D. Karvekar, A. K. Das, Biological importance of organoselenium compounds, Indian J. Pharm. Sci., 69 (2007) 344-351.

[6] E. J. Lenardão, C. Santi, L. Sancineto, Organoselenium compounds as reagents and catalysts to develop new green protocols, New Frontiers in Organoselenium Compounds, 2018, pp. 1–97, 2018.

[7] H. D. S. Souza, R. P. F. de Sousa, B. F. Lira, R. F. Vilela, N. H. P. B. Borges, J. P. de Siqueira-Junior, E. O. Lima, J. U. G. Jardim, G. A. T. da Silva, J. M. Barbosa-Filho, P. F. de Athayde-Filho, Synthesis, in silico study and antimicrobial evaluation of new selenoglicolicamides, Braz. Chem. Soc., 30 (2019) 188-197.

[8] C. Santi, R.G. Jacob, B. Monti, L. Bagnoli, L. Sancineto , E.J. Lenardão , Review: Water and aqueous mixtures as convenient alternative media for organoselenium chemistry,   Molecules, 21 (2016) 1482.

[9] A. Tepecik, Z. Altin, S. Erturan, The Diorganoselenium and Selenides Compounds Electrochemistry J. Autom. Methods Manage. Chem. 1 (2008) 1-6.

[10] S. Möhle, M. Zirbes, E. Rodrigo, T. Gieshoff , A. Wiebe, S. R. Waldvogel, Modern Electrochemical Aspects for the Synthesis of Value-Added Organic Products, Angew.Chem. Int. Ed., 57 (2018) 6018-6041.

[11] A. Kunai, J. Harada, J. Izumi, H. Tachihara, K. Sasaki, Anodic oxidation of diphenyldiselenide in acetonitrile, Electrochim. Acta, 28 (1983) 1361-1366.

[12] O. Niyomura, M. Cox, T. Wirth, Electrochemical Generation and Catalytic Use of Selenium Electrophiles, Synlett, 2 (2006) 251-254.

[13] M. Tingoli, M. Tiecco, D. Chianelli, . Balducci, A. Temperini, Novel azido-phenylselenenylation of double bonds: Evidence for a free-radical process, J. Org. Chem., 56 (1991) 6809–6813.

[14] D. S. Smith, J. Winnick, Y. Ding, L. A. Bottomley, Electrosynthesis of Alpha-keto Acetals, Electrochim. Acta, 43 (1998) 335-339.

[15] M. Tingoli, M. Tiecco, L. Testaferri, R. Andrenacci, R. Balducci, Intramolecular nucleophilic deselenenylation reactions promoted by benzeneselenenyl triflate. stereospecific synthesis of vicinal amino alcohol precursors J. Org. Chem. 58 (1993) 6097.

[16] B. I. Kharisov, Direct synthesis of metal complexes, Elsevier, Switzerland, 2018.

[17] Fundamentals and applications of organic electrochemistry: synthesis, materials, devices, T. Fuchigami, M. Atobe, S. Inagi, Wiley, United Kingdom, Edition 2015.

[18] E. Steckhan, Topics in Current Chemistry, Vol. 185, Springer-Verlag, Berlin, 1997, Chapter 3.

[19] C. Gütz, B. Klöckner, S. R. Waldvogel, Electrochemical screening for electroorganic synthesis, Org. Process Res. Dev., 20 (2016) 26–32.

[20] S. Torri, K. Uneyama, K. Handa, Research articleAbstract only A facile access to α-phenylselenenyl carbonyl compounds by electrochemical oxidation, Tetrahedron Lett., 21 (1980) 1863-1866.

[21] R. Mundil, A. Sokolohorskyj, J. Hošek, J. Cvačka, I. Císařová, J. Kvíčala, J. Merna, Nickel and palladium complexes with fluorinated alkyl substituted α-diimine ligands for living controlled olefin polymerization, Polym. Chem., 9 (2018) 1234-1248.

[22] L. M. Bouchet, J. E. Argüello, Photoinduced one-electron oxidation of aromatic selenides: effect of the structure on the reversible dimerization reaction, J. Org. Chem., 83 (2018), 5674–5680